Geometric properties of spin models: cluster size heterogeneity

Amanda de Azevedo-Lopes

UNIVERSIDADE FEDERAL DO RIO GRANDE DO SUL

INSTITUTO DE FÍSICA

PROGRAMA DE PÓS-GRADUAÇÃO EM FÍSICA

Tese de Doutorado

Geometric properties of spin models: cluster size heterogeneity *

(Propriedades geométricas de modelos de spin: heterogeneidade de tamanhos de domínios)

Amanda de Azevedo-Lopes

Tese realizada sob orientação do Prof. Jeferson J. Arenzon e apresentada ao Instituto de Física da UFRGS em preenchimento parcial dos requisitos para a obtenção do título de Doutora em Ciências.

Porto Alegre, Brasil

Março de 2021

Acknowledgements

First and foremost, I would like to thank my supervisor, Jeferson Arenzon. I am profoundly grateful for his support, guidance, and useful critique. His advice during these years has made me a better scientist and has helped me in the writing of this thesis. Without his encouragement and patience, this work would never have been possible.

I am profoundly grateful to Prof. Federico Corberi, without whom my internship in Italy would not have been possible. Thank you for receiving me with great hospitality during my stay at the Università degli studi di Salerno. Despite the pandemics, it has been a pleasant and fruitful experience.

I must acknowledge the people I have collaborated and learned from during this period. I had the pleasure of working with Paulo Oliveira (Murilinho), Onofrio Mazzarisi, and Renan Almeida, whom I thank for several interesting discussions.

From the Graduate Program in Physics, I am grateful to Liane Thier Ruschel and Marcos Roberto Gonçalves for the kind and efficient assistance in dealing with the most diverse bureaucratic processes.

A special mention goes to all my friends and colleagues from UFRGS. My sincere thanks goes to Vinícius Ferreira, Felipe Selau, Rafael Barfknecht, Marion Silvestrini, Demétrius Lima, Sabrina Tigik, Nicole de March, Lucas Secco, Matheus Heinemann, Eduardo Stock and Marcos Pérez. They all contributed, in one way or another, in making my graduation a more stimulating and pleasing journey.

From Salerno, I am especially grateful to Matheus Chaves, Philipp Ritzinger, and my companions of Yama Arashi dojo. You all have made the experience of being in lockdown in a foreign country much better. Grazie Maestro Antonio per l'accoglienza, Carmine, la cui dedica sarà sempre fonte di ispirazione, Marcello per le infinite chiacchierate ed Elettra e Maria Rita per essere grandi compagni di kendo.

A special thanks to Mariana Timm, whose friendship in all these years has made life more enjoyable. Thank you for being the Best Frau Forever. I thank André Antonitsch for his patience, support and cheering. Last but not least, I would like to thank my mother, Andréia, for her support throughout all these years and for always believing in me.

A todos e a todas, um grande obrigado.

"Leggere è andare incontro a qualcosa che sta per essere e ancora nessuno sa cosa sarà..."

—Italo Calvino, *Se una notte d'inverno un viaggiatore*

Abstract

Many systems are continually evolving in nature. In contrast to phenomena at, or close to, equilibrium, the behavior of out of equilibrium systems is much less understood. The geometrical characterization of the structures, e.g., domains and hulls, common for certain classes of non-equilibrium dynamics and their time evolution are important in determining the macroscopic properties of many systems. For example, consider the problem of phase-ordering kinetics, when a system is suddenly quenched from a high temperature state, driving the system from a disordered phase to an ordered one. After the quench, ordered regions begin to form and grow via domain coarsening. The morphology of the domain structure holds information about the system's geometric properties and also grasp information about its phase transition. Many systems exhibit domain growth, with examples varying from magnetic domain growth in ferromagnetic materials to the phase separation in bacterial populations.

In particular, only recently, the role of the critical percolation point on the dynamical properties of $2d$ spin systems after a sudden temperature quench has been considered. In equilibrium, it is possible to resolve the thermal and percolative effects on finite lattices by studying the cluster size heterogeneity, $H_{\mathrm{eq}}(T)$, a measure of how heterogeneous the domains are in size. In this thesis, we extend the equilibrium measure $H_{\mathrm{eq}}(T)$ to out of equilibrium configurations, deriving an analytical expression for the dynamical cluster size heterogeneity $H(t)$, based on the analytical equations for domain size distributions. We study its temporal evolution and explore its usefulness in studying out of equilibrium situations after driving the system out of equilibrium by a sudden quench in temperature. Our analysis shows that $H(t)$ detects and distinguishes between different time regimes related to the two timescales in the system, namely the short percolative one and the long coarsening one. Besides, we also study a simple statistical model that generates independent domains whose only constraint is to fill the system area. We focus on evaluating the heterogeneity for algebraic distributions and showing that there is an exponent that maximizes the heterogeneity.

Resumo

Muitos sistemas na natureza estão em constante evolução. Ao contrário de fenômenos em equilíbrio, ou perto do equilíbrio, o comportamento de sistemas fora do equilíbrio é muito menos compreendido. A caracterização geométrica de estruturas comuns para certas classes de dinâmicas fora do equilíbrio, como domínios e hulls, e a sua evolução temporal são importantes para determinar propriedades macroscópicas de muitos sistemas. Por exemplo, considere o problema de ordenamento de fases dinâmico, quando a temperatura do sistema é repentinamente resfriada, levando o sistema de uma fase desordenada para uma ordenada. Após o resfriamento, regiões ordenadas começam a se formar devido à interação entre os spins e ocorre o crescimento de domínios. A morfologia da estrutura dos domínios contém informação sobre as propriedades geométricas do sistema e também guardam informação sobre sua transição de fase. Há diversos sistemas que apresentam crescimento de domínios, com exemplos variando de crescimento de domínios em materiais ferromagnéticos a separação de fase em populações de bactérias.

Em particular, apenas recentemente, o papel do ponto crítico de percolação nas propriedades dinâmicas de sistemas de spin $2d$ após um súbito resfriamento na temperatura foi considerado. Em equilíbrio, é possível separar os efeitos térmicos e percolativos em redes finitas através da heterogeneidade de tamanhos de domínios, $H_{eq}(T)$, uma medida de quão heterogeneos os tamanhos dos domínios são. Nesta tese, apresentamos uma extensão da medida de equilíbrio $H_{eq}(T)$ para configurações fora de equilíbrio, através de uma expressão analítica para a heterogeneidade de tamanhos de domínios dinâmica $H(t)$, baseada na solução analítica para a distribuição das áreas dos domínios. Estudamos a evolução temporal de $H(t)$ e demonstramos sua utilidade para analisar situações fora de equilíbrio após tirar o sistema de equilíbrio através de uma diminuição súbita na temperatura. Nossa análise mostra que $H(t)$ detecta e distingue entre os diferentes regimes temporais relacionados às duas escalas de tempo do sistema, isto é, à escala curta percolativa e à longa de crescimento de domínios. Além disso, também estudamos um modelo estatístico simples que gera domínios independentes cujo único vínculo é preencher a área do sistema. Focamos em estimar a heterogeneidade para distribuições de probabilidade algébricas e mostramos que há um expoente para a qual a heterogeneidade é maximizada.

Resumo simplificado estilo nota de imprensa (Press release)

Propriedades geométricas de modelos de spin: heterogeneidade de tamanhos de domínios

Amanda de Azevedo Lopes

Orientador: Jeferson J. Arenzon

Muitos sistemas na natureza estão em constante evolução, longe de estarem em equilíbrio. Ao contrário de fenômenos que ocorrem em equilíbrio, o comportamento de sistemas fora do equilíbrio é muito menos compreendido. Por exemplo, ao agitar uma mistura de dois líquidos, como água e óleo, tirando-a do que chamamos de estado de equilíbrio, um grande número de pequenas gotículas se formam. Mas se a deixarmos em repouso, estas gotas (domínios) crescem até as duas fases se separarem completamente (equilíbrio), formando duas camadas de água e óleo. Esse tipo de fenômeno é chamado de crescimento de domínios e pode ser visto nos mais diferentes contextos, desde bolhas de sabão e domínios em materiais ferromagnéticos até segregação espacial em populações de bactérias. Em particular, o estudo de domínios formados durante a evolução temporal desses sistemas possui grande importância teórica e inúmeras aplicações tecnológicas, sendo ainda um problema não completamente esclarecido. Podemos caracterizar geometricamente esses domínios: suas áreas, perímetros, números de lados, etc. Com isso, é possível determinar propriedades macroscópicas dos sistemas. A morfologia da estrutura dos domínios contém informação sobre as propriedades geométricas e também guarda informação sobre a transição de fase do sistema.

A informação que pode ser obtida desses sistemas depende das quantidades que serão medidas. Recentemente, um novo observável geométrico foi introduzido para estudar estados de equilíbrio. Neste trabalho exploramos, pela primeira vez, seu comportamento em situações fora do equilíbrio. Essa quantidade, a heterogeneidade dos tamanhos de domínios, H, fornece detalhes sobre a uniformidade das áreas desses domínios e é sensível às diferentes escalas de comprimento de sistemas em equilíbrio. Estudamos então a evolução temporal desse observável H em modelos simples para sistemas fora do equilíbrio após realizar uma perturbação brusca que os tira do equilíbrio (por exemplo, um rápido resfriamento). Nossa análise mostra que, através da medida de H, é possível detectar e distinguir os diferentes comportamentos relacionados às escalas de tempo presentes no sistema, isto é, uma escala curta e uma longa, associada ao crescimento de domínios.

List of Figures

Contents

Chapter 1

Introduction

Equilibrium statistical mechanics studies the complicated behavior of systems constituted of a huge number of building blocks - particles, spins, etc. It provides well-developed general tools to approach complex physical problems in statistical equilibrium. However, many systems in nature are constantly evolving over time. In contrast to phenomena at, or close to, equilibrium, the behavior of out of equilibrium systems is much less comprehended. Studies over the past few decades have provided important information to understand these systems dynamics better. In particular, one of the key issues is to geometrically characterize the structures that are common for certain classes of non-equilibrium dynamics.

One approach to studying out of equilibrium systems is by perturbing a system in equilibrium and observing its relaxation. The equilibrium state of some systems corresponds to different macroscopic configurations, e.g., a magnetic system with magnetization m and $-m$. Therefore, when perturbing such systems, different regions of the system attempt to equilibrate in different equilibrium phases locally. These locally ordered regions grow (or coarsen) until, if possible, reaching the new equilibrium state [1].

A classic example of systems that exhibit such domain growth behavior are systems quenched through a phase transition, such as magnets quenched through the disordered (paramagnetic) phase to the ordered (ferromagnetic) one. After the quench, the system tries to adapt and locally equilibrate with its environment, dividing itself into several regions called domains. The domains will not order instantaneously but typically will have a slow relaxation until they eventually reach the new equilibrium state [1]. Other systems that manifest similar behaviors are depicted in Figure 1.1. Figure 1.1a shows the coarsening of a superconducting magnetic froth as the temperature is increased [2]. The domain interfaces are in a superconducting phase, while the inside of the domains is in a normal magnetic phase. Another example is the magnetic domain growth during the heat treatment of a FeRh alloy [3,4]. Upon heating, domains nucleate and grow, and the system undergoes an antiferromagnetic to ferromagnetic phase transition (Figures 1.1b and 1.1c).
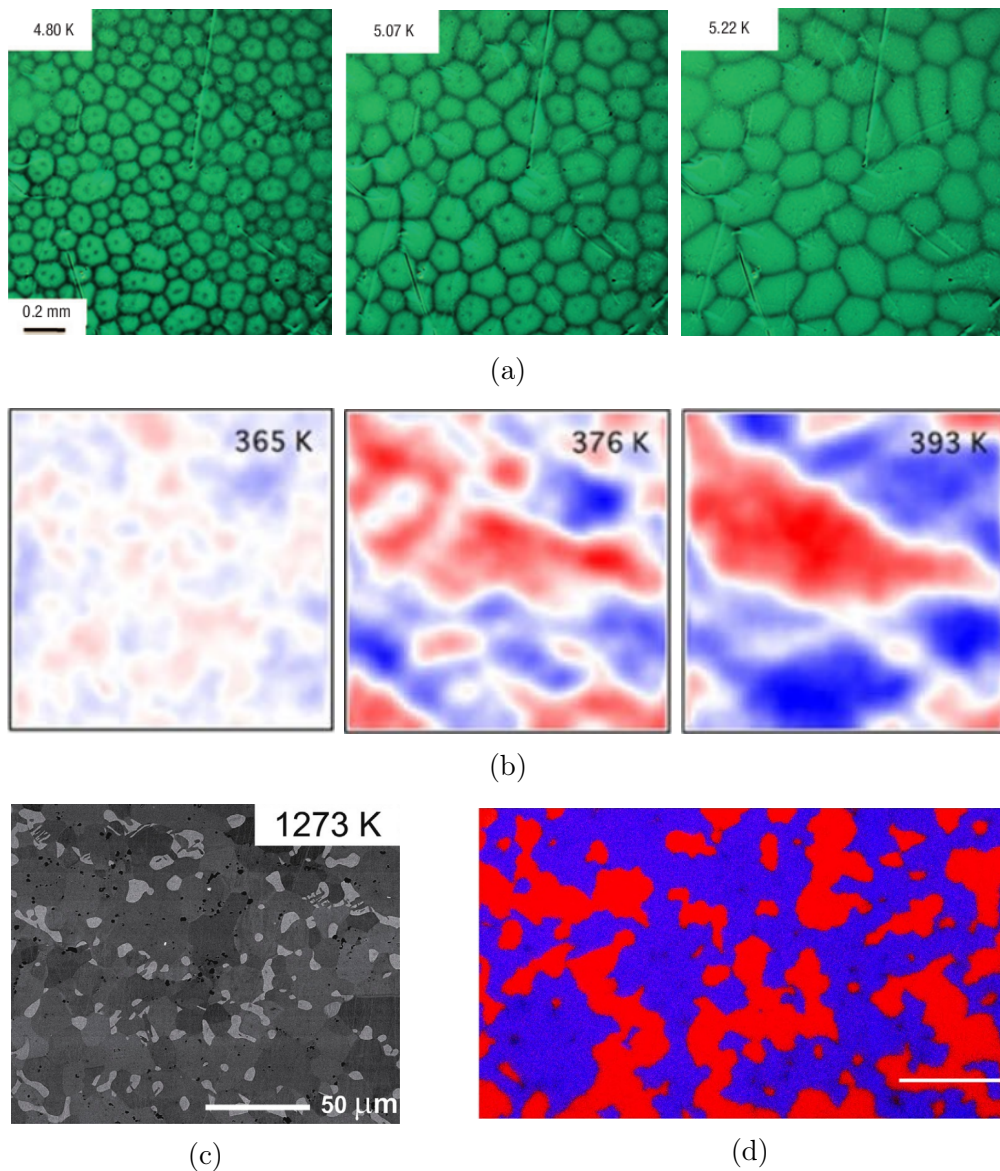
Figure 1.1: Examples of systems that exhibit coarsening. (a) Coarsening of magnetic froth on a superconducting lead disc as temperature increases, extracted from Prozorov *et al.* [2]. The inside of the cells are in a normal magnetic phase and the interfaces are in a superconductor one. (b) X-ray photoemission electron microscopy images of magnetic domain growth in a FeRh thin film, extracted from Keavney *et al.* [3]. Upon heating, the system undergoes an antiferromagnetic to ferromagnetic phase transition at ~ 375K. Local domain magnetization in red and blue. (c) Backscattered electron images during heat treatment of a FeRh alloy displaying magnetic domain growth, extracted from Chirkova *et al.* [4]. Bright and dark correspond to different phases. (d) Phase separation in bacterial populations, extracted from McNally *et al.* [5]. Initially, two strains of *Vibrio cholerae* bacteria (represented in red and blue, respectively) are in a well-mixed state. One of these strains kills the adjacent bacteria through a secretion mechanism that intoxicate other strains, promoting spatial separation between the different strains and enhancing cooperation with kin.

These patterns are not restricted to magnetic systems, also occurring in several other systems as biological tissues [6], spatial patterns in ecological ecosystems [7], and bacterial populations [5]. Figure 1.1d shows the spatial separation in two well-mixed bacterial populations, where each population is represented in red and blue, respectively [5]. One of these strains kills the adjacent bacteria through a secretion mechanism that intoxicate other strains and predators, promoting phase separation between the strains and enhancing cooperation with kin.

The examples above demonstrate that the study of ordering processes is essential to understand pattern formation, which is a relevant problem for many areas. A common characteristic of the coarsening regime is that there is a single relevant length scale $R(t)$ so that all spatial quantities are statistically invariant in time when measured with respect to $R(t)$ [1]. Figure 1.2 presents five snapshots of the coarsening process in a liquid crystal, illustrating the scale invariance during the evolution. The experimental system is a liquid crystal made of achiral bent-core molecules that exhibit electric-driven deracemization, which is the formation of chiral domains from an achiral solution [8]. Initially, the cooled liquid crystal is isotropic, with the bent-core or "banana" molecules (Figure 1.3a) organized in layers, aligned parallel to each other. Their alignment has a tilt direction with two possible orientations due to their bent shape (Figure 1.3b). There is no preferential direction of the tilt in the absence of an external field, and there are no domains formed. The tilt direction can be controlled by applying an electric field, which induces the formation of chiral domains. Domains of opposite chirality have different optical properties and polarize the light differently. Through polarizer filters, both alignments can be distinguished – with crossed polarizers, the domains cannot be distinguished (Figure 1.3c, left). By decrossing polarizers, chiral domains can be seen (Figure 1.3c, right). Upon the application of an external electric field, chiral domains are formed and grow as a function of time (Figure 1.2).

Phase ordering processes are qualitatively well understood, but there are still many open questions regarding the morphology of the spatial structures [11]. A series of works have studied the morphology of the domain structure [8,12–14] focusing on the geometrical distributions. The morphology of the domain structure holds not only information about the system's geometric properties but also grasps information about its phase transition and the occurrence of metastable states [15–17]. Various works [12, 13, 18] have shown that very early in the evolution of two-dimensional coarsening systems, the distribution of domain sizes approaches the expected form at critical percolation. The percolating state persists across the dynamics, evolving through the usual coarsening dynamics. Also, not only the short time dynamics is influenced by the critical percolation, but also the final state of the zero temperature Ising model. The probabilities that a $2d$ coarsening system reaches the ground state or evolves to a frozen stripe are equal to those of a spanning cluster at critical percolation [15, 16].
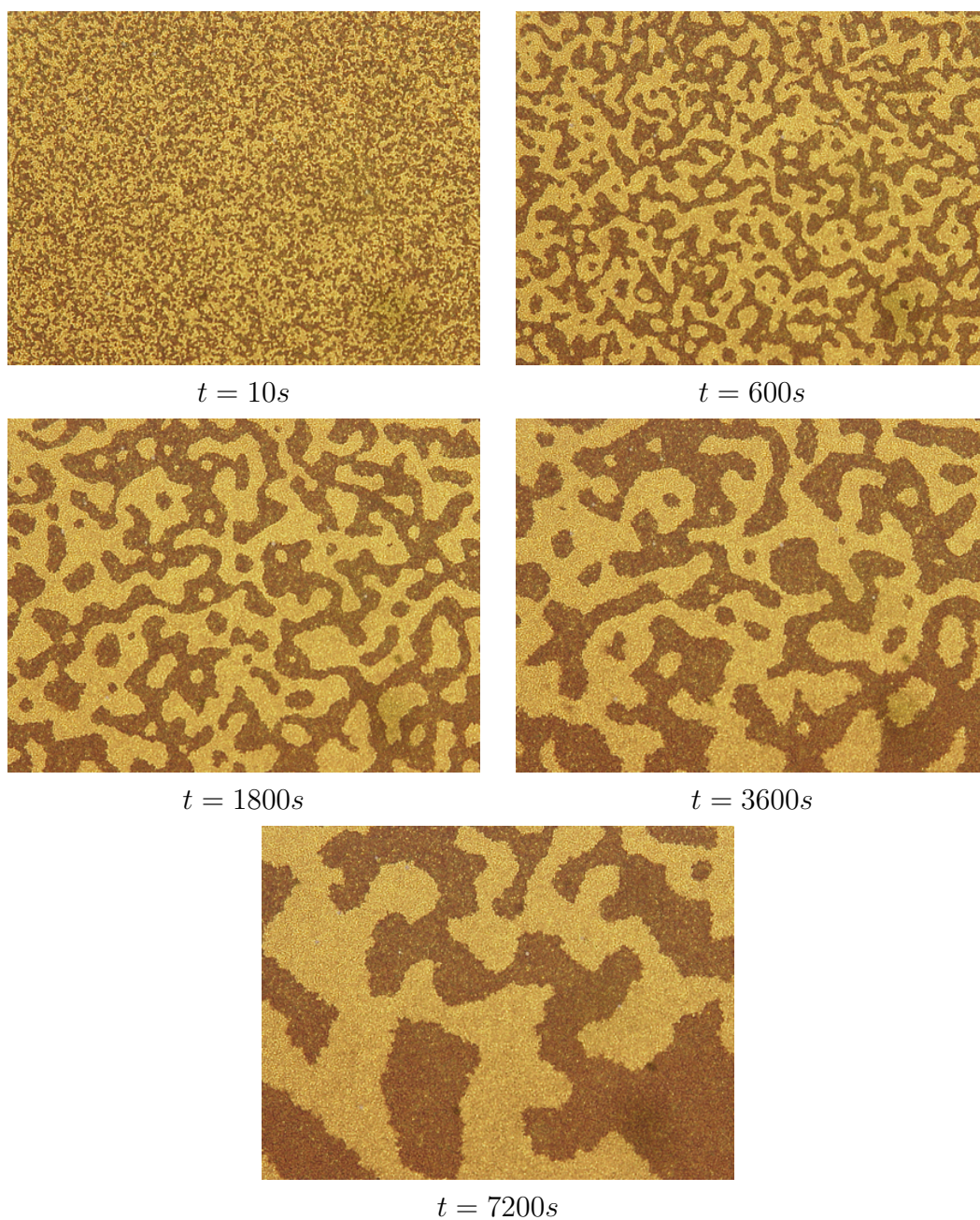
Figure 1.2: Snapshots of the formation and coarsening of chiral domains formed by an electric-field-induced deracemization in a liquid crystal made of achiral bent-core molecules for times $10, 600, 1800, 3600, 7200s$. Initially, the cooled system is isotropic. Upon the application of an external electric field, chiral domains start to form. Bright and dark regions correspond to domains with opposite chiralities. Time measured in seconds. Figures extracted from Sicilia *et al.*. [8].

(a) (b)

(c)
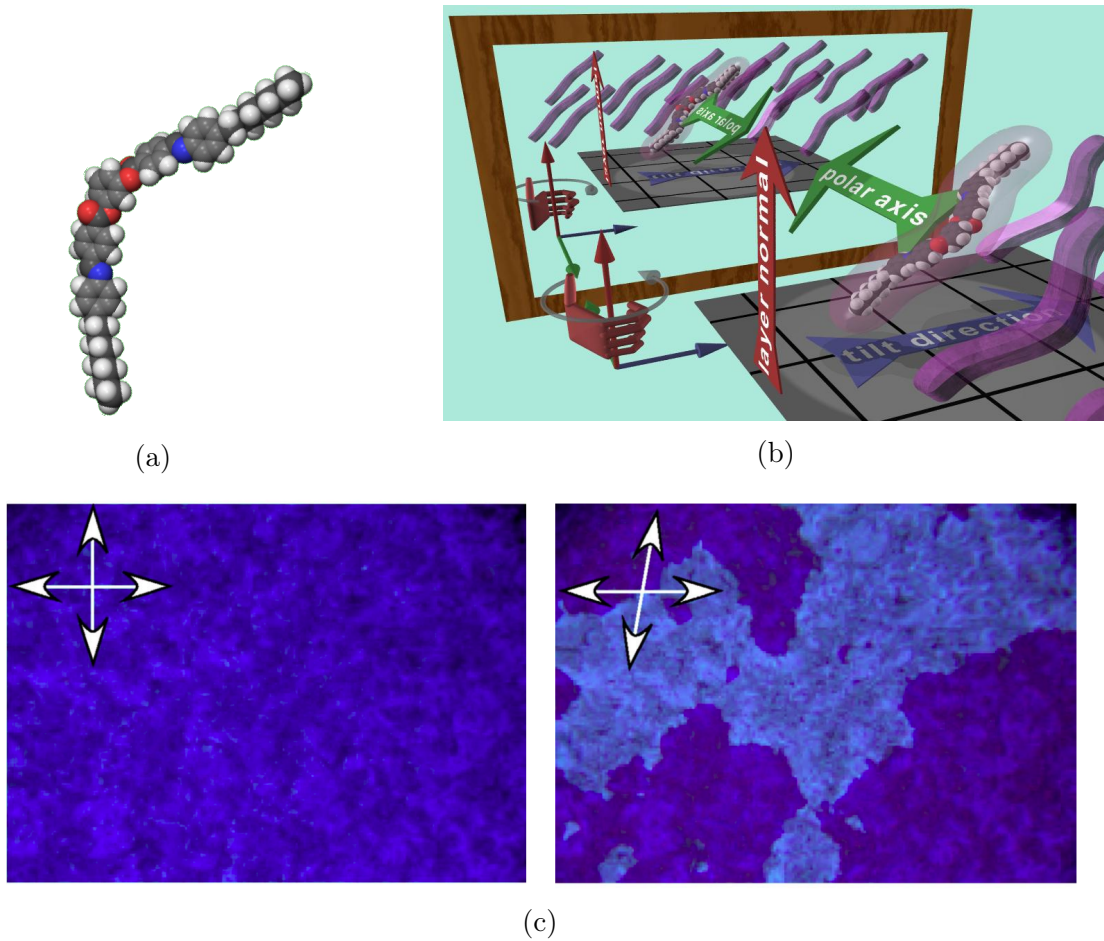
Figure 1.3: (a) Schematic representation of a liquid crystal bent-core molecule. (b) Schematic representation of a chiral layer consisting of achiral bent-core molecules (purple rods). The molecules are parallel to each other, with their long axis tilted with respect to the layer normal (vertical red arrow). Due to the molecules "banana" shape, each one possesses a dipole moment (green arrow) in the molecular plane and perpendicular to the long axis of the molecules. The layer normal, tilt direction (blue arrow), and the polar axis define a right-handed coordinate system (denoted by curled fingers), whereas in the mirror image, these vectors define a left-handed system, demonstrating the chirality of the layer structure. (c) By applying an electric field and decrossing polarizers (right panel), two chiral domains can be seen (bright and dark regions). Top row figures extracted from Keppke and Moro [9]. Bottom row figures extracted from Earl *et al.* [10].

The relation between coarsening dynamics and percolation is surprising due to their differing natures. Percolation is a paradigm of a noninteracting problem, which is defined as the process of a liquid moving slowly through a substance that has tiny holes [19]. On the other hand, coarsening dynamics depends on the interactions between the spins, which contrasts with the percolation process. Thus, apparently paradoxical, the interactions between the spins provide the environment for the formation of percolative features.

1.1 Motivations

There are several quantities to characterize systems geometrically, e.g., the space-time correlation function or the distribution of cluster sizes. In this thesis, we take a different approach to analyze the geometrical structures. We explore a recently proposed quantity called cluster size heterogeneity, which measures how heterogeneously sized the equilibrium domains in a distribution are [20]. Rather than taking into account the whole distribution, the heterogeneity only considers whether a given size is present in a system configuration. Despite the simplicity to define this quantity, the heterogeneity successfully determined the nature of the explosive percolation transition [20], which motivated a detailed study of its scaling properties and its application in other models, such as the site and bond percolation models [21], the Ising [22, 23] and Potts models [24].

The results for the equilibrium cluster size heterogeneity $H_{eq}(T)$ of the geometrical domains in the $2d$ Ising model showed two peaks at two very distinct temperatures. The first, small peak is associated with the thermal transition [22]. It occurs close to $T_1 \simeq T_c$ and is only observed for large systems [23]. The second peak is much larger than the first one, and appears at $T_2(L) > T_c$ [23]. The second peak is identified as an effect from the percolative transition. As the system size increases, the position of the second peak $T_2(L)$ approaches T_c. Despite the thermal and percolative transitions occurring at the same T_c, for finite systems these effects have not yet merged. Therefore, for equilibrium finite samples, the equilibrium cluster size heterogeneity was able to untangle the percolative and thermal effects.

Although the equilibrium cluster size heterogeneity has been properly characterized [20–24], whether this measure may be useful to study out-of-equilibrium configurations remains an open question. In particular, some of the questions we want to address are:

(i) Extend the measurement of the cluster size heterogeneity to out-of-equilibrium configurations and characterize its dynamical properties.

(ii) Analyze the dynamical size heterogeneity in the $2d$ Ising model. Is this quantity able to give information on the approach to the critical percolation point and the following coarsening evolution? How do different initial states, e.g., infinite or finite range correlations, change the behavior of $H(t)$?

(iii) How do different values of the exponent τ of the domain size distribution change the behavior of the heterogeneity? What value of this exponent τ maximizes the heterogeneity and how do we compare it with the known values for different models, i.e., how do we compare different long tailed distributions?

(iv) What geometrical properties play a role in the early time dynamics? What microscopic processes play a role in the formation of the first percolating cluster?

The first and second questions were the subject of a publication in *Physical Review E* [25], which is included in Appendix A. We have shown that the dynamical cluster size heterogeneity $H(t)$ is a suitable observable that distinguishes among different dynamical regimes, and provides information on the scaling laws related to domain growth and percolation transition during the dynamics. The third and fourth questions are the subject of forthcoming works [26,27], respectively. The preprint version of Ref. [26] is included in Appendix B.

1.2   Organization of the manuscript

This thesis is organized as follows: Chapter 2 contains a brief review of the Ising model, and of geometrical and statistical properties of domains, focusing on the coarsening process and the dynamic scaling hypothesis. It also addresses briefly the percolation problem and its relation with the coarsening dynamics. Chapter 3 is dedicated to a review of the equilibrium cluster size heterogeneity and its properties. Chapter 4 contains the results of the cluster size heterogeneity in a more general model, in which domains are independently chosen, with only a constraint on the total area of the system. Section 4.1 presents the model, while sections 4.2 and 4.3 illustrate the results for a general domain distribution and an algebraic one, respectively. In chapter 5 are the results for the cluster size heterogeneity in out of equilibrium configurations. Section 5.1 presents a brief description of the Ising dynamics, and the quench protocol used to drive the system out of equilibrium. The following sections 5.1.1 and 5.1.2 contain the results for the different initial temperatures. Chapter 6 summarizes the results and presents the final remarks on this thesis. At the end of that chapter, we discuss some perspectives of this thesis.

Chapter 2

Coarsening, domain growth, and percolation

One of the simplest examples of phase-ordering kinetics is a magnetic system quenched from above to below its critical temperature. The interactions between the spins drive the system towards an ordered state, where the spins initially form small domains of the different equilibrium phases and compete to select the new equilibrium state. Thus, coarsening dynamics is when a system initially in a disordered state starts to order locally in one of the competing equilibrium phases. Such domain growth exhibits a scaling phenomenon that, according to the dynamical scaling hypothesis, possesses a single characteristic length $R(t)$, such that all spatial quantities are independent of time when measured with respect to $R(t)$ [1].

In recent years there has been considerable interest in the role of percolation in the coarsening dynamics of magnetic systems [12, 13, 15–17, 28–31]. Investigations on the domain size distribution in curvature-driven coarsening dynamics have found that after a short time, the statistical and geometrical properties of spin clusters of neighboring sites have the same properties of clusters in critical percolation [12, 13]. The percolating state persists throughout the dynamics, with the system continuing to evolve through the usual curvature-driven coarsening dynamics. Similar results were found for coarsening with weak disorder [32] and for conserved order-parameter dynamics [18]. However, not only the short time scale is influenced by the critical percolation, but also the final state of the zero temperature Ising model. The relation between coarsening dynamics and percolation is surprising due to the diverse nature of both problems. This chapter begins with a brief overview of geometrical and statistical properties of domains, focusing on domain growth and the scaling hypothesis. It also addresses the percolation problem and its relation with the coarsening dynamics.

2.1 Ising model

The Ising model [33], used to describe the behavior of magnetic systems, is one of the simplest and most widely studied models. The physicist Wilhelm Lenz proposed it to his student Ernst Ising, who exactly solved the one-dimensional version in his Ph.D. thesis in 1924. It was proposed to explain the transition from the paramagnetic phase (P) at high temperature to the ferromagnetic one (F) that occurs below the Curie temperature T_c.

The model consists of a set of spins that may assume the values $+1$ or -1, disposed on a lattice with a given geometry, where each spin interacts with its neighbors. In the absence of an external magnetic field, the Ising model is described by the hamiltonian:

$$\mathcal{H} = -J \sum_{\langle i,j \rangle}^{N} S_i S_j, \tag{2.1}$$

where J is the exchange interaction between the spins, the sum is over all pairs of spins that are neighbors, and N is the total number of spins. For $J > 0$, the interaction is ferromagnetic, while for $J < 0$ it is antiferromagnetic. It has analytical solutions for one and two-dimensional cases. In the one-dimensional case, there is no phase transition. The two-dimensional case was exactly solved by Lars Onsager in 1944 [34] on a square lattice without an external magnetic field. The phase transition is continuous and occurs at the critical temperature $T_c = 1/\ln(1 + \sqrt{2}) \simeq 2.269$.

2.2 Geometrical definitions

A system initialized in an out-of-equilibrium configuration or quenched to a subcritical temperature tries to order locally in two or more competing equilibrium phases or absorbing states. This competition promotes the appearance of locally aligned regions corresponding to each state. A group of nearest neighbor sites with aligned spins is defined as a geometric domain or cluster. An example of a domain configuration is shown in Figure 2.1. The area of a domain corresponds, for discrete spin systems, to the number of spins contained in it. Geometric domains may have other, smaller geometric domains inside their external interface, creating "holes", and being inside even larger domains. The outer domain boundary is called the "hull", and the hull enclosed area corresponds to the total number of sites inside the hulls, i.e., the area of the whole domain plus the area of all domains inside it. In the example of Figure 2.1, the corresponding hull enclosed area for the domains 1 and 2 is $A_h^{(1)} = \pi R_1^2$ and $A_h^{(2)} = \pi R_2^2$, respectively. The area of the corresponding geometric domains is $A_d^{(1)} = \pi R_1^2$, and $A_d^{(2)} = \pi(R_2^2 - R_1^2)$ respectively.
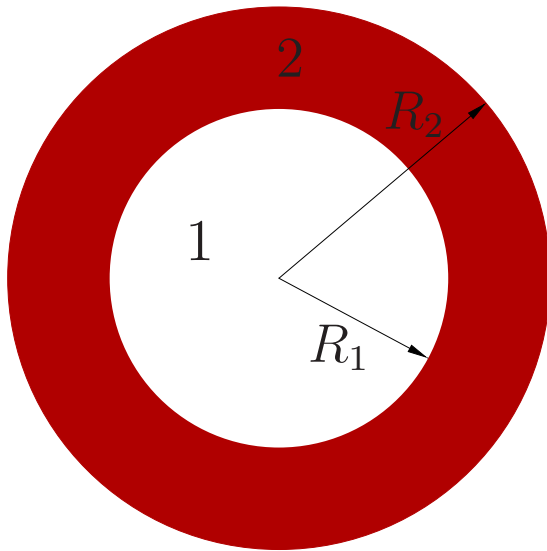
Figure 2.1: Example of hull enclosed and domain areas in a configuration with two circular interfaces. There are two hull enclosed areas, $A_h^{(1)} = \pi R_1^2$ and $A_h^{(2)} = \pi R_2^2$, and two domains with areas $A_d^{(1)} = \pi R_1^2$ and $A_d^{(2)} = \pi(R_2^2 - R_1^2)$.

2.3   Dynamical scaling hypothesis

The theory of coarsening or phase-ordering kinetics is connected with the dynamical evolution of the system toward the final equilibrium state [1]. An example of the patterns formed by a system quenched from the disordered phase and left to evolve is shown in Figure 2.2. After the quench, locally ordered regions grow in time (coarsen), and the typical length scale of the ordered regions increases as the different phases compete to achieve the final equilibrium state. Apart from a scaling factor, this domain structure remains statistically similar at different times. This observation gave rise to the dynamical scaling hypothesis, which states that there is a single growing length $R(t)$ (the average domain size at time t), such that the domain structure is statistically independent of time when distances are measured with respect to it [1].

The characteristic length grows as a power-law

$$R(t) \simeq t^{1/z_d}, \tag{2.2}$$

where z_d is the dynamical exponent and depends on the dynamic universality class. The universality classes are defined by the nature of the dynamics, the symmetries, the conservation laws, and the spatial dimensions. For the non-conserved order parameter class, which includes the Ising model with Glauber dynamics, $z_d = 2$, while for the conserved order parameter class, e.g., the Ising model with Kawasaki dynamics, $z_d = 3$ [1].

There are several ways to measure the characteristic length of the domains. One possibility is to measure the correlations between the spins. The correlation function at equal times $C(r, t)$ measures the correlation between two spins in two sites at a distance r at a
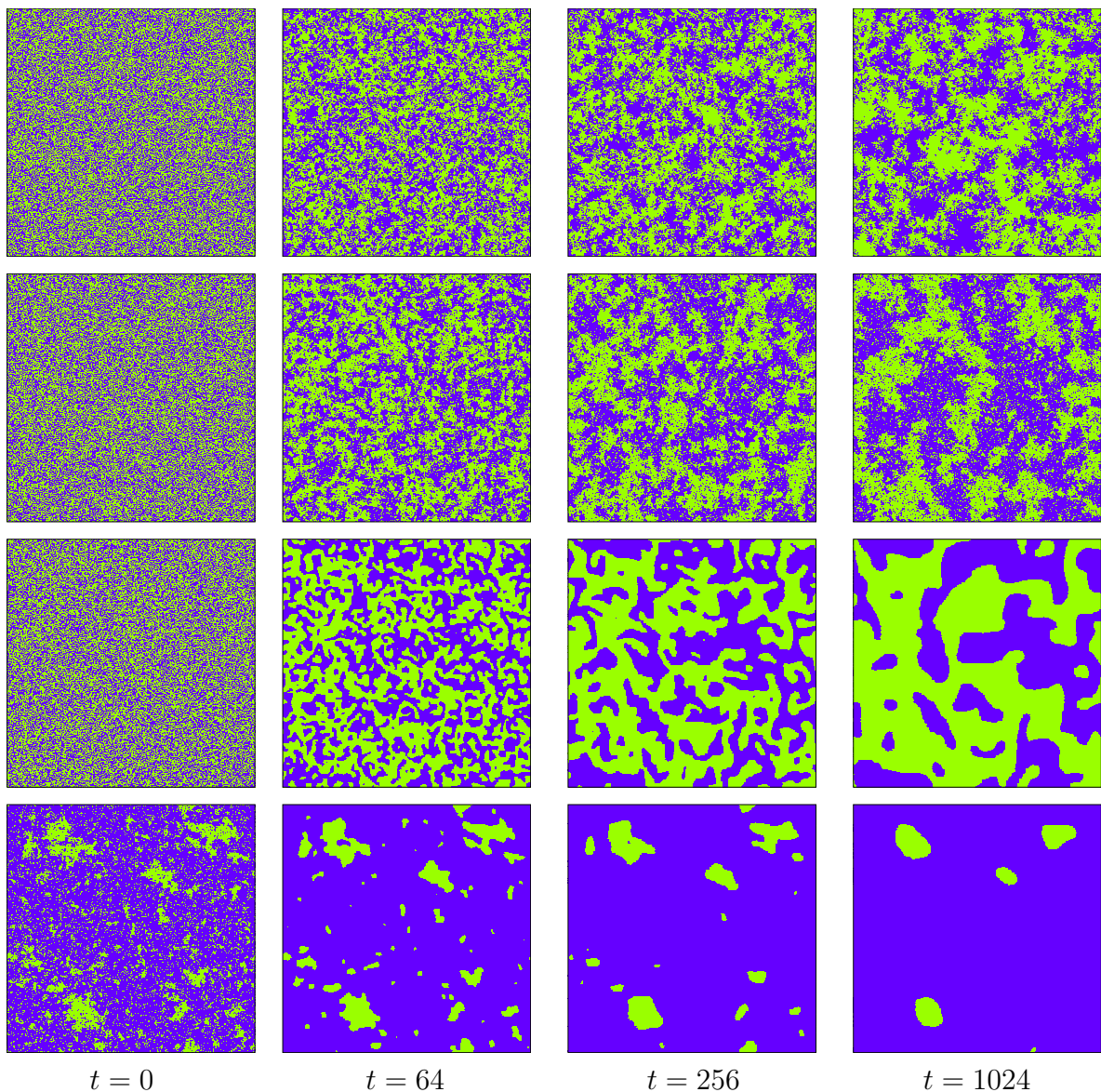
Figure 2.2: Snapshots of a Monte Carlo simulation of the $2d$ voter (first row) and Ising (second, third and fourth rows) models with linear size $L = 640$ and periodic boundary conditions. For the first to the third row, the initial state was $T_0 \to \infty$, corresponding to an uncorrelated state. On the fourth row, the system was equilibrated at $T_0 = T_c$, corresponding to an initial state with long range correlations. Each color represents a spin orientation, $+1$ or -1. On the second row, the Ising model was quenched from $T_0 \to \infty$ to $T_f = T_c$, while on the third and fourth rows, the final temperature was $T_f = 0$. Note that the voter model has a different coarsening process than the zero temperature Ising model. The $T = 0$ dynamics is purely curvature driven, while the voter dynamics is driven by interfacial noise. The voter model also differs from the Ising model critical relaxation (second row), especially due to the absence of bulk fluctuations. The temperature generates an excess of small domains and roughens the domain walls. Snapshots were taken at times (measured in Monte Carlo steps, MCS) indicated below the images.

time t

$$C(r,t) = \frac{1}{N} \sum_{i=1}^{N} \langle S_i(t) S_j(t) \rangle \big|_{|\vec{r_i} - \vec{r_j}| = r} \,, \tag{2.3}$$

where N is the total number of spins and the brackets $\langle ... \rangle$ denote the average over different initial conditions. According to the dynamic scaling, the correlation function can be rescaled as

$$C(r,t) \sim f(r/R(t)) \,, \tag{2.4}$$

where $f(x)$ is the scaling function.

At high temperatures, $T > T_c$, the correlations between the spins are short ranged, and in the limit $T \to \infty$, the spins are uncorrelated. The equilibrium state at zero temperature is homogeneous, all spins are aligned and the correlation is of the order of the linear system size L. After a quench from infinite temperature to a temperature $T < T_c$, the correlation between the spins increases over time, as shown in Figure 2.3a. At a short range, the spins have a higher probability of being in the same state, thus the correlation is higher. As the distance r increases, this probability decreases and the correlation between the spins is lower. Figure 2.3b shows the correlation function as a function of the rescaled distance $r/R(t)$. The characteristic length $R(t)$ is computed as the distance r at which the correlation is $C(R,t) = 0.3$, but the scaling does not depend on this value and other choices give equivalent results. The inset shows that the characteristic length grows as a power-law, $R^2(t) \sim t$, as predicted from the scaling hypothesis. The correlation function was also measured experimentally. For example, the experimental results of the liquid crystal system in Ref. [8] displayed a good agreement with the scaling hypothesis.

Despite several numerical studies and experimental results supporting the scaling hypothesis, the proof of its validity has been restricted to a few simples models such as the one-dimensional Ising model with Glauber dynamics [35, 36], the nonconserved $O(n)$ model in the limit $n \to \infty$ [37], and the one-dimensional XY model [38]. The validity of the scaling hypothesis was also demonstrated for two-dimensional coarsening systems with nonconserved order parameter dynamics [12], which will be discussed in the next section.

2.4 Domain growth

At zero temperature, there are no thermal fluctuations; hence the system excess energy is located at the domain walls. Therefore, energy can only decrease by reducing the total interface length. In 1979, Allen and Cahn [39] verified that the domain walls movement is related to the superficial tension; thus, the coarsening process is purely curvature driven. Allen and Cahn have shown that the velocity v of each element of a domain boundary is
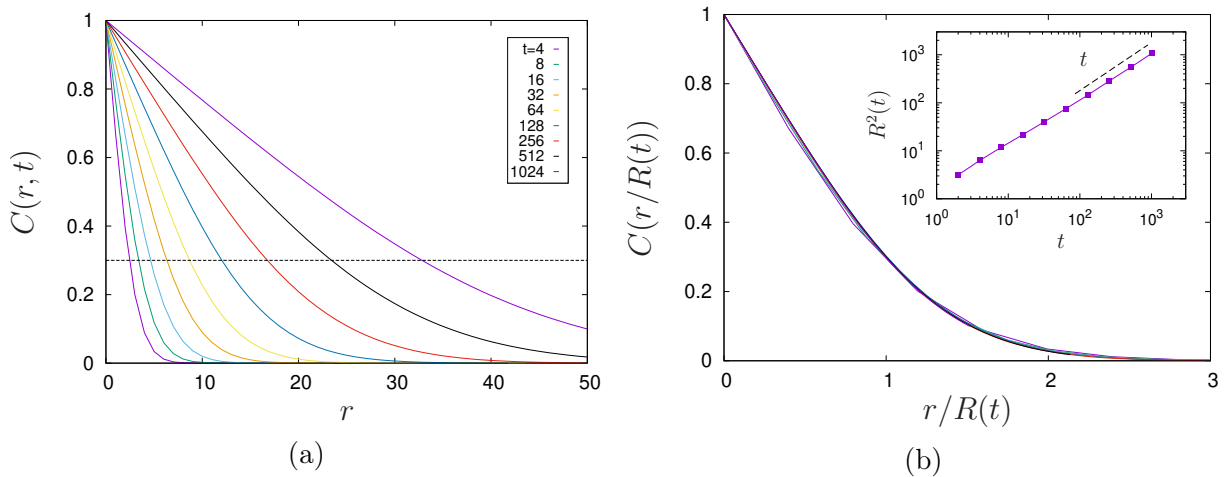
Figure 2.3: Correlation function $C(r, t)$ for the $2d$ Ising model after a quench from $T_0 \to \infty$ to $T_f = 0$ and several different times $t = 2^2, ..., 2^{10}$. (a) Initially, the spins are uncorrelated and the correlation between the spins grows as the system evolves. At short distances, the probability of the spins being in the same state is higher, hence a higher correlation. This probability decreases as the distance between the spins increases, so the correlation is lower. (b) Collapsed correlation function using the characteristic length measured as the distance R at which the correlation is $C(R, t) = 0.3$ (dashed horizontal line in panel (a)). On the inset, the time evolution of the squared characteristic length $R^2(t)$. As predicted from the dynamical scaling, the characteristic length grows as a power-law, $R^2(t) \sim t$. The linear system size is $L = 640$.

proportional to the local interfacial curvature [1,39]:

$$v = -\frac{\lambda}{2\pi}\kappa\,, \tag{2.5}$$

where λ is a temperature-dependent constant, with the dimensions of a diffusion constant, κ is the local curvature, and the velocity is normal to the interface, with its direction setting the reduction of the curvature, $\kappa \sim r^{-1}$ (Figure 2.4a). As the interface velocity depends on the curvature, domain walls of smaller domains move faster than the domain walls of larger ones (Figure 2.4b). Since the interface length (and area) of smaller domains is smaller than in larger ones, we will see that smaller domains disappear before bigger ones.

To highlight the curvature driven growth, Figure 2.5 shows a comparison of the evolution of a circular domain for the curvature driven $2d$ zero-temperature Ising model and the $2d$ voter model. The voter model is a simple spin model without an associated energy function named after its interpretation in terms of opinion dynamics [40–42]. In the voter model, a site chosen at random aligns with a randomly chosen nearest neighbor. Thus, the probability of a spin flip does not depend on the energy variation, as in the Ising model, but is given by the fraction of nearest neighbors with opposite orientation. Hence, there is no bulk noise and the motion of the interfaces does not depend on the curvature, but is driven by interfacial fluctuations [43]. For curvature driven growth, a large bubble shrinks with time due to the surface tension, with the density of interfaces (or domain

boundaries) decaying with $\rho \sim t^{-1/z_d}$. A large bubble under the voter model dynamics does not shrink as in curvature driven growth but slowly disintegrates as the boundary of the domain roughens, with the density of interfaces decaying with $\rho \sim 1/\ln t$ [43]. A special case is the one-dimensional lattice where the voter dynamics is equivalent to the zero temperature Ising-Glauber dynamics [44, 45].

(a)

(b)
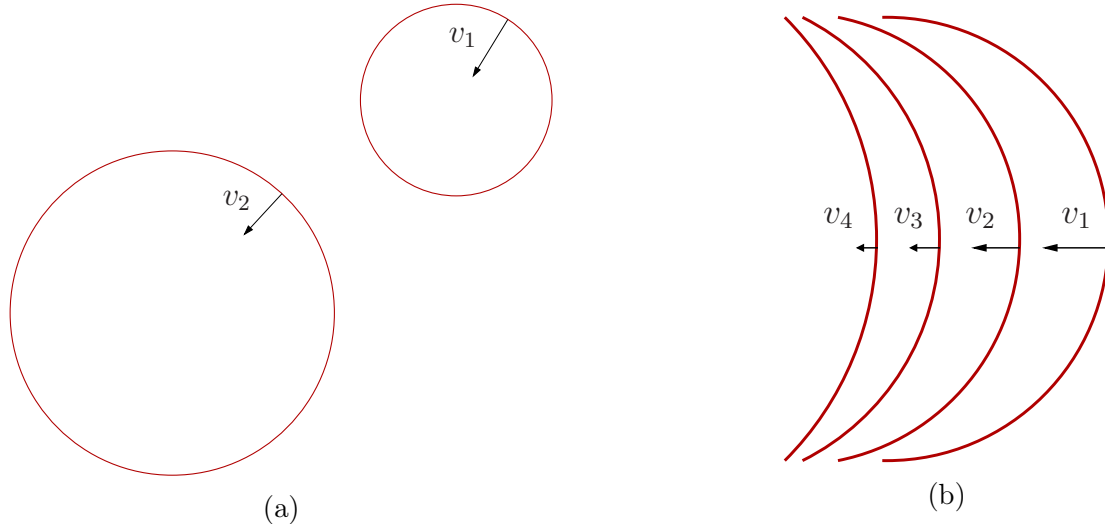
Figure 2.4: Schematic of the velocity of a domain boundary and the local interfacial curvature. Panel (a) illustrates two domains: the interface velocity is normal to the interface and is proportional to the local curvature, thus $v_1 > v_2$. Panel (b) shows that a domain wall moves faster for a higher local curvature, $v_1 > v_2 > v_3 > v_4$.

The time-dependence of the area contained within a hull may be derived from the Allen-Cahn equation by integrating the velocity around the hull:

$$\frac{dA_h}{dt} = \oint \vec{v} \cdot d\vec{\ell} = -\frac{\lambda_h}{2\pi} \oint \kappa d\ell = -\lambda_h \,, \tag{2.6}$$

where the final equality is obtained from the Gauss-Bonnet theorem [12]. Integrating the above equation in time, one obtains the area of a hull at any time t,

$$A_h(t) = A_h(0) - \lambda_h t \,. \tag{2.7}$$

Note that all hulls shrink at the same rate. As a result, at a time t, all hulls with an initial area smaller than $\lambda_h t$ will have disappeared, while the enclosed areas of the remaining hulls will have decreased by $\lambda_h t$. Considering the number of hulls with areas between A and $A + dA$ in a given time t, the distribution of hull enclosed areas $n_h(A, t)$ is:

$$n_h(A, t) = n_h(A + \lambda_h t, 0) \,. \tag{2.8}$$

Therefore, when the initial distribution is known, the distribution at any later time may be determined. Also, the shape of the distribution is not altered during the evolution but is uniformly shifted to the left at rate λ_h. At zero temperature, the Ising model is

16
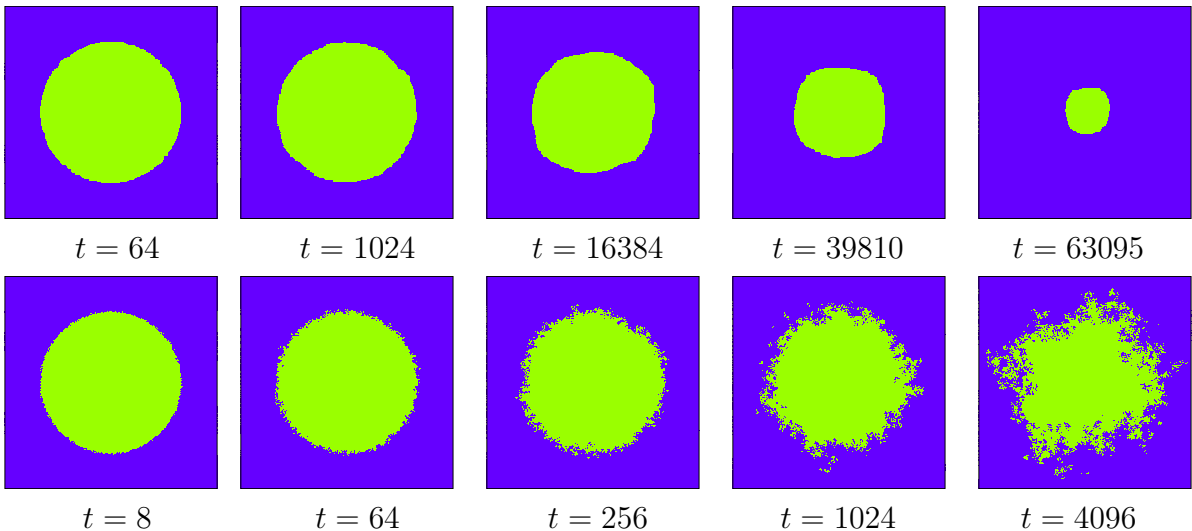
Figure 2.5: Snapshots of a Monte Carlo simulation of the 2d zero-temperature Ising model with linear size $L = 640$ and periodic boundary conditions evolving from an initial state with a bubble of radius $r = 0.3L$. Each color represents a spin orientation, $+1$ or -1. Snapshots were taken at times (measured in Monte Carlo steps, MCS) indicated below the images. To highlight the curvature-driven evolution of the zero-temperature Ising model, the bottom row displays the 2d voter model driven by the interfacial fluctuations.

purely curvature driven, and the interfaces tend to disappear or become flat, with the smallest domains disappearing first from the domain distribution. The thermal fluctuations roughen the domain walls at finite temperature, opposing the curvature driven growth and slowing it down [13]. They also generate thermal domains that are not related to the coarsening dynamics. This effect is easily noted in figure 2.2 comparing the evolution towards $T = 0$ and $T = T_c$. This temperature-dependent behavior is encoded in the parameter λ_h.

2.5 Hull enclosed area and domain-size distributions

As seen in the previous sections, the coarsening process is curvature-driven. The interfaces tend to disappear independently of one another with a velocity proportional to the local curvature. If the initial distribution is known, the time evolution of the distribution $n(A, t)$ can also be determined.

The equilibrium distribution is known for two particular cases. Cardy and Ziff [46] have determined the equilibrium hull enclosed area distribution for a 2d, two-state system, as the Ising model, at the critical temperature T_c:

$$n_h(A, 0) \sim \frac{c_h}{A^2}, \qquad T_0 = T_c, \qquad (2.9)$$

where $c_h = 1/(8\pi\sqrt{3}) \approx 0.022972$ is an adimensional universal constant. This expression is valid for $A_0 \ll A \ll L^2$, with A_0 a microscopic area and L^2 the system size.

Cardy and Ziff [46] also computed the equilibrium hull enclosed area distribution for

the random site percolation at the critical density p_c. In random site percolation, a site is occupied with probability p, and empty with probability $1 - p$. For $p > p_c$, a cluster spans the system with probability 1. Further details of random site percolation will be addressed in the next section, 2.6. For a square lattice, the percolation threshold is $p_c \approx 0.5927$. The Ising model in a square lattice with a disordered configuration (corresponding to the equilibrium state at $T \to \infty$) has spins pointing up or down with probability 1/2, which corresponds to an occupation probability of $p = 0.5$. Hence, this initial state is below the percolation threshold.

However, after a quench from $T_0 \to \infty$ to $T < T_c$, the system is rapidly attracted to a critical percolation state [13]. At a very short time t_{p_1} a percolating cluster with geometrical properties of critical percolation appears for the first time in the system [13]. Therefore, the equilibrium hull enclosed area distribution at critical percolation may be used as the initial equilibrium distribution at $T \to \infty$,

$$n_h(A, 0) \sim \frac{2c_h}{A^2}, \qquad \text{critical percolation } (T_0 \to \infty), \qquad (2.10)$$

where the extra factor 2 arises from the counting of the two phases of hull enclosed areas in the coarsening dynamics, while the result of Cardy and Ziff only accounts for clusters of occupied sites in random percolation [12]. Indeed, for a quench from infinite temperature to a subcritical temperature, the Ising model rapidly attains the critical percolation distribution, as shown in Figure 2.6, so this distribution can be considered as the starting point for the $T_0 \to \infty$ case [13].

Using these distributions in (2.9) and (2.10) as the initial conditions $n(A_i, t_i)$ of the equation (2.8), Arenzon *et al* [12,13] have shown that the hull-enclosed area density is

$$n_h(A, t) = \frac{c_h}{(A + \lambda_h t)^2}, \qquad T_0 = T_c, \qquad (2.11)$$

$$n_h(A, t) = \frac{2c_h}{(A + \lambda_h t)^2}, \qquad T_0 \to \infty, \qquad (2.12)$$

assuming a time much greater than the initial time $t \gg t_i$ and areas much larger than microscopic areas, but still much smaller than the system size, $A_0 \ll A \ll L^2$. Both distributions correspond to a system with a characteristic area proportional to t, which corresponds to a characteristic length scale proportional to $t^{1/2}$, validating the dynamical scaling hypothesis [12].

Similarly, approximate expressions for the domain area distributions can be obtained, which have a form similar to the hulls,

$$n_d(A, t) \sim \frac{c_d}{(A + \lambda_d t)^\tau}, \qquad T_0 = T_c, \qquad (2.13)$$

$$n_d(A, t) \sim \frac{2c_d}{(A + \lambda_d t)^{\tau'}}, \qquad T_0 \to \infty, \qquad (2.14)$$

18

with the constants $c_d \approx c_h$, $\tau' = 187/91 \approx 2.055$, $\tau = 379/187 \approx 2.027$, and the equilibrium distribution of domain areas at critical percolation given by [19]

$$n_d(A, 0) \sim \frac{2 c_d A_0^{\tau'-2}}{A^{\tau'}} , \tag{2.15}$$

and at the critical temperature [47]

$$n_d(A, 0) \sim \frac{c_d A_0^{\tau-2}}{A^{\tau}} . \tag{2.16}$$

The agreement between the analytical equations (2.13) and (2.14) is shown in Figures 2.7 and 2.8. Figure 2.7 shows the time-dependent domain distribution, after a quench from $T_0 \to \infty$ to $T = 0$, at different times of the evolution. The lines are the analytical distributions from Eq. (2.14) with the fitting parameters $c_d = 0.025$, $\tau' = 2.055$, and $\lambda_d = 2.1$. The agreement between the analytical results and the simulations are very good, apart from the bump at the end of the distribution. The overshoot of the distribution for large areas is due to the finite size effects. The spanning domains are limited by the lattice finite length and have a size much smaller than they would have on an infinite system. Figure 2.8 shows the rescaled data, highlighting the collapse over time for the simulations and the analytical data. The data were obtained on a square lattice with linear size $L = 640$ using the continuous-time Monte Carlo dynamics, and the average was taken over 2000 independent system realizations.
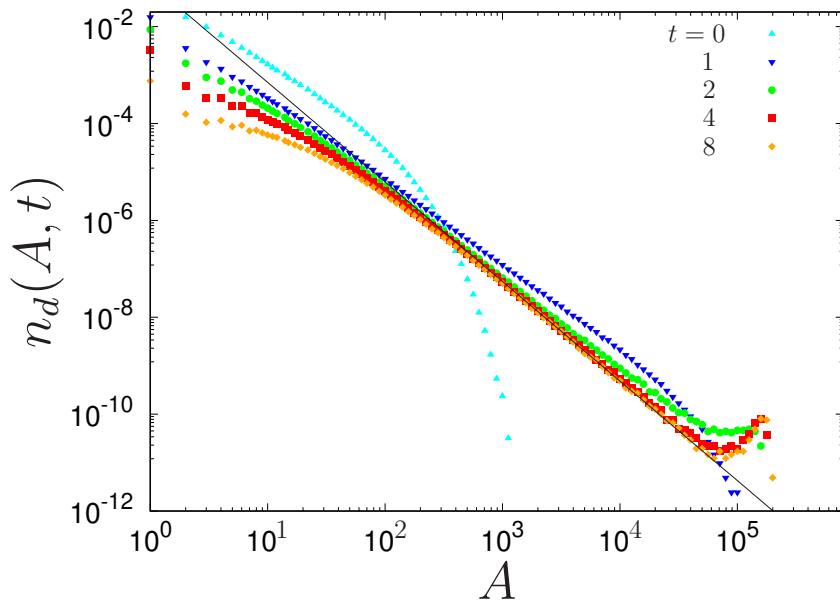
Figure 2.6: Early evolution of the domain distribution of the $2d$ Ising model with linear size $L = 640$ and periodic boundary conditions quenched from the infinite temperature initial condition to $T = 0$. The average was taken over 2×10^3 samples. The distribution quickly converges to the critical percolation. The straight line corresponds to $A^{-2.055}$. Results agree with those of Sicilia et al [13], validating the code that was used in Chapter 5.
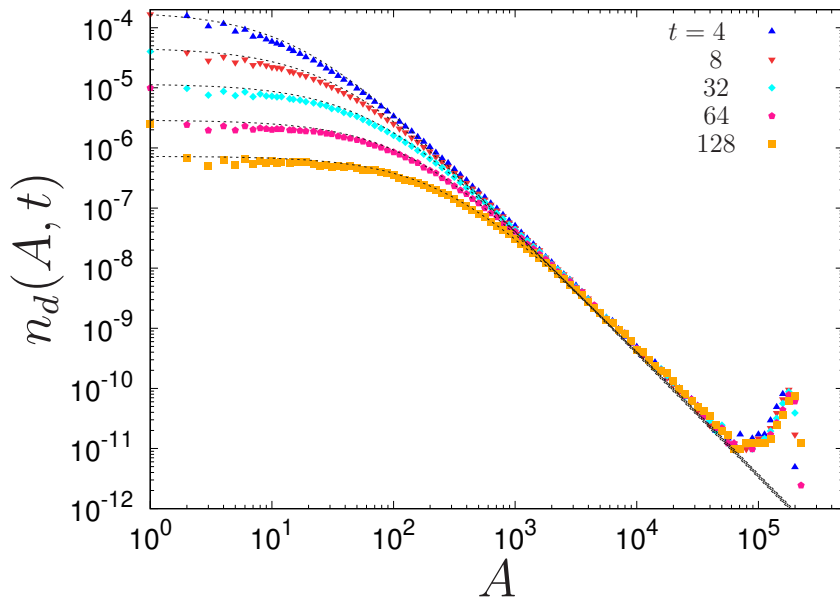
Figure 2.7: Evolution of the domain-size distribution of the $2d$ Ising model quenched from the infinite temperature initial condition to $T = 0$. Same data as in Fig. 2.6, but at larger times. The average was taken over 2×10^3 samples. Dashed lines correspond to equation (2.14), with $\lambda_d = 2.1$, $c_d = 0.025$ and $\tau' = 2.055$.
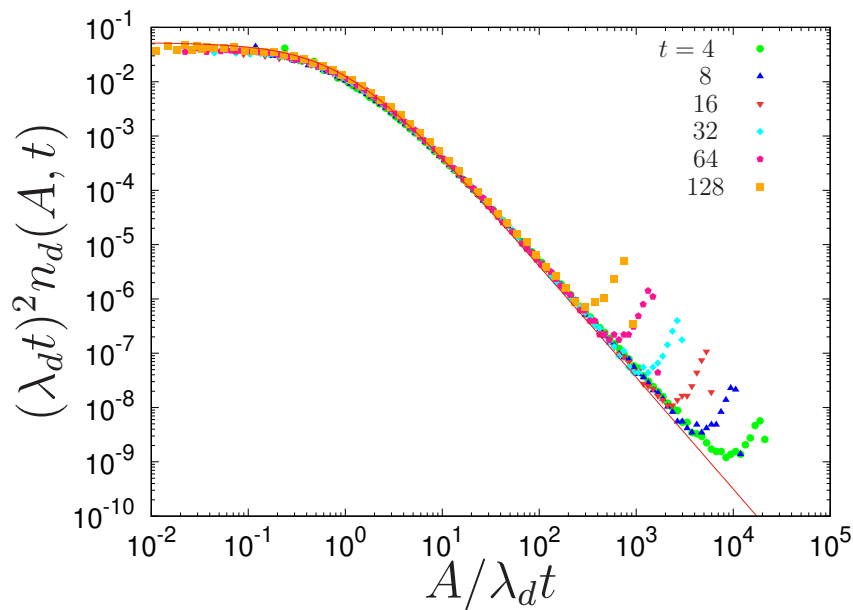
Figure 2.8: Data collapse of the domain-size distribution of the $2d$ Ising model quenched from the infinite temperature initial condition to $T = 0$. Same data as in Figure 2.7. The analytical results of Eq. (2.14) (red line) have a good agreement with the simulation results (points).

20

2.6 Percolation

Percolation is a paradigm of a non-interacting problem, a purely geometrical phenomenon. Broadbent and Hammersley proposed this model in 1957 [48] to model how the random properties of a medium, e.g., the structure or the porosity of the medium, influence the percolation of a fluid. For example, percolation can be defined as the process of a fluid moving slowly through a substance that has tiny holes in it [19]. Another example of percolation is coffee making, in which the water has a preferential direction of flowing through the ground coffee. The fluid (water) percolates when it spreads from one side of the structure to the other (in this case, the ground coffee), and percolation in networks, which considers the propagation of activities through connected space. Though there are many variants of the percolation problem, in this section, only site percolation is addressed.

In general terms, site percolation is defined by randomly occupying a lattice site with probability p and leaving it empty with probability $(1 - p)$. Here, clusters are groups of neighboring occupied sites [19]. Examples of clusters in the square lattice are shown in Figure 2.9. In an infinite system, if the occupation probability is greater than the percolation threshold, $p > p_c$, the probability $P(p)$ that a cluster extends from one side of the system to the other is 1 (Figure 2.9c), while for $p < p_c$, this probability is 0 (Figure 2.9a). Thus, in the limit $L \to \infty$ at the percolation threshold p_c a phase transition occurs – a spanning or giant domain emerges (Figure 2.9b). Notice the highlighted cluster in Figure 2.9b – a cluster connecting two opposite borders of the system is a percolating cluster that spans (free boundary conditions) or wraps around the system (periodic boundary conditions). This threshold p_c depends on the lattice geometry and on its dimension d. For the square lattice, $p_c \simeq 0.59$, while for the triangular lattice, $p_c = 0.5$.

(a) $p < p_c$ (b) $p \simeq p_c$ (c) $p > p_c$
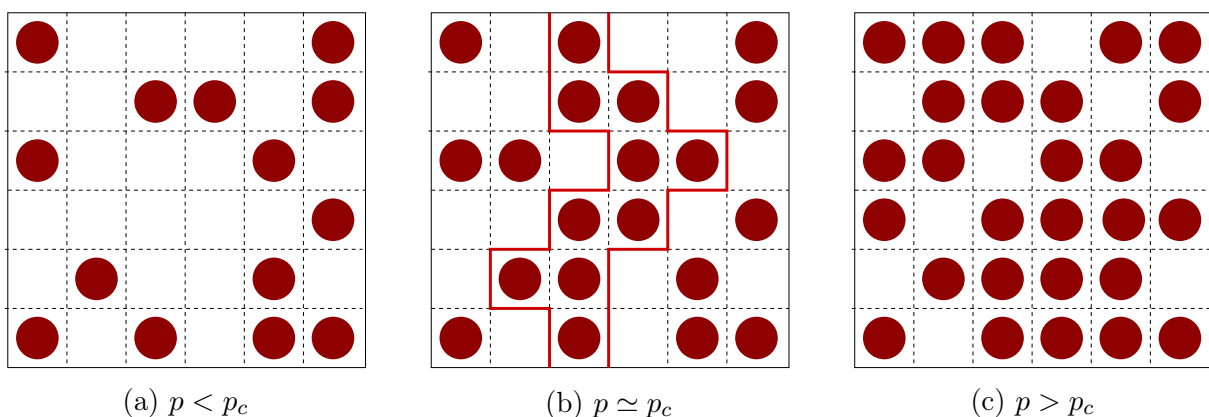
Figure 2.9: Examples of random site percolation for various values of occupation probability p on a 6×6 square lattice with free boundary conditions. Occupied sites are marked by a red circle, while unoccupied sites are left empty. Neighbouring occupied sites form clusters. The corresponding occupation probability p is indicated below each configuration. Notice that there is a cluster spanning (perimeter highlighted in red) from the top to the bottom at (b).

Around the critical point p_c the distributions of cluster sizes, hull enclosed areas, perimeter lengths, etc. have a scaling behavior [19], i.e., there is a single relevant scale that diverges as $\xi \sim |p - p_c|^{-\nu}$, where ν is the associated critical exponent. Near the percolation threshold, ξ is limited in finite systems. Far from the critical region, $\xi < L$ and it behaves as if the system is infinite. The correlation length corresponds to the average radius of a typical percolation cluster, contributing to the mean cluster size and similar properties. The critical behavior of other quantities of interest are controlled by ξ, that acts as a characteristic length.

The cluster size distribution, $n(A)$, follows a power-law at the critical point [19],

$$n(A) \sim A^{-\tau}, \tag{2.17}$$

where τ the associated critical exponent. Approaching the critical region from below, $p \lesssim p_c$, large clusters are exponentially rare, and the cluster size distribution is

$$n(A) \sim A^{-\tau} \exp(-A/A_c), \tag{2.18}$$

where A_c acts as a cutoff on the cluster sizes. It is related to the correlation length, $A_c \sim \xi^{d_f}$, where d_f is the fractal dimension. The exponents d_f and ν have the relation $\sigma = 1/(\nu d_f)$, therefore the cutoff can be written as

$$A_c \sim |p - p_c|^{-1/\sigma}, \tag{2.19}$$

where σ is associated with the extension of the cluster size distribution power-law tail. From the scaling relations, several critical exponents are related and may be written in terms of the other exponents. For example, the fractal dimension d_f can be expressed in terms of the Fisher exponent τ, $d_f = d/(\tau - 1)$, where d is the dimensionality of the lattice [49]. For $2d$ percolation some of the critical exponents are known, $\tau = 187/91$, $d_f = 91/48$, $\nu = 4/3$, and $1/\sigma = 91/36$ [19].

2.7 Critical percolation and coarsening

Even though percolation is a non-interacting problem, in recent years several papers [12, 13, 15, 16, 18, 28–30, 50–52] have shown that it has an important role in the coarsening dynamics of magnetic systems. As shown in Section 2.5, the initial distribution for the infinite temperature does not have large domain sizes ($t = 0$, Figure 2.6). After the quench, very early in the evolution, at a time t_{p_1}, the distribution of domain sizes approaches the expected form at critical percolation, and a percolating cluster is formed for the first time [12, 13]. Other recent works have shown [17, 28, 29] that, despite a percolating cluster first appearing in the early dynamics at a time t_{p_1}, only at a longer timescale t_p a percolating cluster becomes stable.

If the approach to a percolative state occurs in the early regime, how does it happen if the occupation probability is below p_c? The initial state at an infinite temperature in a square lattice with spins pointing up or down with probability $1/2$ corresponds to a percolation problem with an occupation probability $p = 0.5$, below the percolation threshold $p_c \simeq 0.59$. Hence, the formation of a percolating cluster is an effect of the coarsening dynamics and not of the occupation probability p. Indeed, the first percolating cluster is formed when the magnetization is still close to zero, meaning $p \simeq 0.5$.

The approach to a percolative state can be understood by looking at the typical domain scale, $R(t)$ [13]. When the typical domain size is much smaller than the lattice spacing a_0, $R(t) \ll a_0$, the system has a disordered configuration. As $R(t)$ increases, $a_0 \ll R(t) \ll L$, one approaches the continuum percolation, for which $p_c = 1/2$ in $2d$ [53]. Therefore, instead of increasing p, the dynamics self-tunes to a critical percolation state as the correlation between spins increases.

Turning to the final evolution of the $2d$ Ising model quenched to zero temperature, studies of an anomalous scaling for the equilibration time have shown that the ground state is not always reached and the system may remain frozen in a striped state [50–52]. In one dimension, the ground state is always reached, but in two dimensions, there is a non-zero probability that the system freezes into a stripe configuration. Spirin *et al* [51, 52] have found that in two dimensions, the ground state is reached with an approximated probability of 0.6 and a state with two horizontal or vertical stripes with an approximated probability of 0.3, while configurations with more stripes or diagonal ones are reached with lower probabilities. Later, the probabilities of occurrence of such stripe states were shown to correspond to the crossing probabilities in critical percolation for periodic and free boundary conditions [15, 16].

The frozen stripes occur because, at zero temperature, a straight domain wall is a stable configuration. Therefore, at zero temperature, a percolating domain crossing the system horizontally or vertically will eventually coarsen into a frozen striped state. The most common stripe configuration is one with two stripes, typically with both stripes of the same width [51, 52]. States with more than two parallel stripes are extremely rare (Figure 2.10f), and contain alternating stripes whose width is at least two sites [51, 52]. Such a minimum width is necessary to have a stable stripe, otherwise, the stripe will collapse under the dynamics. Conversely, a diagonal stripe has a low but nonzero probability and is extremely long lived ($t_{eq} \sim L^3$), eventually reaching the ground state in a much longer timescale [51] (Figure 2.10e). On the other hand, a percolating domain crossing the system in a cross configuration will grow into the ground state in a time $t_{eq} \sim L^2$. At finite temperature, striped states also exist but are not a stable configuration. The metastable stripes persist for a finite long time compared to the usual relaxation time scale but will eventually approach the ground state [15].

A spin cluster percolates in a $2d$ system with periodic boundary conditions (a model defined on a torus) if the cluster wraps around the system, i.e., if there is a path of con-

nected sites belonging to this cluster that winds around at least one of the two directions of the system (horizontally or vertically). A percolating cluster in this system may have the following configurations (Figure 2.10):

- a configuration with at least one cluster wrapping the system along only one direction, either vertically or horizontally. This configuration corresponds to the vertical or horizontal stripes in Figures 2.10a and 2.10b;

- a configuration with an unique cluster wrapping the system in both directions (cross configuration, Figure 2.10c);

- a configuration with at least one cluster wrapping in both directions but that does not self-intersect. This configuration corresponds to the diagonal stripes in Figure 2.10d.
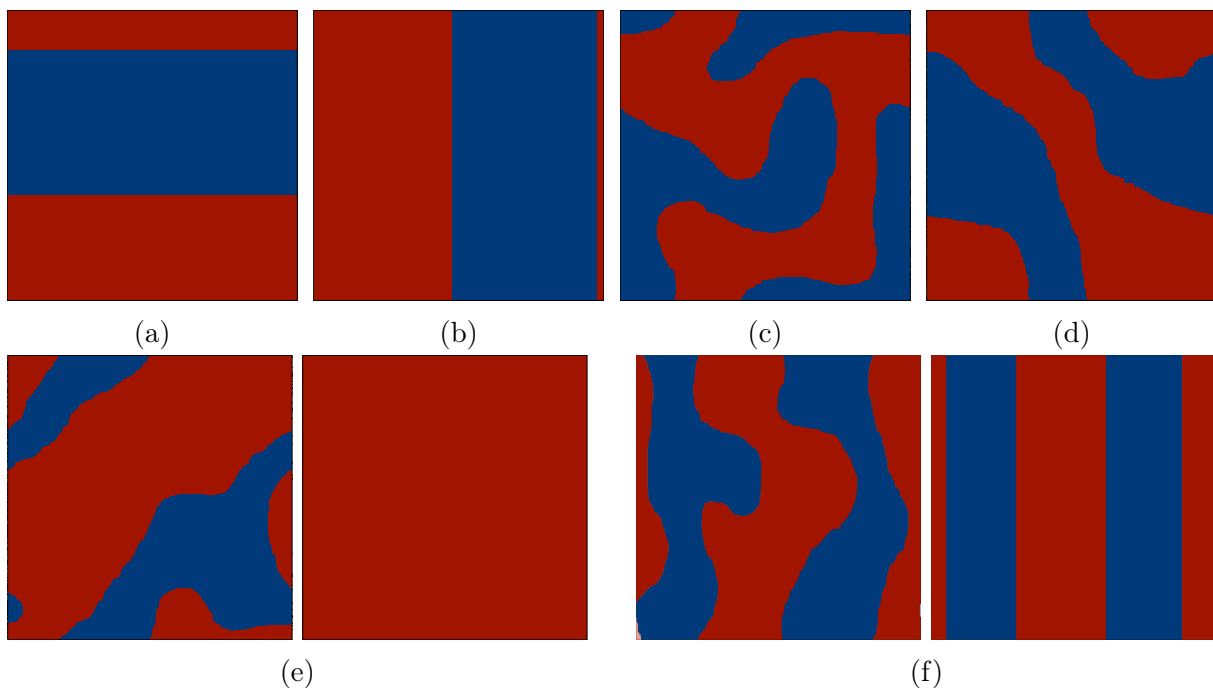
Figure 2.10: Illustration of wrapping cluster configurations on a $2d$ lattice with periodic boundary conditions (on a torus). Panel (a) shows two clusters wrapping the system horizontally, and in (b) vertically. Panel (c) shows a cross configuration, with only one cluster percolating in both directions, while in panel (d) both clusters percolate diagonally. In panels (a), (b) and (d), the presence of the red wrapping cluster implies in the existence of at least one blue percolating cluster next to them. On the other hand, the red percolating cluster in both directions in (c) forbids the existence of other wrapping clusters. The diagonal stripes eventually reach the ground state, shown in panel (e). The evolution of the rare case of more than two parallel stripes is highlighted in panel (f).

The wrapping probabilities for site critical percolation on lattices with periodic boundary conditions were calculated by Pinson [54]. The probability of having a cluster percolating in both directions with a cross topology is $\pi_{hv} \simeq 0.6190$, the probabilities of having a cluster wrapping the system either vertically, π_v, or horizontally, π_h, is

$\pi_{h,v} = \pi_h + \pi_v \simeq 0.3388$, as both configurations are equivalent. The probability of having a cluster wrapping in both directions in a diagonally striped configuration is $\pi_{\text{diag}} \simeq 0.0418$. Similar probabilities were calculated for systems with free boundary conditions [55, 56], where the percolating cluster spans the system from one border to the opposite one instead of wrapping around the system.

Despite a percolating cluster appearing early in the dynamics, only at a longer timescale t_p does the percolating cluster becomes stable, and its wrapping will determine the final evolution. The time t_p is defined [28] as the time the number and type of the wrapping clusters (horizontally, vertically, diagonally, or in both directions) are equal to the amount and kind of stripes in the final state [15, 16, 28]. This time is size dependent, $t_p \sim L^{z_p}$, where z_p depends on the dynamical exponent z and the lattice coordination n_c. Arguments for the necessity of a dynamical measurement of the lattice spacing and the influence of another growing length, different from $R(t) \sim t^{1/2}$ have been put forward in Ref. [29]. This implies in a percolation-related length, $R_p(t) \sim t^{1/z_p}$. Through a more detailed argument, the authors of Ref. [29] argued that the appropriate exponent is $z_p = 2/5$.

Chapter 3

Cluster size heterogeneity: the statics

In this chapter, we review the equilibrium properties of the cluster size heterogeneity, H_{eq}, originally introduced in the context of explosive percolation [20]. This quantity is defined as the number of distinct domain-sizes present in a given system configuration. Therefore, instead of considering the whole domain size distribution, H_{eq} only considers whether a given size is present in a configuration and corresponds to the number of such distinct domain sizes. The success of the cluster size heterogeneity in determining the nature of the explosive percolation transition [20] motivated the detailed study of this quantity and its application to other models, as the site and bond percolation models [21], the Ising [22, 23] and Potts models [24].

The cluster size heterogeneity H_{eq} is measured from each sample distribution, and not from the averaged ones. The cluster size distribution, $n(A)$, is defined as the number of clusters of size A per site. Unlike the averaged domain size distributions shown in the last chapter, a single configuration of a finite system does not have all possible domain sizes present due to space restrictions. For example, consider a square lattice as in Figure 3.1. A cluster is formed by neighbouring squares occupied by the same color. In this example there are four clusters of size 1, two clusters of size 2, a cluster of size 3, a cluster of size 4 and a cluster of size 34. The heterogeneity of this configuration is $H_{\mathrm{eq}} = 5$. The domain size distribution $n(A)$ for this configuration is shown on the right, notice that there are several missing cluster sizes. Therefore, the domain size distribution of a single sample, $n(A)$, is not continuous (Figure 3.2a), but for a sufficient number of samples or an infinite system, the averaged distribution $\langle n(A) \rangle$ is indeed complete (Figure 3.2b).

3.1 Heterogeneity in random site percolation

As discussed in the section 2.6, site percolation is defined by randomly occupying a lattice site with probability p and leaving it empty with probability $1 - p$. Clusters are defined as groups of neighboring occupied sites [19]. When $p = 0$, there are no occupied sites. In the limit $p \to 0$, the clusters are isolated particles, therefore $H_{\mathrm{eq}} = 1$. In the opposite limit $p \to 1$, there is only one giant cluster extending over the system, and
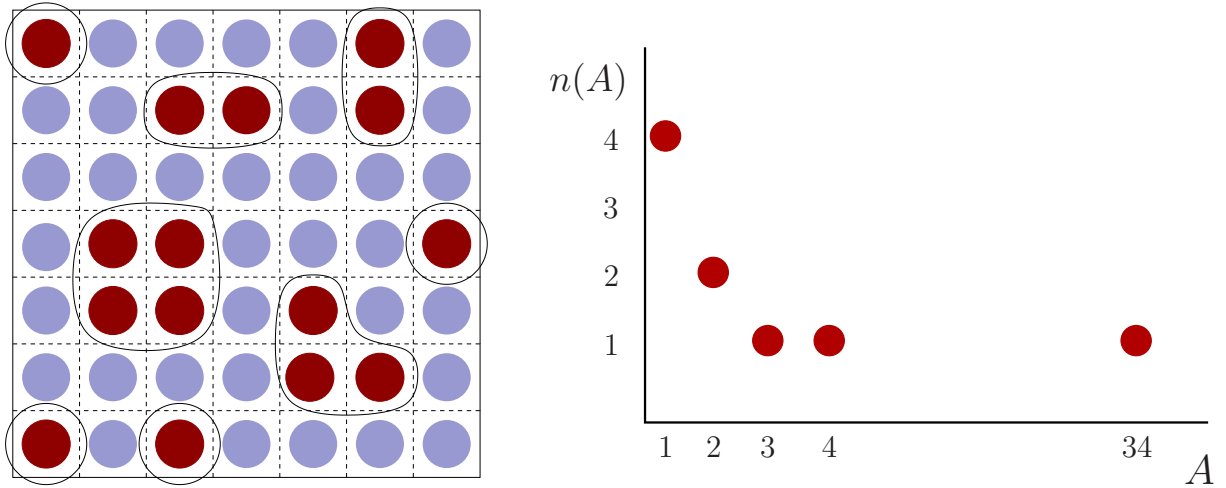
Figure 3.1: Sketch of a 7×7 square lattice with free boundary conditions. Groups of neighbouring squares occupied by the same color form a cluster. There are four clusters of size 1, two clusters of size 2, a cluster of size 3, a cluster of size 4 and a cluster of size 34. Hence, the heterogeneity for this configuration is $H_{\mathrm{eq}} = 5$. Notice that the largest cluster (blue) crosses the system (percolates) in both directions. The domain size distribution $n(A)$ for this configuration is shown on the right.

$H_{\mathrm{eq}} = 1$ once again. In an infinite system, at the percolation threshold p_c a phase transition occurs – a spanning or giant domain emerges. A cluster extending from one side of the system to the other connecting two opposite borders is a percolating cluster that spans (free boundary conditions) or wraps around the system (periodic boundary conditions). For all $p > p_c$, there is a percolating cluster, while for $p < p_c$, there is no such cluster [19].

As p increases from $p = 0$, sites start being populated, clusters nucleate and aggregate. The diversity of cluster sizes increases, the distribution of domain sizes becomes broader and H_{eq} grows. Likewise, decreasing p from $p = 1$, the diversity of cluster sizes also increases, as there is space for smaller clusters apart from the giant cluster and H_{eq} increases. Close to the transition, the distribution of cluster sizes follows a power law, which further increases the likelihood of the clusters having different sizes. Therefore, H_{eq} is expected to have a maximum between these two limits.

The heterogeneity, along with a finite-size scaling (FSS), was first used by Lee *et al.* [20] to clarify the nature of the explosive percolation transition. Still, neither have the scaling properties of H_{eq} been fully understood nor have they been fully explored in the ordinary percolation problems. Noh *et al.* [21] studied the heterogeneity in site and bond percolation models and found that the standard FSS form was not valid. The cluster heterogeneity peak position (p^*, H^*) scaled algebraically with the system size L with apparently universal exponents for the site and bond percolation on the square and triangular lattices. However, the peak position, p^*, did not scale as $L^{-1/\nu}$, as would be expected from the usual FSS hypothesis, where $\nu = 4/3$ is the correlation length exponent in two dimensions.
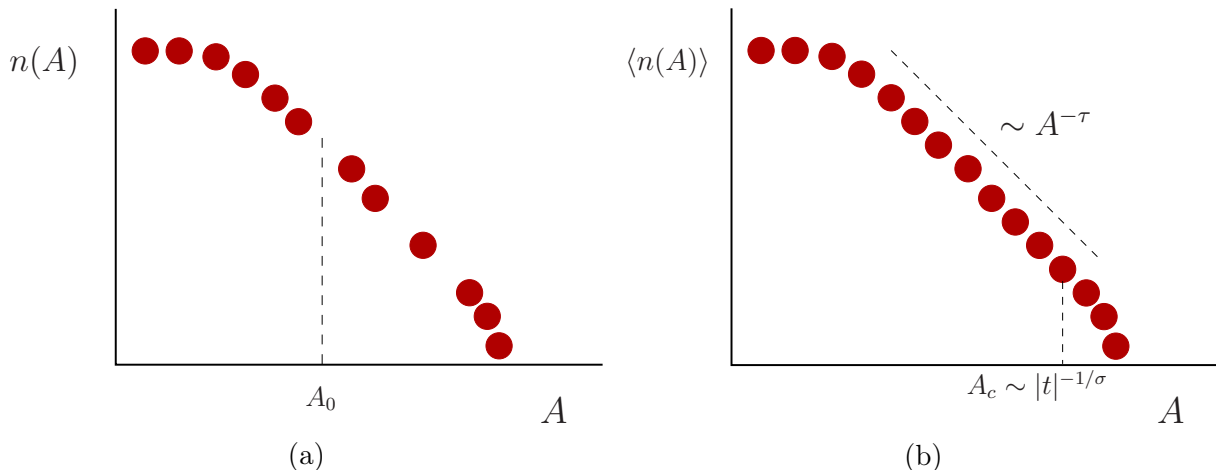
Figure 3.2: Schematic of a cluster size distribution of (a) a single, finite sample, $n(A)$, and (b) of an averaged ensemble, $\langle n(A) \rangle$. Due to finite-size restrictions, a single sample of a finite system does not have all possible cluster sizes present. The smallest missing size, A_0, is indicated by a vertical dashed line. All sizes smaller than A_0 are present, while sizes greater than A_0 may not be present in the system. On the right, the distribution's power-law behavior $\sim A^{-\tau}$ is indicated by a slanted dashed line. The cut-off term, A_c, marks where the distribution deviates from the power-law behavior and is indicated by a vertical dashed line.

Therefore, Not *et al.* [21] derived an appropriate FSS form for H_{eq}

$$H_{\mathrm{eq}}(\epsilon, L) = L^{d/\tau} f(|\epsilon| L^{1/\nu_H}) \,, \tag{3.1}$$

where $\epsilon \equiv p - p_c$, L is the lattice linear size, d is the lattice dimension, τ is the Fisher exponent, ν_H is a new critical exponent, and $f(x)$ is a scaling function, that is constant close to the transition and $\sim x^{-1/\sigma}$ far from the critical region.

The standard FSS considers the region around the critical point where the correlation length ξ differs from its behavior in an infinite system size, $\xi \sim |\epsilon|^{-v}$. In finite systems, the correlation length is constrained by the linear system size L and it is cutoff when $\xi > L$, so the width of the critical region is thus $|\epsilon| \sim L^{-1/\nu}$. However, H_{eq} displayed a different scaling behavior. Instead of scaling with the correlation length exponent ν as would be expected from the usual FSS, $|p - p_c| \sim L^{-1/\nu}$, the critical region scales with the new exponent ν_H, $|p - p_c| \sim L^{-1/\nu_H}$.

To characterize H_{eq} and derive the above FSS expression, Noh *et al.* started by specifying the size of each cluster, following the approach of Jan *et al.* [57] to find the FSS behavior of the r-th largest cluster size at the critical percolation and extending this approach to the off-critical region.

Near the percolation threshold, the cluster size distribution, $n(A)$, for a finite cluster size A is a contribution of a power-law and a cutoff term [19],

$$n(A) \sim A^{-\tau} \exp(-A/A_c) \,, \tag{3.2}$$

where A_c is a characteristic cluster size that acts as a cutoff on the cluster sizes (Fig. 3.2, right). Near the critical region the characteristic cluster size diverges, $A_c \sim |\epsilon|^{-1/\sigma}$, as the correlation length also diverges, $\xi \sim |\epsilon|^{-\nu}$. Far from the critical region, where the correlation length $\xi \ll L$, no finite size effect is observed and the observables are indistinguishable from an infinite system. Thus,

$$A_c \sim \begin{cases} L^{d/(\tau-1)} & \text{for } |\epsilon| \ll L^{-1/\nu} \\ |\epsilon|^{-1/\sigma} & \text{for } |\epsilon| \gg L^{-1/\nu} \end{cases}. \tag{3.3}$$

At the critical percolation point $p = p_c$ the giant cluster is fractal, with a fractal dimension $d_f = 91/48$ in $2d$, and the cluster size distribution follows a power-law $n(A) \sim A^{-\tau}$. The critical exponents also obey scaling relations, and τ can be written in terms of d_f, $\tau = 1 + d/d_f = 187/91$, where $d = 2$ is the dimension of the system.

The dependence of H_{eq} on the system size L may be understood as follows. We define A_0 as the average smallest cluster size not present in a distribution. Therefore, all domain sizes $A < A_0$ are present in the distribution, that is, the expected number of clusters in this region is $L^d n(A < A_0) > 1$, and we say the distribution in this range is dense (Figure 3.2a). Since we are considering a finite system, above A_0 some cluster sizes are not present, $L^d n(A > A_0) < 1$, i.e., there are some holes in the distribution, and this region is said to be sparse. These two regions are separated at $A = A_0$, defined as $L^d n(A_0) \sim 1$. Noh *et al.* [21] argued that the contributions to H_{eq} from these two regions are of the same order.

Thus, to estimate H, we need to understand how both the dense and sparse regions contribute to H_{eq}. At the critical region, from Eq. (3.2), $n(A_0) \sim A_0^{-\tau} \sim L^{-d}$, so A_0 scales as $A_0 \sim L^{d/\tau}$. As there is at least one cluster of each size in the region $A < A_0$, this region contributes to H_{eq} with $A_0 \sim L^{d/\tau}$. The remaining contribution is from the sparse region, $A > A_0$. Ranking those clusters by size from the largest one, the largest cluster lies in the interval $[A_1, \infty)$, with an expected number of clusters of

$$L^d \int_{A_1}^{\infty} n(A) dA = 1. \tag{3.4}$$

The second-largest cluster is in the interval $[A_2, \infty)$, such that the expected number of clusters in this region is 2,

$$L^d \int_{A_2}^{\infty} n(A) dA = 2. \tag{3.5}$$

Likewise for the r-th largest cluster, the expected number of clusters in the range $[A_r, \infty)$ is

$$r \sim N \int_{A_r}^{\infty} n(A) dA = L^d \int_{A_r}^{\infty} A^{-\tau} dA \sim L^d A_r^{1-\tau}, \tag{3.6}$$

where A_r is the average size of the r-th largest cluster at $p = p_c$,

$$A_r \sim \left(\frac{L^d}{r}\right)^{\frac{1}{\tau-1}} . \tag{3.7}$$

As we are ranking the clusters in reverse order, as r increases, $A_r \to A_0$. As $A_0 \sim L^{d/\tau}$, for a very large r_0, $L^{d/\tau} \sim (L^d/r_0)^{\frac{1}{\tau-1}}$. Hence, there are $r_0 \sim L^{d/\tau}$ clusters in the sparse region [21] and indeed both contributions to H_{eq} scale in the same way,

$$H \sim A_0 + r_0 \sim L^{d/\tau} . \tag{3.8}$$

As noted by Jo *et al.* [22], the competing scales here are not the usual system size L and the correlation length ξ, but the competition between A_0 and A_c, which reflect the limitations in cluster sizes due to the finite system size. The characteristic cluster size, that is the cutoff from the power-law distribution, grows as $A_c \sim |\epsilon|^{-1/\sigma}$. When $A_c \gg A_0$, the distribution is a well-developed power law, and the distribution for a single configuration has many holes. Far from the critical region, A_c decreases and the critical region extends up to the point in which $A_c \sim A_0$. By definition, $L^d n(A_0) \sim 1$. So, $L^d A_c^{-\tau} \sim 1$, which leads to the scaling $A_c \sim L^{d/\tau}$. However, A_c diverges at the critical point, $A_c \sim |\epsilon|^{-1/\sigma}$, which allows us to estimate the size of the critical region as $|\epsilon| \sim L^{-d\sigma/\tau} \equiv L^{-1/\nu_H}$, where ν_H is the new exponent defined as $\nu_H = \tau/d\sigma = \nu\tau/(\tau - 1)$.

Hence, the scaling behavior of H_{eq} is given by

$$H(\epsilon, L) \sim \begin{cases} L^{d/\tau} & \text{in the critical region, } |\epsilon| \ll L^{-1/\nu_H} \\ |\epsilon|^{-1/\sigma} & \text{otherwise} \end{cases} , \tag{3.9}$$

which can be summarized by equation (3.1).

The behavior of the equilibrium cluster size heterogeneity as a function of the occupation probability p for the site percolation model on the $2d$ square lattice and several system sizes L is shown in Figure 3.3a [21]. The cluster heterogeneity is expected to be maximal at the transition, and the cluster heterogeneity peak approaches the transition from below the critical point p_c. Due to the finite size, the percolating cluster that is formed at p_c occupies a large part of the system, leaving less space for other clusters, and reducing H_{eq}. Thus, the peak acts as a precursor effect to the transition in finite systems. In the limit $L \to \infty$, the maximal heterogeneity converges to p_c. The data for all different sizes in Figure 3.3a collapse onto a single curve using Eq. (3.1) with $\nu_H = 187/72$ and $\tau = 187/91$, confirming the predicted scaling form (Figure 3.3b). Thus, the FSS is not governed by the correlation length exponent ν, but the new exponent ν_H, in contrast with the standard FSS.
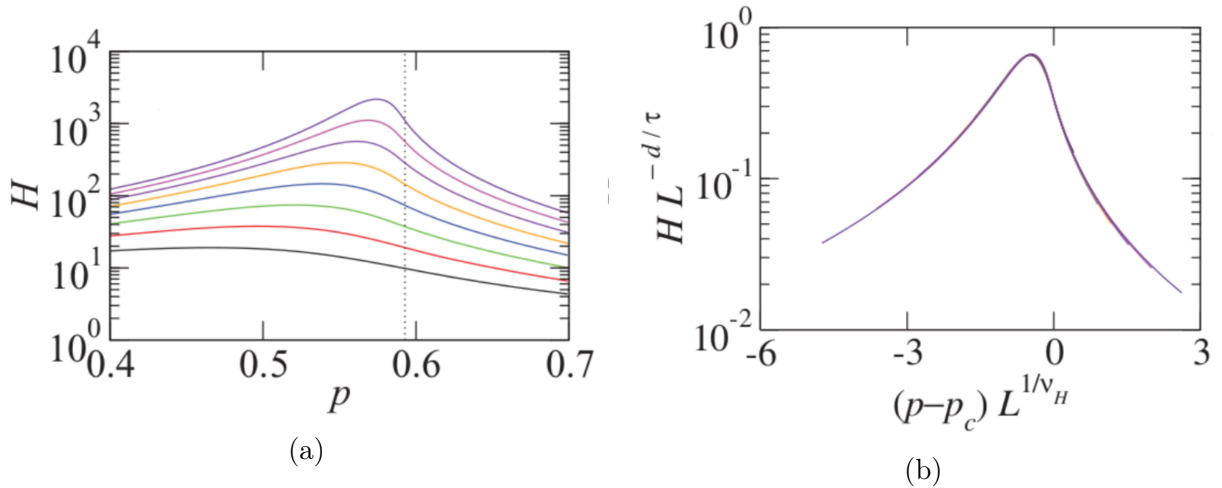
Figure 3.3: Cluster heterogeneity in site percolation on the square lattice as a function of the occupation probability p. In panel (a) the dotted lines represent the critical percolation threshold p_c. Lattice sizes are $L = 2^5, ..., 2^{12}$. As the system size L increases, H_{eq} is higher and the position of the peak approaches p_c. Panel (b) shows the collapsed data using the scaling function of Eq. (3.1). Figure extracted from Noh *et al.* [21].

3.2 Heterogeneity in the Ising model

The heterogeneity in cluster sizes in the two-dimensional Ising model was first investigated by Jo *et al.* [22]. They were able to verify the scaling proposed by Noh *et al.* [21] through Monte Carlo simulations and found numerical values of the fractal dimension d_f and the Fisher exponent τ for the cluster distribution agreeing with the known exact values obtained via conformal field theory. For the considered system sizes, no peak was observed at T_c but only a kink, although they argued the existence of such a peak.

Later, de la Rocha *et al.* [23] presented new results using larger system sizes for both geometric and physical clusters. A geometric cluster considers all nearest neighbor parallel spins belonging to the same domain. In contrast, a physical cluster only takes the fraction of the parallel spins effectively correlated [58, 59]. This distinction is important for interacting spins under thermal noise: the heterogeneity of physical clusters H_p differs from the geometrical one H_g. They have shown that in a square lattice, for equilibrium states, varying the temperature, H_g has two distinct peaks for sufficiently large systems, one small peak close to T_c and another, large and broad peak far above T_c.

The first peak is close to T_c (Figure 3.4a), and grows as expected with $L^{d/\tau}$, while the size of the critical region scales with L^{1/ν_H}. The value of τ and ν_H used in the collapse (Figure 3.5a) are $\tau \simeq 2.016(4)$ and $\nu_H \simeq 1.984$, very close to the exponents for the geometric domains in the Ising model, $\tau = 379/187 \simeq 2.027$ and $\nu_H = 379/192 \simeq 1.974$.

The second peak is much broader than the first one (Figure 3.4b). In the large temperature limit, $T \to \infty$, due to the entropic contribution of uncorrelated spins, as discussed in [22], H_g is a slowly increasing function of L, $H_g(T \to \infty) \sim \log L$, which are depicted as horizontal lines in Figure 3.4b. This asymptotic state can be measured on a random

configuration with, on average, half the spins up and the other half down, and this state is approached as $H_g(T) - H_g(T \to \infty) \sim T^{-1}$.

This second peak is harder to collapse (Figure 3.5b). Due to the excess heterogeneity at high temperatures, this peak does not collapse well with the exponents used in the first peak. Still, a satisfactory collapse was obtained with $\tau \simeq 2.048$ and $\nu \simeq 1.25$, values closer to the exponents for the random site percolation, $\tau_{\text{perc}} = 187/91$ and $\nu = 4/3$ (thus, $\nu_H = 187/72$).

In $2d$, both the thermal and percolative transitions for the geometric clusters happen at the critical temperature T_c in the thermodynamic limit. However, for finite systems, these transitions have not yet merged. As the system sizes increase, both peaks move towards T_c, indicating that the exponents obtained collapsing both peaks should converge. The authors of Ref. [23] argue that in the thermodynamical limit these exponents will converge to the ones of the Ising model.
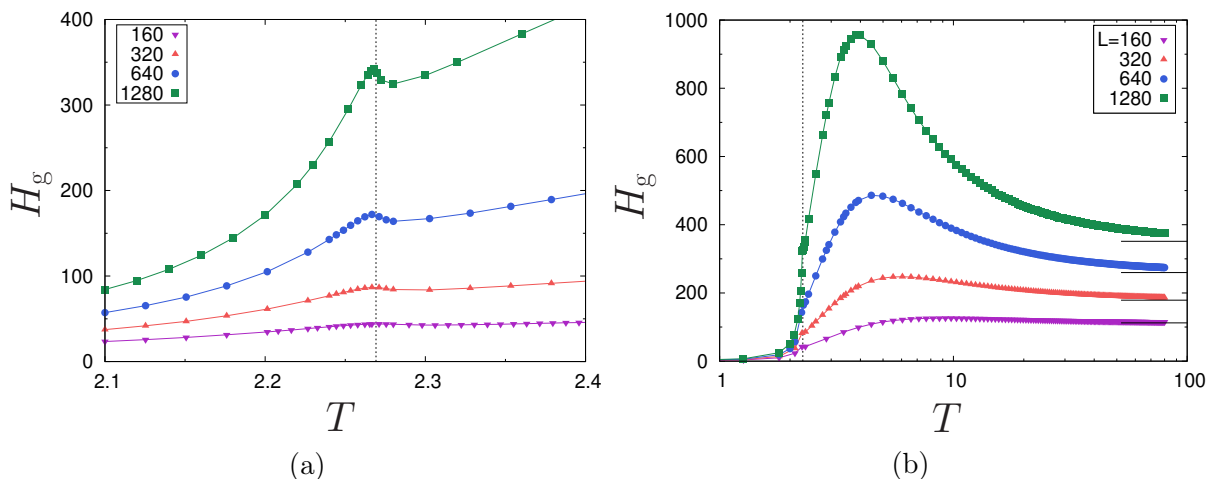
Figure 3.4: Cluster size heterogeneity H_{eq} for the $2d$ Ising model in equilibrium as a function of the temperature for several system sizes. The vertical dotted line locates the critical temperature $T_c = 2/\ln(1 + \sqrt{2})$. The horizontal lines indicate the asymptotic behavior, $H_g(T \to \infty) \sim \log L$. Note the different scale and temperature ranges in (a) and (b). Figures extracted from de la Rocha $et\ al.$ [23].

De la Rocha $et\ al.$ [23] also analyzed the heterogeneity of the physical clusters, which considers only the effectively correlated spins from the geometrical domains. The physical clusters are also referred as Coniglio-Klein [59] or Fortuin-Kasteleyn [58] in the literature. To obtain these domains, starting from a geometric cluster, for every pair of parallel spins, a bond between them is created with a temperature-dependent probability $p = 1 - e^{-2\beta}$. The parallel spins connected by these bonds form the physical cluster. In Figure 3.6 we highlight the difference between the geometrical and physical clusters through two snapshots of the geometrical and physical clusters of the $2d$ Ising model evolving from an initial disordered state $(T \to \infty)$ to $T_f = T_c$. Sites with $+1$ and -1 spins are represented by green and white sites, respectively. The largest clusters are highlighted in different colors, red for spin $+1$ clusters and blue for spin -1 clusters. Notice the difference between both configurations – the navy geometrical cluster is wrapping the system vertically, while the
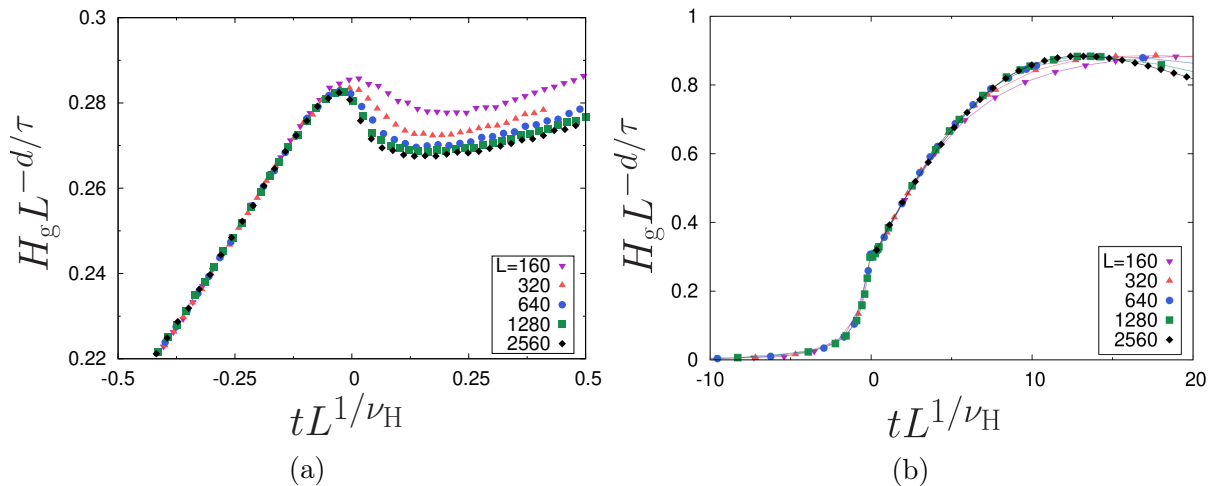
Figure 3.5: Collapsed data for the cluster size heterogeneity H_{eq} from Figure 3.4. In panel (a) the exponents τ and ν_H used to collapse the peak close to T_c are close to the ones of the geometrical domains in the Ising model, while in panel (b) the exponents used to collapse the second bigger peak are closer to the exponents for the random site percolation. As the system size L increases, these values are expected to converge to the ones of the geometrical domains in the Ising model. Figures extracted from de la Rocha et $al.$ [23].

corresponding physical cluster is divided into many others; thus, the largest cluster with $m = -1$ is much smaller. Even though the percolative and the thermal transitions occur at the same temperature for both types of domains, only the physical clusters encode the proper critical exponents, i.e., the percolative and thermal transitions are in the same universality class. Thus, the geometrical fluctuations correspond to the thermal ones, reflecting on the behavior of H_p.

Measurements for H_p for equilibrium states as a function of the temperature are shown in Figure 3.7. Different from the case of the geometrical clusters, H_p presents a clear peak near T_c even for the smaller sizes, which grows closer to the critical temperature as the system size increases. Its behavior at large temperatures is also different from the geometrical clusters, as the spins become uncorrelated as the temperature increases. Indeed, when $T \to \infty$, all spins are effectively uncorrelated and form clusters of unit size, resulting in $H_p(T \to \infty) \to 1$. The proposed scaling form also collapses very well the data for the physical clusters (Figure 3.8). The collapse used the Ising thermal exponents, $\nu = 1$, $\tau_p = 31/15$, and $\nu_H = 31/16$.

The measurements of the heterogeneity in the Ising model show that H_g is very sensitive to the thermodynamical transition, even though the geometrical domains do not encode the proper critical properties. This suggests that H_g may be used to obtain a preliminary estimate for the thermal transition. Moreover, by resolving the transition into two peaks, it may help disentangle the percolative effects from the thermal ones. Exploring this dissociation when the system is driven out-of-equilibrium is the subject of chapter 5.

(a)   (b)
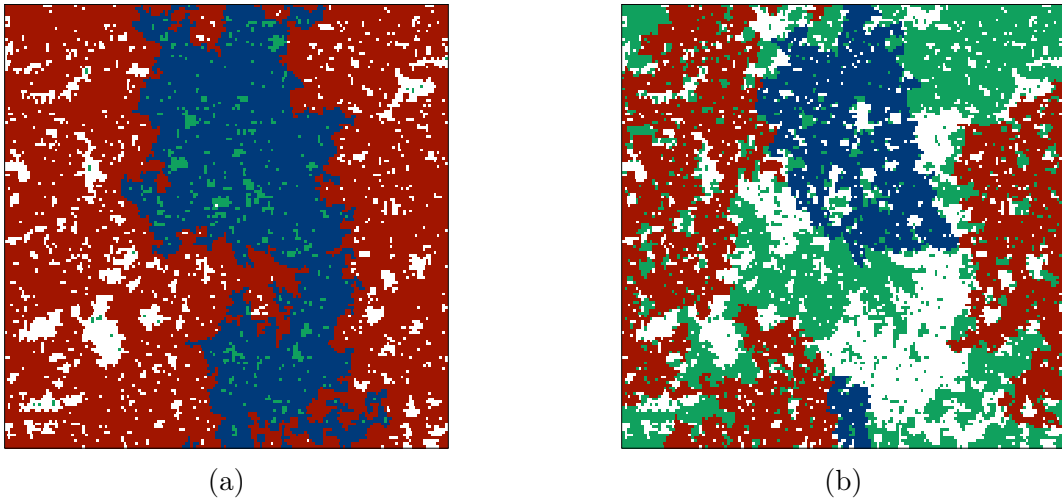
Figure 3.6: Snapshots of geometrical and physical clusters of the $2d$ square lattice Ising model with linear size $L = 160$ and periodic boundary conditions evolving from an initial disordered state to $T_f = T_c$. Green and white sites represent $+1$ and -1 spins, respectively. The largest clusters are highlighted in different colors, red for spin $+1$ clusters and blue for spin -1 clusters. Both snapshots are for the same system evolution (a) illustrating the geometrical domains, and (b) the physical ones. Notice the difference between both configurations – the blue geometrical cluster is wrapping the system vertically, while the corresponding physical cluster is broken into many others, thus the largest blue (red) cluster is much smaller. The snapshots were taken at 10^4 MCS.
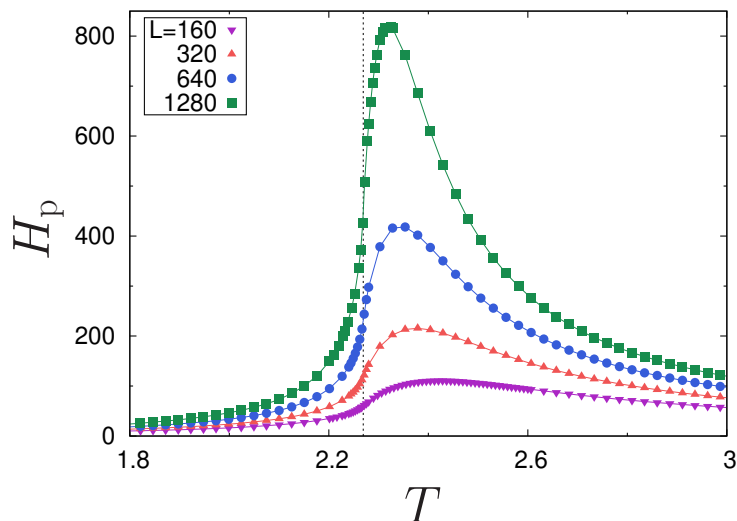
Figure 3.7: Cluster size heterogeneity H_p of the physical domains for the $2d$ Ising model in equilibrium as a function of the temperature for several system sizes. The vertical dotted line locates the critical temperature $T_c = 2/\ln(1 + \sqrt{2})$. In this case, there is a single pronounced peak close to T_c. Figure extracted from de la Rocha *et al.* [23].
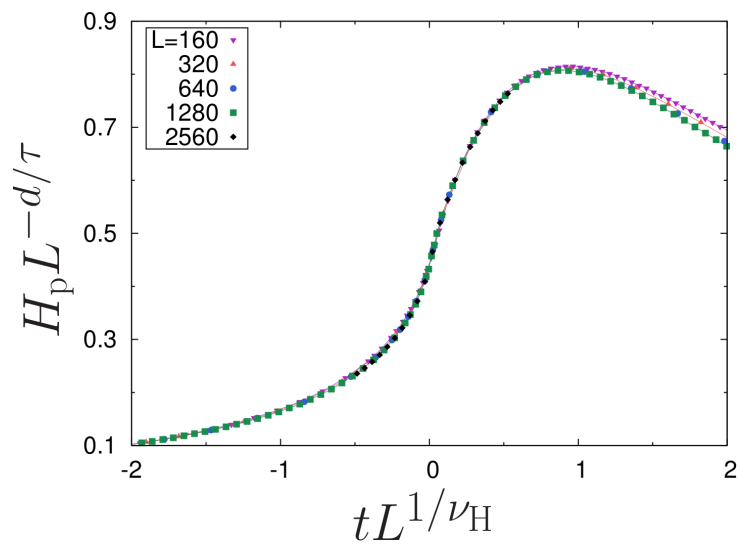
Figure 3.8: Collapsed data for the cluster size heterogeneity H_p of physical domains from Figure 3.7. There is an excellent collapse with the critical exponents of the physical clusters in the Ising model $\tau_p = 31/15$, $\nu = 1$ and $\nu_H = 31/16$. Figure extracted from de la Rocha *et al.* [23].

Chapter 4

Cluster size heterogeneity: a mean-field approach

In the previous chapter, we have reviewed the equilibrium cluster size heterogeneity in random site percolation and the Ising model. In this chapter, we investigate how the exponent of a power-law distribution changes the behavior of the heterogeneity in a finite system. Motivated by the results of the equilibrium cluster size heterogeneity in the $2d$ Ising model [23] and the recent results of the dynamical cluster size heterogeneity [25], that will be shown in chapter 5, a natural question that one may ask is what value of the exponent τ maximizes the heterogeneity and how do we compare it with the known values for different models, specifically, the Ising model?

Throughout this chapter, we will study a general model of independent and identically distributed integer random variables, i.e., a general simple model that generates independent domains whose only constraint is to fill the system area S. This is a sort of a mean-field approach, as there are no correlations between the domains. The only constraint imposed on the system is on the set of chosen domains, although imposing a global constraint somewhat reintroduces correlations. In the cases shown so far, e.g., geometric domains in the Ising model, the equilibrium dynamics imposes correlations between them, which is different from the model considered in this chapter. We focus on the evaluation of the heterogeneity for a general case and algebraic distributions. Therefore, this chapter is somewhat different from the previous one since it does not directly address the Ising model, nor percolation, but has a mean-field approach to investigate H.

4.1 General model with independent and identically distributed random variables

We consider a model where independent and identically distributed random variables $\{s_d\}$ are extracted from a generic probability distribution $p(s)$. In the analogy with domains, the variables s_d represent the size, i.e., the volume, of the d-th domain. The prob-

ability distribution $p(s)$ is denoted as *bare* distribution, since the effective (or *dressed*) distribution of the s_d will be shaped by the presence of the global constraint

$$\sum_{d=1}^{D} s_d = S \, , \tag{4.1}$$

where S is a parameter playing the role of the system size, and D stands for the fluctuating number of domains that, according to the particular extraction of the $\{s_d\}$, is needed to fulfill Eq. (4.1). As it is, this approach is rather general. However, it can be adapted to describe specific models (e.g., random percolation or the Ising model) by using an appropriate domain size distribution $p(s)$.

The probability of a configuration $\mathcal{C} \equiv [\{s_1, \ldots, s_D\}; D]$ is given by

$$p_S(\{s_1, \ldots, s_D\}; D) = \frac{1}{Z_S} \prod_{d=1}^{D} p(s_d) \delta_{\sum_{d=1}^{D} s_d, S} \, , \tag{4.2}$$

where the constraint given by Eq. (4.1) is imposed by the Kronecker delta. The quantity Z_S plays the role of a partition function

$$Z_S = \sum_{D=1}^{\infty} Z_S(D) \, , \tag{4.3}$$

where $Z_S(D)$ is the partial partition function

$$Z_S(D) \equiv \sum_{s_1=1}^{S} \sum_{s_2=1}^{S} \cdots \sum_{s_D=1}^{S} \prod_{d=1}^{D} p(s_d) \delta_{\sum_{d=1}^{D} s_d, S} \, , \tag{4.4}$$

corresponding to an ensemble with a fixed number of domains D, while Z_S corresponds to an ensemble where D can fluctuate. From this simple observation, one obtains the probability of having a number D of domains,

$$p_S(D) = \frac{Z_S(D)}{Z_S} \, , \tag{4.5}$$

and the average number of domains,

$$\langle D \rangle_S = \sum_{D=1}^{S} D p_S(D) \, . \tag{4.6}$$

As already mentioned, the *dressed* probability distribution of finding a domain of size s is different from the *bare* one due to the constraint on the total size, Eq. (4.1). It can

be obtained from Eq. (4.2) by marginalization as

$$p_S(s) = D \sum_{s_1=1}^{S} \sum_{s_2=1}^{S} \cdots \sum_{s_{D-1}=1}^{S} p_S(\{s_1, \ldots, s_{D-1}, s\}; D) \tag{4.7}$$

$$= \frac{p(s)}{\sum_{D=1}^{\infty} D Z_S(D)} \sum_{D=1}^{\infty} D Z_{S-s}(D-1), \tag{4.8}$$

where the extra factor D appears because it does not matter which domain takes the specific size s.

Therefore, the average domain size is

$$\langle s \rangle_S = \sum_{s=1}^{S} s\, p_S(s). \tag{4.9}$$

Similarly, the average heterogeneity is

$$\langle H \rangle_S = \sum_{H=1}^{S} H\, p_S(H), \tag{4.10}$$

where $p_S(H)$ is the probability of observing a certain value of H for a given *bare* probability function. In the next section, we will introduce an alternative approach for evaluating $\langle H \rangle_S$, so the demonstration of $p_S(H)$ will be omitted here. For the derivation of $p_S(H)$, please refer to Ref. [26] (in preparation).

4.2 Solution for a general bare distribution

In principle, all probabilities can be computed with the expressions given in the last section. However, this approach becomes rapidly impracticable already for moderate values of S without a clever approach to handling those equations. Let us consider, for example, the computation of $p_S(s)$ or $p_S(D)$, Eqs. (4.8) and (4.5), which involve the functions Z_S defined in Eq. (4.3). The sums in Z_S contain, *a priori*, S^S terms, which cannot be enumerated by a fast computer even for relatively small values of S. However, due to the constraint over the area imposed by the δ function in Eq. (4.4), only a small fraction of those terms does not vanish. This suggests that the algorithmic complexity involved in the determination of Z_S can be softened by resorting to a clever summation scheme. The following recursive relation

$$Z_S(D) = \sum_{s=1}^{\infty} p(s) Z_{S-s}(D-1) \tag{4.11}$$

allows us to express $Z_S(D)$ in terms of $Z_S(D-1)$, that can be easily proved upon writing $\delta_{\sum_{d=1}^{D} s_d, S} = \delta_{\sum_{d=2}^{D} s_d, S-s_1}$ in Eq. (4.4). It was shown in Ref. [60] that using the above

recurrence relation the algorithmic complexity is lowered to polynomial.

With this convenient recursive method, we can obtain an exact solution of the model up to relatively large values of S. Let us first look at the *dressed* probability distribution, $p_S(s)$. This quantity is plotted in Figure 4.1 using an algebraic bare probability, $p(s) \sim s^{-\tau}$, for different values of τ. We compare the exact dressed probability distribution obtained from Eq. (4.8) with the results of numerical simulations where, after extracting the random variables s_d, only the configurations respecting the constraint (4.1) are kept. One sees a perfect agreement between the exact $p_S(s)$ and the numerical simulations. As expected, the dressed and the bare distributions coincide, $p_S(s) \simeq p(s)$, up to values $s \lesssim S$, beyond which $p_S(s)$ gets strongly depressed. This suggests that the bare $p(s)$ can be used in place of the dressed distribution $p_S(s)$ as an approximation to evaluate the different quantities of interest, thus simplifying the calculations.
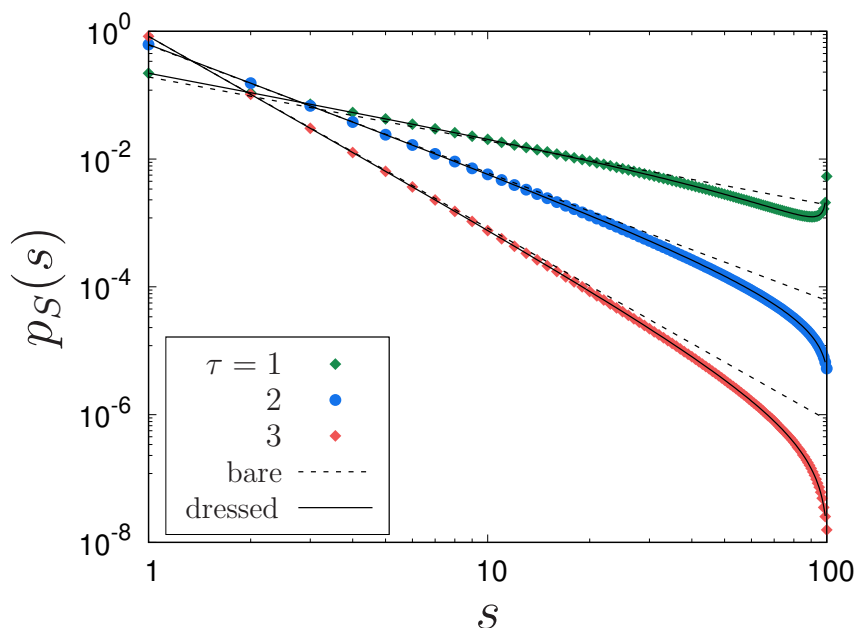
Figure 4.1: The exact dressed probability distribution $p_S(s)$ (solid lines) obtained from Eq. (4.8) is compared with numerical simulations (points) using a bare probability distribution $p(s) \sim s^{-\tau}$ (dashed lines) and different values of τ for a system size $S = 100$. Deviations only become large when s is close to S.

To compute the heterogeneity, instead of turning to Eq. (4.10), which requires the evaluation of $p_S(H)$ (and its huge number of terms in the sums), we make use of a different approach, which directly provides the value of $\langle H \rangle_S$, without resorting to $p_S(H)$.

As defined in the previous chapter, the contributions for the heterogeneity come from two regions of the cluster size distribution, $s \leq s^*$ and $s > s^*$, namely the dense and sparse regions, where s^* separates both regions and is defined by

$$\langle D \rangle_S \, p_S(s^*) = 1 \,. \tag{4.12}$$

From this definition, as discussed previously, there is at least one domain of each size $s \leq s^*$, and this region contributes with s^* to the heterogeneity. For $s > s^*$, differently, a

domain of size s is found with probability $p_S(s)$. Thus, combining both contributions, we obtain an expression for the average heterogeneity

$$\langle H \rangle_S \simeq s^* + \langle D \rangle_S \sum_{s=s^*}^{S} p_S(s). \tag{4.13}$$

It has been shown in Ref. [25] that this is an excellent approximation for $\langle H \rangle_S$, agreeing very well with the results from numerical simulations. Thus, with Eq. (4.13) the evaluation of $\langle H \rangle_S$ only depends on $\langle D \rangle_S$ and $p_S(s)$, which can be computed with the recurrency method discussed above.

4.3 Solution for an algebraic bare distribution

One of the important applications of cluster size heterogeneity is exploring spatial models critical properties, as previously discussed. Thus, it is particularly relevant to consider the case of an algebraic bare distribution

$$p(s) = \begin{cases} N^{-1}(\tau, S)s^{-\tau} & ; \quad \text{for} \quad 1 \leq s \leq S \\ 0 & ; \quad \text{for} \quad s > S, \end{cases} \tag{4.14}$$

where the normalization is a generalized harmonic number and can be written in terms of the Riemann and Hurwitz zeta functions, $\zeta(x)$ and $\zeta(x, y)$, respectively:

$$\begin{aligned} N(\tau, S) &= \sum_{s=1}^{S} p(s) = \sum_{s=1}^{\infty} s^{-\tau} - \sum_{s=S+1}^{\infty} s^{-\tau} \\ &= \zeta(\tau) - \sum_{s=0}^{\infty} (s + S + 1)^{-\tau} \\ &= \zeta(\tau) - \zeta(\tau, S + 1). \end{aligned} \tag{4.15}$$

The exact value of the average number of domains, $\langle D \rangle_S$, can be computed from Eqs. (4.5) and (4.6), and is shown in Figure 4.2 against S for three values of τ. To compute the approximate expression for $\langle D \rangle_S$, we use the approximation $p_S(s) \simeq p(s)$, so Eq. (4.9) can be written as

$$\begin{aligned} \langle s \rangle_S &\simeq \sum_{s=1}^{S} s p(s) = \frac{1}{N(\tau, S)} \sum_{s=1}^{S} s^{1-\tau} = \frac{1}{N(\tau, S)} \left(\sum_{s=1}^{\infty} s^{1-\tau} - \sum_{s=S+1}^{\infty} s^{1-\tau} \right) \\ &= \frac{\zeta(\tau - 1) - \zeta(\tau - 1, S + 1)}{N(\tau, S)} = \frac{N(\tau - 1, S)}{N(\tau, S)}, \end{aligned} \tag{4.16}$$

from which the analytical approximation for $\langle D \rangle_S$ is obtained

$$\langle D \rangle_S \simeq \frac{S}{\langle s \rangle_S}. \tag{4.17}$$

Hence, evaluating Eq. (4.17) using Eq. (4.16) and considering the limit for large S, we obtain an approximate expression for the average number of domains. The asymptotic behavior of the normalization $N(\tau, S)$ is obtained through the the Euler-Maclaurin sum formula [61]

$$N(\tau, S) \simeq \zeta(\tau) + \frac{1}{1 - \tau} S^{1-\tau}, \tag{4.18}$$

and

$$N(\tau - 1, S) \simeq \zeta(\tau - 1) + \frac{1}{2 - \tau} S^{2-\tau}, \tag{4.19}$$

which for τ close to 1 reduces to [62]

$$N(1, S) \simeq \ln S + \gamma, \tag{4.20}$$

where $\gamma \simeq 0.577$ is the Euler constant. Thus, for the case $\tau = 1$, we have

$$\langle D \rangle_S = \frac{S\,N(1, S)}{N(0, S)} \simeq \ln S + \gamma \tag{4.21}$$

and for the case $\tau = 2$,

$$\langle D \rangle_S \simeq \frac{\pi^2}{6} \frac{S}{\ln S}, \tag{4.22}$$

where $\zeta(2) \simeq \pi^2/6$. Similarly, considering the large S limit, all cases are summarized below

$$\langle D \rangle_S \simeq \begin{cases} \dfrac{2 - \tau}{1 - \tau} & ; \text{ for } \quad \tau < 1 \\ \ln S & ; \text{ for } \quad \tau = 1 \\ \zeta(\tau)(2 - \tau)S^{\tau-1} & ; \text{ for } \quad 1 < \tau < 2 \\ \dfrac{\zeta(2)S}{\ln S} & ; \text{ for } \quad \tau = 2 \\ \dfrac{\zeta(\tau)}{\zeta(\tau - 1)}S & ; \text{ for } \quad \tau > 2\,. \end{cases} \tag{4.23}$$

The agreement between these results and the exact determination, shown in Figure 4.2, is very good even for $\tau = 1$ where the leading term in the approximation is not a simple power-law.

Using the approximation $p_S(s) \simeq p(s)$ on the definition of s^* from Eq. (4.12), we obtain

$$s^*(S, \tau) \simeq \left(\frac{S}{\gamma + \frac{S^{2-\tau}-1}{2-\tau}} \right)^{1/\tau}, \tag{4.24}$$

where the asymptotic behavior of the Riemann zeta function is approximated by $\zeta(x) \simeq (x - 1)^{-1} + \gamma$. Substituting s^* in Eq. (4.13), we obtain an approximate expression for the
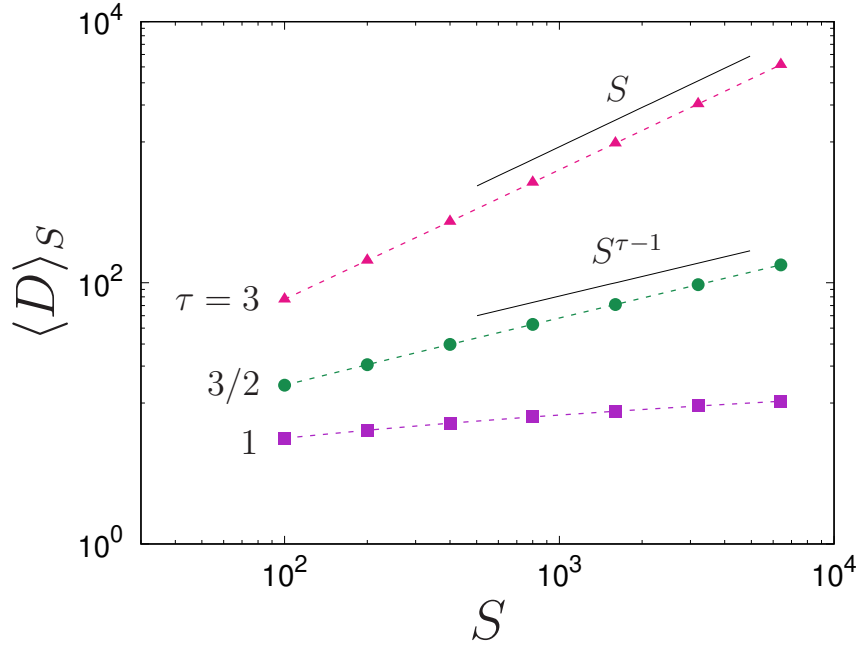
Figure 4.2: Average number of domains as a function of the system size S for different values of τ evaluated through Eq. (4.6). The solid lines indicate the predicted asymptotic behaviour given by Eq. (4.23), while for $\tau = 1$, $\langle D \rangle_S \simeq \ln S$.

average heterogeneity

$$\langle H \rangle_S \simeq s^* + \langle D \rangle_S \sum_{s=s^*}^{S} p(s)$$

$$\simeq \frac{\tau s^* - (s^*)^\tau S^{1-\tau}}{\tau - 1} \, . \tag{4.25}$$

This determination of $\langle H \rangle_S$ is shown in Figure 4.3 for the smallest and largest sizes only and compared with numerical simulations. The agreement between the analytical and numerical results is very good. In particular, both cases present a peak at $\tau \simeq 2$, which becomes more pronounced as S increases.

As shown for the average number of domains $\langle D \rangle_S$, for large S the leading contribution of Eq. (4.25) is

$$\langle H \rangle_S \simeq \begin{cases} \dfrac{2-\tau}{1-\tau} & ; \text{ for } \quad \tau < 1 \\[2mm] \ln S & ; \text{ for } \quad \tau = 1 \\[2mm] \dfrac{\tau(2-\tau)^{1/\tau}}{\tau - 1} S^{1-1/\tau} & ; \text{ for } \quad 1 < \tau < 2 \\[2mm] 2\left(\dfrac{S}{\ln S}\right)^{1/2} & ; \text{ for } \quad \tau = 2 \\[2mm] \dfrac{\tau}{\tau - 1}\left[\dfrac{S}{\gamma + (\tau - 2)^{-1}}\right]^{1/\tau} & ; \text{ for } \quad \tau > 2 \, . \end{cases} \tag{4.26}$$

42
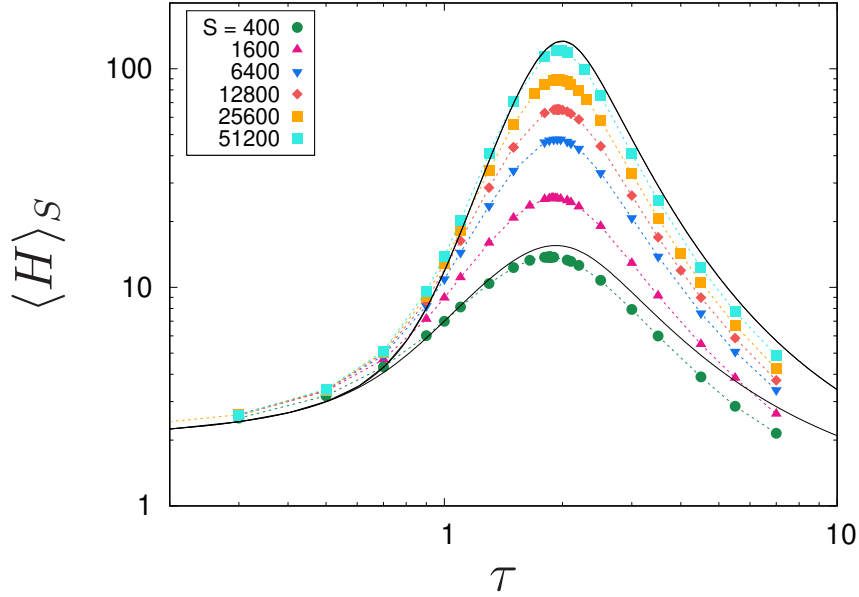
Figure 4.3: Cluster size heterogeneity, $\langle H \rangle_S$ as a function of the exponent τ for different system sizes S obtained through numerical simulations. The results present averages over a large number of samples (10^6 for the smallest size, and 10^4 for the largest). Solid lines are the approximate analytical solution given by Eq. (4.26), whose agreement with the numerical results is very good (shown only for the smallest and largest sizes).

It is possible to analyze how the size dependence of $\langle H \rangle_S$ observed in Figure 4.3 relates to the exponent τ from Eq. (4.26). The hetetogeneity size dependence may be written as $\langle H \rangle_S \sim S^{\alpha(\tau)}$, with

$$\alpha(\tau) \sim \begin{cases} 0 & ; \text{for} \quad \tau < 1 \\ 1 - 1/\tau & ; \text{for} \quad 1 < \tau < 2 \\ 1/\tau & ; \text{for} \quad \tau > 2. \end{cases} \tag{4.27}$$

The exponent $\alpha(\tau)$ evaluated from the above expression is plotted with a dashed line in Figure 4.4 and compared with simulation results. The results were obtained by fixing the value of τ for different system sizes in the simulation data in Figure 4.3 and extrapolating the results through a power-law fit to obtain an estimate of $\alpha(\tau)$.

Thus, from Figure 4.4 it is clear that there is a maximum value of the heterogeneity at $\tau = 2$ for an algebraic bare function, signaled by the abrupt change of behavior at $\tau = 2$. This result can be interpreted with a similar reasoning used in chapter 3 for random site percolation. If one considers a fixed number of domains D, it is intuitive that the steeper the bare power-law distribution (i.e., a larger τ), there is a higher probability of repeatedly extracting small domains than selecting larger domains, hence a smaller H. On the other hand, for a slow decaying function, i.e., a smaller τ, the probability of extracting different sizes is higher, thus a higher H. However, the average number of domains $\langle D \rangle_S$ depends on the (fixed) system size S and varies with τ.

(i) For $\tau > 2$, the average number of domains $\langle D \rangle_S$, Eq. (4.23), does not depend on τ, only on S. Even though $\langle D \rangle_S \sim S$, the heterogeneity depends on the number
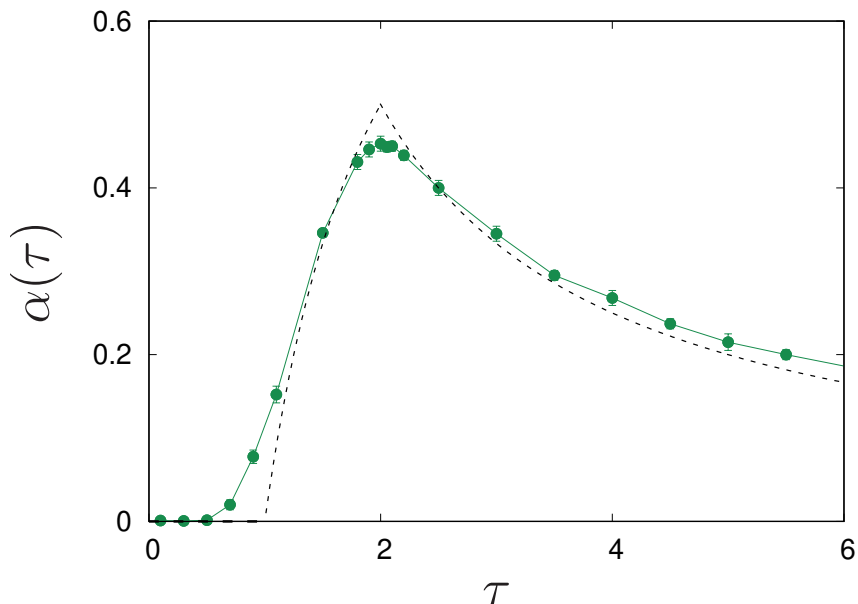
Figure 4.4: Behavior of exponent $\alpha(\tau)$ as a function of τ. Fixating a value of τ in the simulation data in Figure 4.3, we obtain an estimate of $\alpha(\tau)$ through an extrapolation through a power-law fit. The dashed line is the approximate analytical solution in Eq. (4.27).

of *different* sizes in a given configuration. Since the probability of extracting small domains is much higher than selecting larger ones, the size diversity is low; thus, the heterogeneity is small, $\langle H \rangle_S \sim S^{1/\tau}$.

(ii) On the opposite limit, when $\tau \leq 1$, comparing Eqs. (4.23) and (4.26), one sees $\langle D \rangle_S \simeq \langle H \rangle_S$. Therefore, most of the clusters have a distinct size (meaning that $s^*(S, \tau)$ is very small). When $\tau \leq 1$, there is a high probability of extracting a cluster comparable to the system size, thus reducing the effective space available to additional clusters (due to the imposed constraint on the system size), and $\langle H \rangle_S$ is small irrespective of the system size at this range.

(iii) In between those two limits, $1 < \tau < 2$, $\langle D \rangle_S$ still depends on τ. As τ increases from small values, $\langle D \rangle_S$ also increases. However, for a fixed D, increasing τ, decreases H. Thus, there is a competing effect between lowering the diversity of sizes and the average increase of D. The latter effect prevails, so H increases for $1 < \tau \leq 2$ and presents a pronounced maximum at $\tau = 2$.

Interestingly, the maximum heterogeneity is found at $\tau = 2$, which is close to the exponent for geometrical domains in the Ising model, $\tau = 379/187 \simeq 2.027$ [47, 63], for physical clusters, $\tau = 31/15 \simeq 2.067$ [59], and at critical percolation, $\tau = 187/91 \simeq 2.055$ [19]. Another possibility is to consider the distribution of areas inside every hull. Although the number of hulls is precisely the same as the number of geometric domains, as each hull is associated with a single domain [13], they do not need to obey the area constraint and, indeed, their total area is larger than S. Strikingly, their Fisher exponent τ is exactly 2, which corresponds to the exponent that maximizes the heterogeneity in the model

addressed in this chapter. We thus speculate that the fewer constraints upon the domains, the closer their exponent will be to $\tau = 2$.

The cluster size heterogeneity measurements through a sort of mean-field approach show that there is, indeed, an exponent that maximizes the heterogeneity and is very close to the associated exponents for the Ising model. Also, we have seen that the cluster size heterogeneity measurements in the equilibrium Ising model are very sensitive to the thermodynamical transition and that H_g may be used to disentangle the percolative effects from the thermal ones. Exploring this dissociation when the system is driven out-of-equilibrium is the subject of the next chapter.

Chapter 5

Cluster size heterogeneity: the dynamics

The measurement of the cluster size heterogeneity was useful to resolve both the thermal and percolative transitions in the $2d$ Ising model, but there are many questions related to the time evolution of the cluster size heterogeneity. Despite being proposed to study equilibrium configurations, is the cluster size heterogeneity able to provide additional information on out-of equilibrium systems? Does the temporal evolution of the cluster size heterogeneity shed some light on the percolative and thermal effects? Is $H(t)$ useful to study the geometric properties and the coarsening processes? Such questions motivated a preliminary study [64] of the dynamical cluster size heterogeneity in the Potts model with $q = 2, 3$ and different quench protocols.

To address these questions, in this Chapter, we discuss the dynamical properties of the cluster size heterogeneity, $H(t)$, in the $2d$ Ising model. Our main objective here is to explore whether this new observable may be useful, not only to study equilibrium properties of simple models, but their dynamics as well. The results presented in this chapter have been published in Phys. Rev. E [25], which is included in Appendix A.

5.1 Ising dynamics

We study the dynamical heterogeneity in the $2d$ Ising model, whose Hamiltonian is

$$\mathcal{H} = -J \sum_{\langle i,j \rangle} s_i s_j \,, \tag{5.1}$$

with $J > 0$, $s_i = \pm 1$ is the spin at the site i, and the sum is over the pairs of nearest-neighbours sites on an $L \times L$ square lattice with periodic boundary conditions. There are two possible initial states:

(i) an uncorrelated random spin configuration, where each site has the probability $1/2$ to be in the state $s_i = +1$ or $s_i = -1$. This condition corresponds to an equilibrium

46

infinite temperature state;

(ii) a configuration thermalized at the critical temperature T_c, corresponding to a state with infinite range correlations.

To drive the Ising model out of the equilibrium state, we apply a simple protocol consisting of a sudden quench in temperature, shown in Figure 5.1a. We consider two relevant temperature paths: starting at an initial uncorrelated state, corresponding to an infinite initial temperature, instantaneously quench the system to a subcritical temperature, $T_f < T_c$ (Figure 5.1b, path I, $T_0 \to \infty$, $T_f < T_c$). The other interesting initial configuration is to thermalize the system at the critical temperature T_c for an initial configuration with infinite range correlations, then quench it to a subcritical temperature (Figure 5.1b, path II, $T_0 = T_c$, $T_f < T_c$).
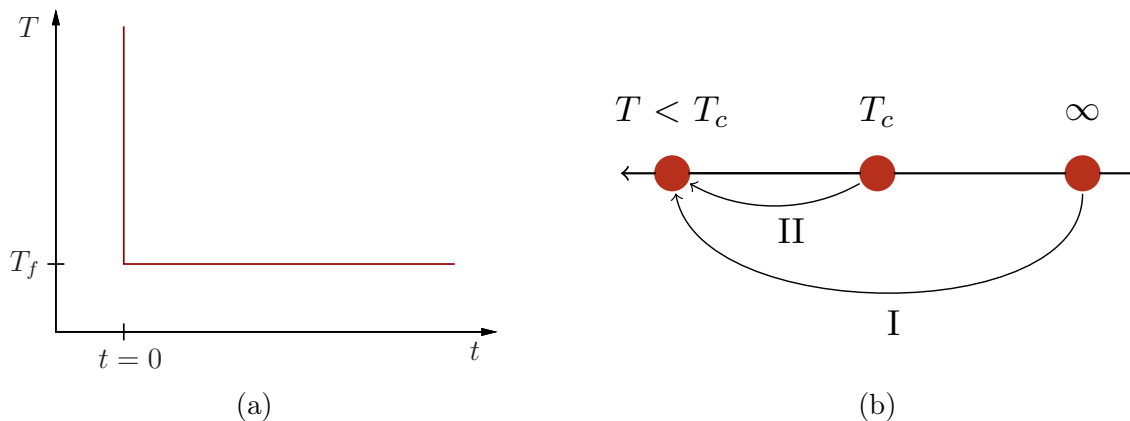
Figure 5.1: Simple quench protocols. (a) Instantaneous quench protocol, when the system is instantaneously quenched to a temperature T_f at time $t = 0$. (b) Temperatures used in the simulations. The initial conditions are $T_0 \to \infty$ or $T_0 = T_\text{c}$ and the final temperature is $T_f < T_\text{c}$.

When $T_0 = T_\text{c}$, the system is equilibrated with a cluster flip algorithm that is more efficient near the critical region when compared to single flip dynamics [65]. Single flip algorithms, like the Metropolis algorithm, have a dynamical critical exponent, $z \approx 2.0$, higher than the values for cluster flip algorithms, like the Swendsen-Wang or Wolff algorithms, $z \approx 0.25$ [65]. This effect is due to the critical slowing down, that makes the transition slower close to the transition, because of the divergence of the correlation length with the exponent z and the significant critical fluctuations. Despite the usefulness in accelerating the thermalization process at T_c, cluster flip algorithms have non-local dynamics, so for the dynamical measurements, we must use a single flip algorithm.

The temperature after the quench is $T_f = 0$. The continuous time Monte Carlo algorithm [65] is used to accelerate the simulations. This algorithm is particularly simple at zero-temperature, since there is no bulk noise and the dynamics is concentrated on the domains' interfaces. Therefore, the spins that can be flipped are those with an opposing local field. The transition probability is

$$w_i(s) \sim \begin{cases} 1, & \text{if } \Delta E_i(s) < 0 \\ p, & \text{if } \Delta E_i(s) = 0 \\ 0 & \text{if } \Delta E_i(s) > 0 \,, \end{cases} \qquad (5.2)$$

where $p \in [0,1]$ is the probability of accepting an $\Delta E = 0$ flip. For the heat bath and Glauber dynamics, $p = 1/2$, while for the Metropolis algorithm, $p = 1$ [66].

In the continuous-time dynamics, we keep a list of the N_{mobile} spins that have a possibility to flip. At zero-temperature, those are the spins where the energy cost if the spin were to flip is $\Delta E \leq 0$. By keeping track of the flippable spins, there is a higher probability that the proposed flip will be accepted. Thus, this algorithm saves computer time by not picking spins that do not have a probability to flip. Each attempt to flip corresponds to a time increment by $1/N_{\text{mobile}}$, instead of $1/N$. The time increment varies as N_{mobile} decreases during the dynamics. Time is measured in Monte Carlo steps (MCS), where one unit corresponds to N attempts to flip.

To compute the heterogeneity, the clusters are identified using the Hoshen-Kopelman algorithm [67]. The geometric domains are computed in a sweep of the lattice, checking which nearest neighbors spins are parallel, and assigning labels to track each cluster. Next, the domain size distribution and the total number of clusters are measured. From the cluster distribution, the heterogeneity and other quantities may be measured, such as the existence and type of percolating clusters, the largest and second largest cluster size, the first absent domain size in the distribution, etc.

5.1.1   Critical initial temperature

At $T_0 = T_c$ the system has infinite range correlations with high thermal fluctuations. The cluster size distribution with this initial condition evolves as [12,13]

$$n_d(A, t) \sim \frac{c \left[\lambda(t + t')\right]^{\tau-2}}{\left[A + \lambda(t + t')\right]^{\tau}} \,, \qquad (5.3)$$

where $n_d(A,t)dA$ is the average number of clusters per unit area, whose size is between A and $A + dA$. The constant $c \simeq 0.029$ [12,13] is very close to the Cardy-Ziff number, $c_h = 1/8\sqrt{3}\pi \simeq 0.023$ [46], the constant λ has the dimensions of a diffusion constant (we consider time and area units unitary). At $T = 0$, $\lambda \simeq 2$, with time and area units unitary, and t' is a microscopic time such that $\lambda t' \simeq 1$.

The cluster size distribution (5.3) is the starting point to derive an analytic expression for the cluster size heterogeneity. The initial state at T_c has a large percolating cluster already established, with the second largest percolating cluster much smaller than the largest one. The time a percolating cluster first appears is indicated by t_{p_1}, and when the percolating cluster becomes stable is t_p. Since there is a percolating cluster at the initial state, $t_{p_1} \simeq 0$, and as this cluster is already stable, being much bigger than the second

largest cluster, $t_p \simeq 0$ [28]. The above distribution is an average, while the heterogeneity H is measured from a single configuration, as discussed in Chapter 3 and shown in Figure 3.2. Differently from the averaged distribution of Eq. (5.3), in a single sample not all possible cluster sizes may be present, therefore there are holes in this distribution.

As done for the equilibrium heterogeneity, we denote $A_0(t)$ as the smallest missing size at time t. Then, the sample cluster size distribution is dense for $A < A_0(t)$, and sparse for sizes greater than $A_0(t)$. If l_0 is a microscopic length and $(l_0 L)^2$ the area of the system, $A_0(t)$ is the size such that $(l_0 L)^2 n(A_0, t) l_0^2 \sim 1$. Using Eq. (5.3) and setting $l_0 = 1$, we obtain an expression for $A_0(t)$

$$A_0(t) \simeq (\lambda t + 1) \left[\left(\frac{L\sqrt{c}}{\lambda t + 1} \right)^{2/\tau} - 1 \right] \Theta(t - t_0), \tag{5.4}$$

where $\Theta(t)$ is the Heaviside step-function. From the Allen-Cahn equation (2.5), we know the areas are decreasing with a rate λ, and the smallest domains will disappear first from the distribution. Therefore, the dense region of the cluster size distribution will have disappeared after a time t_0 such that

$$t_0 \simeq \frac{L\sqrt{c}}{\lambda}. \tag{5.5}$$

The heterogeneity $H(t)$ is given by the contributions of both the dense and sparse regions,

$$H(t) \simeq A_0(t) + L^2 \int_{A_0}^{\infty} dA \, n(A, t), \tag{5.6}$$

where the first term corresponds to the size of the dense region, and the second term to the number of clusters in the sparse region. Using Eqs. (5.3) and (5.4) with Eq. (5.6), we get an expression for $H(t)$ at all times:

$$H(t) \simeq \begin{cases} (\lambda t + 1) \left[\dfrac{\tau}{\tau - 1} \left(\dfrac{L\sqrt{c}}{\lambda t + 1} \right)^{2/\tau} - 1 \right], & t \leq t_0 \\[3ex] \dfrac{L^2 c}{\tau - 1} \dfrac{1}{\lambda t + 1}, & t \geq t_0. \end{cases} \tag{5.7}$$

Analysing both terms, we notice $H(t)$ has a first regime when the coarsening process is slowly removing the smallest clusters, slowly changing $A_0(t)$, up to times $t \simeq t_0$, and a second regime after the dense region has disappeared, and $H(t)$ becomes equivalent to the number of remaining clusters.

The initial value $H(t = 0)$ corresponds to the equilibrium state at T_c

$$H(t = 0) \simeq H_{\text{eq}}(T_c, L) \simeq \frac{\tau}{\tau - 1} c^{1/\tau} L^{2/\tau}, \tag{5.8}$$

whereas $H(t \to \infty) = 0$, because we do not consider the spanning clusters in our definition

of the domain size distribution. At $t = t_0$, both regimes give $H(t_0) \simeq L\sqrt{c}/(\tau - 1)$.

The system initially in equilibrium at $T_0 = T_c$ already has a percolating cluster, therefore $t_{p_1} = 0$. This cluster is already stable against the dynamics, thus $t_p = 0$ [28]. The presence of a percolating cluster at $t_{p_1} = 0$ does not imply $t_p = 0$, as this first may not be stable against the dynamics. For example, an infinite temperature configuration on the triangular lattice, with the same probability $1/2$ of the spins being in the state $+1$ or -1, is already at the critical percolation state and has $t_{p_1} = 0$. However, this cluster from the initial distribution is not stable, therefore $t_p > 0$ [28].

The cluster size heterogeneity, $H(t)$, is shown in Figure 5.2 for several lattice sizes. The simulations are compared with the analytical equation (5.7) (black lines) with a pretty good agreement at all times, except close to t_0, where there is a change of regime. Initially, the coarsening process is removing the smaller clusters from the distribution, without a significant impact on $H(t)$ up to $t \simeq t_0$, since mostly of the removed clusters do not have an unique size. When the dense region is about to disappear, $H(t)$ crosses over to a power-law regime. Almost all remaining clusters have an unique size, and $H(t > t_0)$ may be approximated by the number of clusters, $N_d(t > t_0) \sim t^{-1}$ (Figure 5.3).
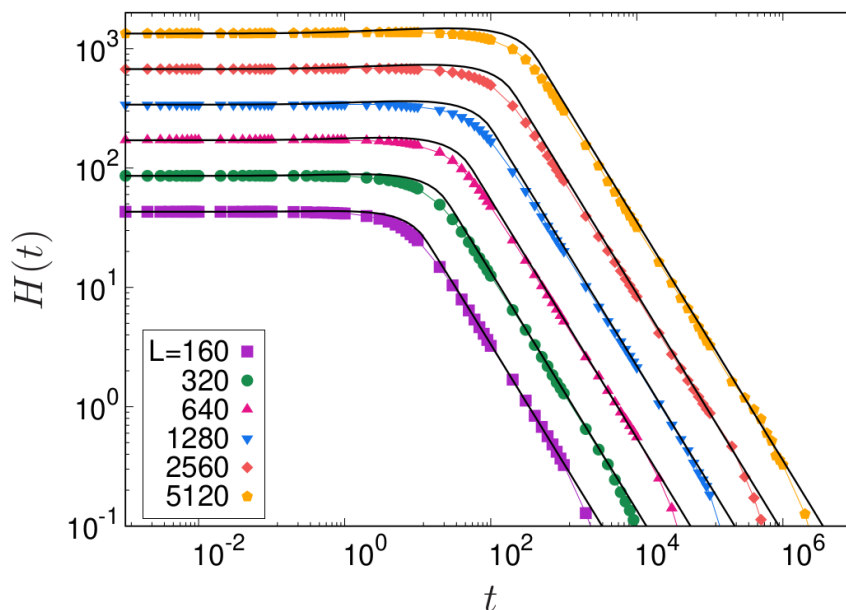
Figure 5.2: Dynamical cluster size heterogeneity $H(t)$ as a function of time (in MCS) for the $2d$ Ising model after a quench from $T_0 = T_c$ to $T_f = 0$. In the first regime, $t \leq t_0$, $H(t)$ changes slowly from its initial value $H_{eq}(T_c, L)$, while the second regime has a power-law behavior with t^{-1}. The behavior of both regimes is well captured by Eq. (5.7) (solid lines). We consider $c \simeq 0.029$, $\lambda \simeq 2$, while τ is used as a fitting parameter to account for finite size effects. For simplicity, only the samples that converged to a fully magnetized state were considered.

The cluster size heterogeneity $H(t)$ collapses well onto a universal curve, $H(t) = L^{-1}f(t/L)$ (Figure 5.4). The time is scaled as $t \rightarrow t/L$ and the cluster size heterogeneity as $H(t) \rightarrow H(t)/L$. The scaling used in the equilibrium case in Ref. [23] considered only the dependency of $H_{eq}(T, L)$ on the system size, $H_{eq}(T, L) \sim L^{-d/\tau}$. The analytic
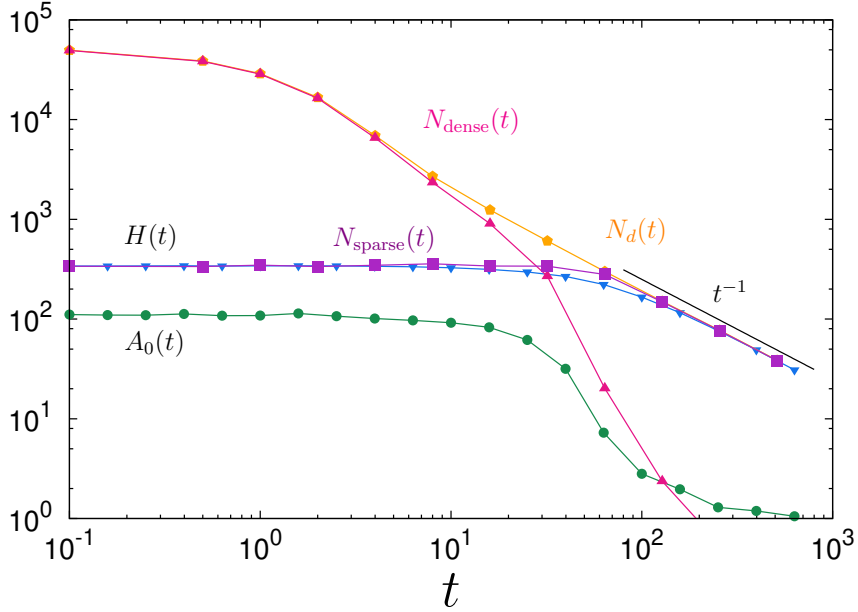
Figure 5.3: Several observables as a function of time after a temperature quench from $T_0 = T_c$ to $T_f = 0$. In the first temporal regime, $H(t)$ presents a slow variation, as well as the number of domains in the dense region, $N_{\text{dense}}(t)$. The coarsening dynamics is removing the smaller clusters in the dense region, thus the number of domains in the sparse region, $N_{\text{sparse}}(t)$, is decreasing quickly. When the dense region is about to disappear, $t \simeq t_0$, the first missing size $A_0(t)$ starts to decrease, and almost all remaining clusters have an unique size, thus $N_{\text{sparse}}(t > t_0) \simeq N_d(t > t_0) \simeq H(t > t_0)$. The solid black line indicates the power-law behavior in the final regime. The system linear size is $L = 1280$ and time is in MCS.

expression (5.7) provides the proper scaling form $f(x)$, and the right dependence on the system size.

Despite the exact value of the Fisher exponent τ for the Ising critical point being known, $\tau_{\text{critical Ising}} = 379/187$, we have considered $\tau = \tau(L)$ as a fitting parameter to take finite size effects into account. As the system size increases, these values $\tau(L)$ converge to the correct value for the Ising critical point, as shown in the inset of Figure 5.4, where each point was obtained from each fit of the analytical expression (5.7). Nevertheless, it is remarkable that $H(t)$ can detect two distinct regimes and that both regions have an excellent collapse.

Another feature of Eq. (5.7) is a small peak $H(t_{\text{max}})$ (Figure 5.5). Both the numerical data and Eq. (5.7) agree on the position of the maximum, t_{max},

$$\frac{\lambda t_{\text{max}} + 1}{L} = \sqrt{c} \left(\frac{\tau - 2}{\tau - 1} \right)^{\tau/2} \simeq 0.004 \,, \tag{5.9}$$

even though the height $H(t_{\text{max}})$ has a small deviation between Eq. (5.7) and the numerical data. This deviation is enlarged in Figure 5.5 due to the chosen vertical scale and can be due to the dependence of Eq. (5.7) on the precise value of c. Furthermore, the analytical results do not account for the coalescence of two domains to form a bigger one, or the fission of a big domain into two smaller ones [13]. Despite these processes not being

important in the analytic results, as given in Eq. (5.3), they may play a role in the small peak of $H(t)$ where there is a change of regime.

5.1.2   Infinite initial temperature

At the initial infinite temperature, despite spins being uncorrelated, there are small clusters present in the system and there is no percolating cluster. The initial heterogeneity $H(t = 0)$ is not very large and corresponds to the equilibrium state at an infinite temperature [21–23]

$$H_{\text{eq}}(T \rightarrow \infty, L) \simeq \ln L. \tag{5.10}$$

Differently from the previous case, the initial state in equilibrium at $T \rightarrow \infty$ is not critical. Soon after the quench, the domains begin to coalesce into larger ones and the domain size distribution approaches in a few MCS the random site percolation critical state [12, 13]. The first occurrence of a percolating cluster is at t_{p_1}, subsequently destroyed by the dynamics. The largest and second largest cluster compete until a later time t_p, when the largest cluster becomes stable and will grow throughout the dynamics. After the cluster size distribution becomes critical at t_{p_1}, it evolves as [12, 13, 29]

$$n_d(A, t) \sim \frac{2c \left[\lambda(t + t_{p_1} + t') \right]^{\tau_p - 2}}{\left[A + \lambda(t + t_{p_1} + t') \right]^{\tau_p}}, \tag{5.11}$$

where $\tau_p = 187/91$ is the Fisher exponent, the factor 2 in the numerator accounts for the existence of clusters with both positive and negative magnetization, while in the related percolation problem only particle clusters are considered and not the empty sites. Similar to the previous case, we obtain an expression for the first missing cluster size $A_0(t)$ from the cluster size distribution,

$$A_0(t) \simeq \left[\lambda(t - t_{p_1}) + 1 \right] \left[\left(\frac{L\sqrt{2c}}{\lambda(t - t_{p_1}) + 1} \right)^{2/\tau_p} - 1 \right] \Theta(t - t_0), \tag{5.12}$$

and the time t_0 at which the dense part of the distribution will have disappeared is

$$t_0 \simeq \frac{L\sqrt{2c} - 1}{\lambda} + t_{p_1}. \tag{5.13}$$

Thus, calculating using Eq. (5.6), the behavior of $H(t)$ is given by the expression

$$H(t) \simeq \begin{cases} (\lambda(t - t_{p_1}) + 1) \left[\dfrac{\tau_p}{\tau_p - 1} \left(\dfrac{L\sqrt{2c}}{\lambda(t - t_{p_1}) + 1} \right)^{2/\tau_p} - 1 \right], & t_{p_1} < t \leq t_0 \\[4mm] \dfrac{2L^2 c}{\tau_p - 1} \dfrac{1}{\lambda(t - t_{p_1}) + 1}, & t \geq t_0. \end{cases} \tag{5.14}$$
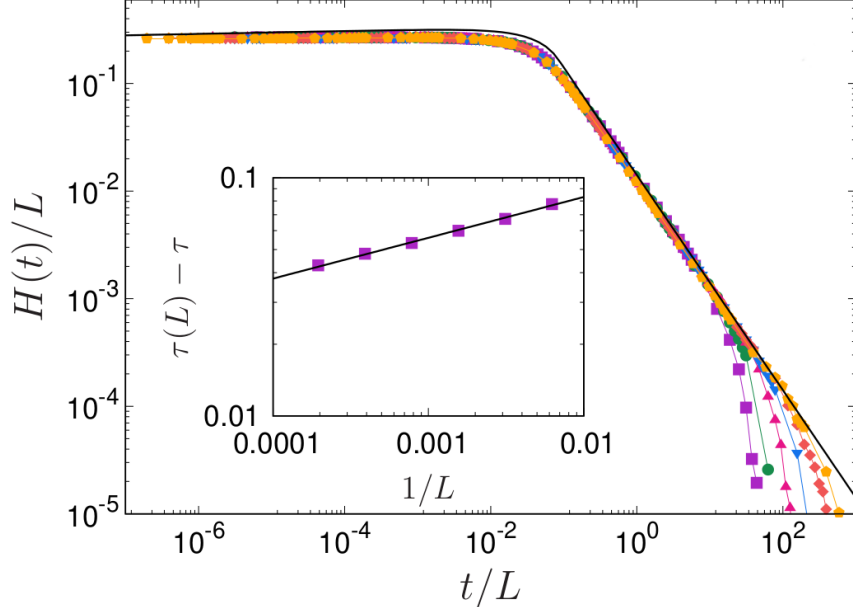
Figure 5.4: Collapse of the cluster size heterogeneity $H(t)$ for the 2d Ising model after the quench from $T_0 = T_c$ to $T_f = 0$ onto an universal curve, $H(t) = Lf(t/L)$. The inset shows that the values of $\tau(L)$ used to fit the analytical curves in the Figure 5.2 do converge to the correct value for the critical Ising as the system size increases. The Fisher exponent τ used here is the one for the geometric domains in the Ising model, $\tau_{\text{critical Ising}} = 379/187$. The agreement in the main panel with Eq. (5.7) (black line) is also good.

Figure 5.5: Zoom into the region close to the end of the plateau for the 2d Ising model after the quench from $T_0 = T_c$ to $T_f = 0$. A small peak at $t_{\max}$ is marked by the vertical line, given by Eq. (5.9). The height of the peak $H(t_{\max})$ depends on the precise value of c in Eq. (5.7). The deviation from the numerical data appears larger because of the chosen scale.

Soon after the quench, $H(t)$ grows rapidly and presents a pronounced peak followed by an intermediate plateau before the final power-law decrease toward the asymptotic state, as shown in Figure 5.6.
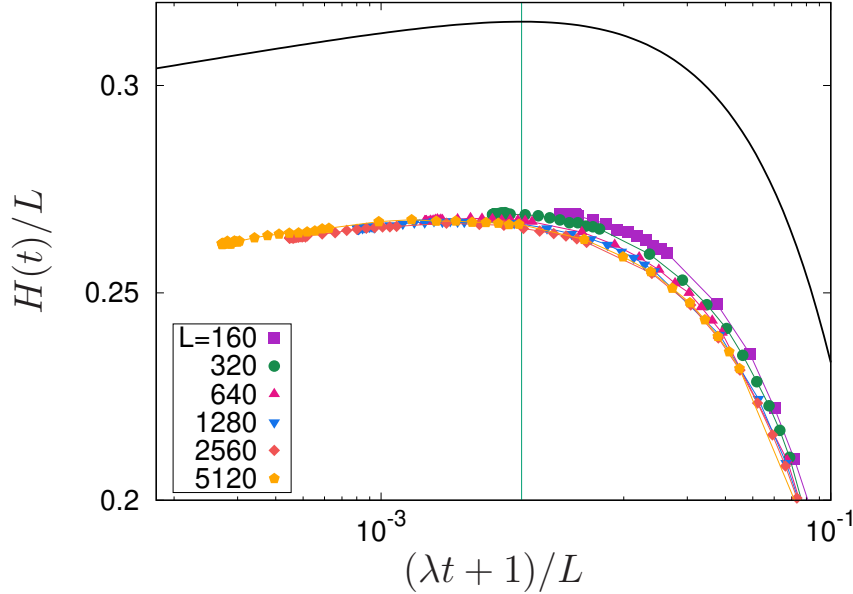

(a)

(b)

Figure 5.6: Dynamical cluster size heterogeneity $H(t)$ as a function of time for the $2d$ Ising model after a quench from $T_0 \to \infty$ to $T_f = 0$. For the largest size, we indicate the times when a percolating cluster first appears, $t_{p_1}(L)$, and when it becomes stable, $t_p(L)$. The black horizontal line indicates $H_{eq}(T_2, L)$, observed in Ref. [23], which agrees well with the peak $H(t_{peak}, L)$. On the right, the black curve is Eq. (5.14) using $\tau_p = 187/91$, showing a good agreement for the regime $t > t_{p_1}$. Notice that panel (a) is in a semi-log scale, while panel (b) is in a log-log scale. For simplicity, only the samples that converged to a fully magnetized state were considered in our numerical data.

As in the previous $T_0 = T_c$ case, the analytical expression of $H(t)$ (5.14) also has a broad and small maximum before t_0, at t_{max}

$$\frac{\lambda t_{max} + 1}{L} = \sqrt{2c} \left(\frac{\tau_p - 2}{\tau_p - 1} \right)^{\tau_p/2} \simeq 0.011. \tag{5.15}$$

However, the numerical data do not have this maximum and decrease after $t > t_0$. We conjecture that this is an effect of the sizes considered here, so the region $t \leq t_0$ may not be fully developed yet, or due to the presence of the initial, precursor maximum that influences the behavior before t_{p_1}. The cluster size distribution in Eq. (5.11) considers the initial state at the critical percolation state, therefore we do not expect the analytical expression for $H(t)$ to capture any features for $t < t_{p_1}$. As a matter of fact, in the analytical expression, $t = t_{p_1}$ corresponds to the beginning of the slowly changing region that precedes the small maximum, which approximately extends between t_{p_1} and t_p (whose separation depends on L), observed in Figures 5.6a and 5.6b:

$$H(t_{p_1}) \simeq \frac{\tau_p}{\tau_p - 1} (L\sqrt{2c})^{2/\tau_p} . \tag{5.16}$$

The pronounced peak before the appearance of the first percolating cluster is a precursor feature of the percolating state. As the domains coalesce after the quench, the domain size distribution widens as shown in Figure 2.6 and $H(t)$ increases. However, as

the largest cluster increases, less space is available for the other clusters, reducing the size heterogeneity. Therefore, the maximum heterogeneity occurs at t_{peak} slightly before t_{p_1}. This early peak is not only a precursor effect of the percolating cluster that appears at t_{p_1}, but also has a strong, mysterious connection with the equilibrium measures of Ref. [23]. For all sizes considered, there is a correspondence between the heights of the dynamical peak, $H(t_{\mathrm{peak}})$, and the second equilibrium peak, $H_{\mathrm{eq}}(T_2)$, observed in Ref. [23], $H(t_{\mathrm{peak}}) \simeq H_{\mathrm{eq}}(T_2)$. This correspondence is indicated by a small horizontal line for the largest L in Figure 5.6a. Indeed, as the temperature decreases, the equilibrium peak at T_2 [23] (Figure 3.4b) also precedes the appearance of a percolating cluster. Furthermore, we also observe that the peak seems to be (roughly) twice the height of the analytical expression at t_{p_1}, which indicates the beginning of the correspondence between the analytical expression and the numerical data:

$$H(t_{\mathrm{peak}}, L) \simeq H_{\mathrm{eq}}(T_2, L) \simeq 2H(0, L) \simeq \frac{2\tau_p}{\tau_p - 1}(L\sqrt{2c})^{2/\tau_p} , \qquad (5.17)$$

indicated in the inset of Figure 5.7. The relation between the peak and the analytical expression $H(t_{\mathrm{peak}}, L) \simeq 2H(0, L)$ is not yet completely understood. This finding suggests that the approach to critical percolation and the formation of the first percolating cluster has to be further investigated.

As expected, the numerical data for $t > t_{p_1}$ is well described by Eq. (5.14) as shown in Figures 5.6b and 5.7, while the peak region clearly grows with a different exponent than the subsequent evolution $t > t_{p_1}$ of $H(t)$. For $t > t_{p_1}$, as in the previous $T_0 = T_{\mathrm{c}}$ case, the evolution follows the usual coarsening process with a t^{-1} power-law growth. By rescaling both $H(t)$ and the time by L, $H(t)$ has a very good collapse for $t > t_{p_1}$, in agreement with Eq. (5.14) (Figure 5.7), despite stronger finite size effects than in the $T_0 = T_{\mathrm{c}}$ case.

For $t \geq t_0$, the power-law behavior of $H(t) \sim t^{-1}$ is similar to the $T_0 = T_{\mathrm{c}}$ case and accounts for the number of clusters $N_{\mathrm{d}}(t)$ (Figure 5.8), differing from the $T_0 = T_c$ case only by the value of τ_p and the factor of 2 in the numerator. Initially, the main contribution to the number of clusters $N_d(t)$ is from the dense region, $N_{\mathrm{dense}}(t)$. Recalling from the Allen-Cahn equation (2.5), the small clusters are being withdrawn first from the distribution at the beginning of the dynamics. These small clusters are concentrated in the dense region for a long period of the dynamics. Meanwhile, the number of clusters in the sparse region, $N_{\mathrm{sparse}}(t)$ has a maximum that coincides with the peak in the heterogeneity. Recalling from Eq. (5.14), in this region $H(t) \simeq A_0(t) + N_{\mathrm{sparse}}(t)$. Even though the sum $A_0(t) + N_{\mathrm{sparse}}(t)$ is greater than $H(t)$ in Figure 5.8, we recall that initially $N_{\mathrm{sparse}}(t)$ does not account for the number of unique sizes in this region, due to repeated cluster sizes. For intermediate times, $t_{p_1} < t < t_0$, the number of domains in the sparse region has a plateau, and while $N_{\mathrm{dense}}(t)$ is reducing rapidly, their removal from the system does not impact $H(t)$ significantly since there are many repeated cluster sizes in this region. When the dense region disappears from the system at times $t \geq t_0$, $A_0(t) \simeq 1$ and $N_{\mathrm{dense}}(t) \sim 0$,
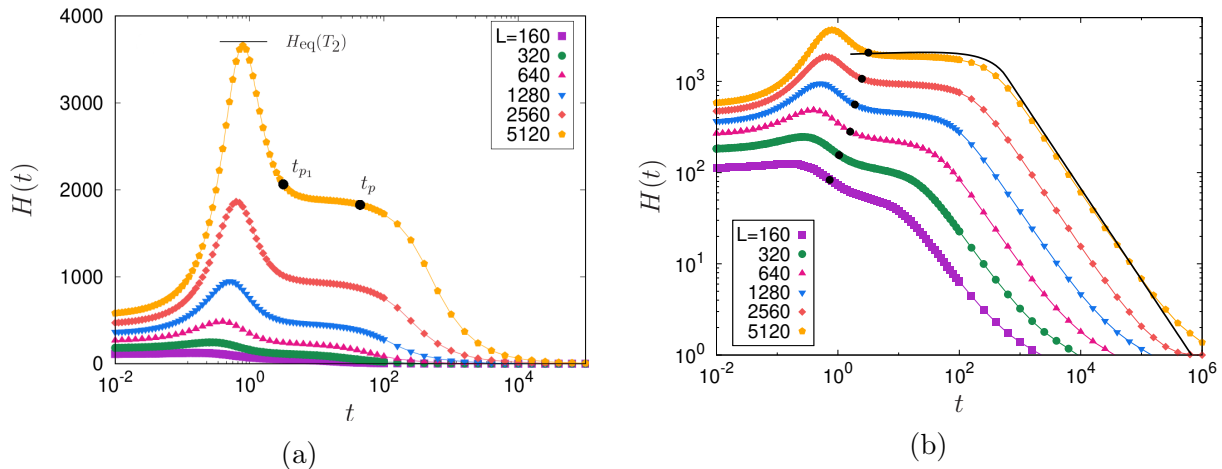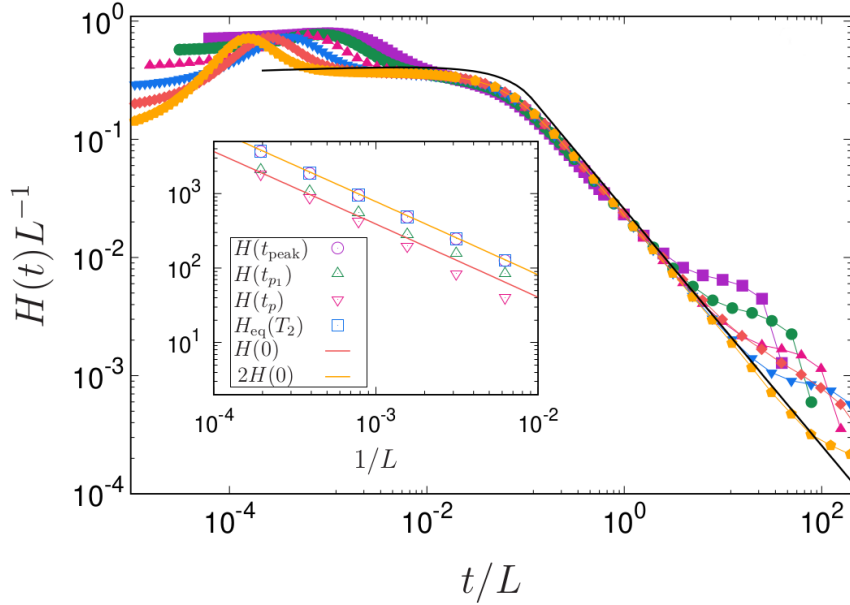
Figure 5.7: Collapse of the dynamical cluster size heterogeneity $H(t)$ as a function of time for the 2d Ising model after a quench from $T_0 \to \infty$ to $T_f = 0$. Both $H(t)$ and time are rescaled by L. The behavior of $t > t_{p_1}$ is well approximated by Eq. (5.14) with $\tau_p = 187/91$ (solid line). The inset shows, in the upper straight line, the height of the peaks $H(t_{\text{peak}}, L)$ (circles) and $H_{\text{eq}}(T_2, L)$ (squares) along with Eq. (5.17), indistinguishable at this scale, as a function of the system size. Below, we compare the data of $H(t_{p_1})$ and $H(t_p)$ (triangles) with Eq. (5.16), that get closer as L increases.

$H(t)$ corresponds to the number of domains $N_d(t) \simeq N_{\text{sparse}}$.

Returning to $t < t_{p_1}$ and the early peak at t_{peak}. The $H(t_{\text{peak}})$ is a precursor effect of the percolating cluster that appears at t_{p_1}. Additionally, this peak has a strong relation with the equilibrium measures of Ref. [23] (Figure 5.6a). Indeed, the equilibrium peak at T_2 [23] also anticipates the first appearance of a percolating cluster as the temperature is decreased from a high temperature. Similar to the equilibrium case, where the equilibrium peak at T_2 had a different scaling from the equilibrium peak at T_c, the data collapse in Figure 5.7 fails in the early regime. This indicates that the dynamical scaling length $R(t) \sim t^{1/2}$ is not the single relevant length scale after the quench.

A good collapse around the heterogeneity peak, $t_{\text{peak}} < t < t_{p_1}$, is obtained with $t \sim L^\alpha$, with $\alpha \simeq 0.22$ (Figure 5.9). Notice that although the peaks are well collapsed, neither the black triangles indicating t_{peak}, nor the black circles indicating t_{p_1} exhibit a good convergence. Only for the larger sizes t_{peak} and t_{p_1} seem to collapse with $H(t)/L$ and t/L^α, with $\alpha \simeq 0.22$. Meanwhile, this exponent does not collapse t_p. Thus, different values of the exponent α can collapse the characteristic times, t_{p_1} and t_p. For t_p, it was shown in Ref. [29] that the exponent corresponding to the stabilization of the percolating cluster is 0.4. On the left side of the peak, it seems that the convergence to a universal curve is slower. This is in agreement with Ref. [23], where it was found that $H(T \to \infty) \sim \log(L)$.

Other estimates of the exponent α are possible. For example, we can check the relation of t_{peak} with the system size L through a power-law $t_{\text{peak}} \sim L^\alpha$. As the peak is very
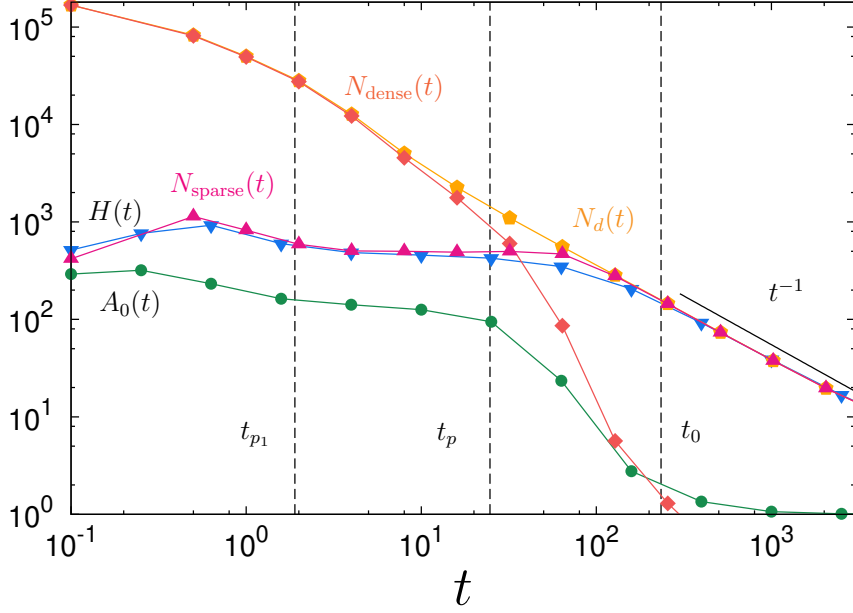
Figure 5.8: Number of clusters as a function of time for the $2d$ Ising model after a quench from $T_0 \to \infty$ to $T_f = 0$ with linear system size $L = 1280$. The total number of clusters $N_d(t) = N_{\mathrm{dense}}(t) + N_{\mathrm{sparse}}(t)$ (orange pentagon), the number of clusters in the dense region $N_{\mathrm{dense}}(t)$ (red lozenges), and the sparse region $N_{\mathrm{sparse}}(t)$ (pink triangles). In blue, the heterogeneity $H(t)$ (triangles) and in green, the first absent cluster size $A_0(t)$ (circles). Vertical dashed lines indicate t_{p_1}, t_p and t_0, respectively. The solid black line has a -1 slope, indicating the coarsening regime.
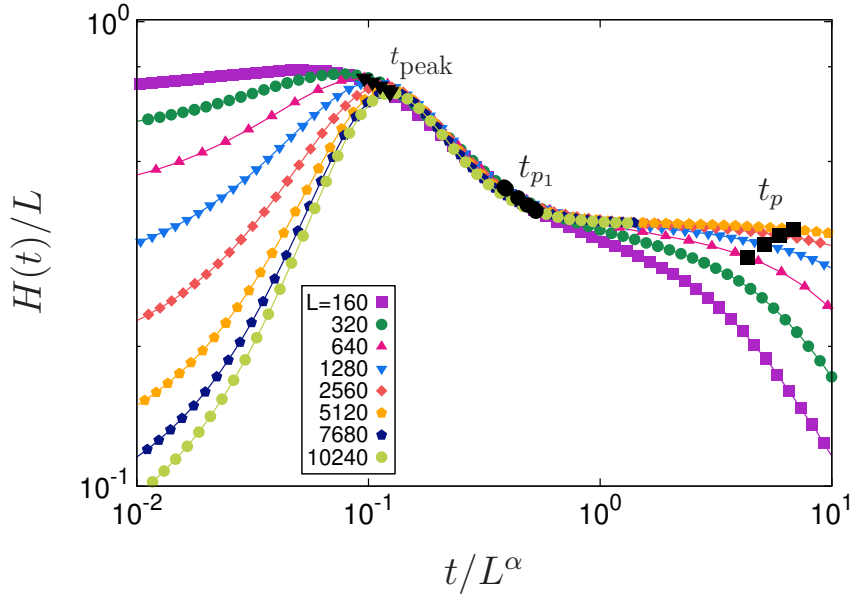
Figure 5.9: Collapse of the dynamical cluster size heterogeneity $H(t)$ as a function of time for the $2d$ Ising model after a quench from $T_0 \to \infty$ to $T_f = 0$. The peak is indicated by t_{peak} (inverted triangles), the appearance of a first percolating cluster by t_{p_1} (circles), and the stabilization of the percolating cluster by t_p (squares). The early time region near the peak, $t_{\mathrm{peak}} < t < t_{p_1}$, is collapsed using an exponent $\alpha \simeq 0.22$. However, only for the larger sizes t_{peak} and t_{p_1} display a good collapse with this exponent, while t_p is not collapsed.

broad for smaller systems, the determination of t_{peak} is not very precise for these sizes. Thus, only linear sizes greater than $L > 640$ were considered in the fit, and an exponent $\alpha \simeq 0.293 \pm 0.03$ was obtained (Figure 5.10). The local slope of this function also provides an estimate for α, $dt_{\text{peak}}/dL \sim L^{\alpha-1}$. Using this relation, we obtain $\alpha \simeq 0.270 \pm 0.03$ (inset, Figure 5.10). However, while this exponent $\alpha \simeq 0.27$ collapses well $t_{\text{peak}}(L)$, it has a poor collapse in the region after the peak, indicating that there is indeed another length scale playing a role in the approach to critical percolation. For comparison, the dashed line in the inset of Figure 5.10 fits well the data and corresponds to $\alpha = 0.22$, which was obtained from the collapse of $H(t)$ (Figure 5.9). Clearly, $H(t)$ has a different dependence on the system size L in the region of the peak, the plateau and the tail. Furthermore, a more detailed analysis of this exponent $\alpha = 0.22$ is necessary to establish with greater reliability if $H(t)$ is well suited as an observable to measure the approach to critical percolation.
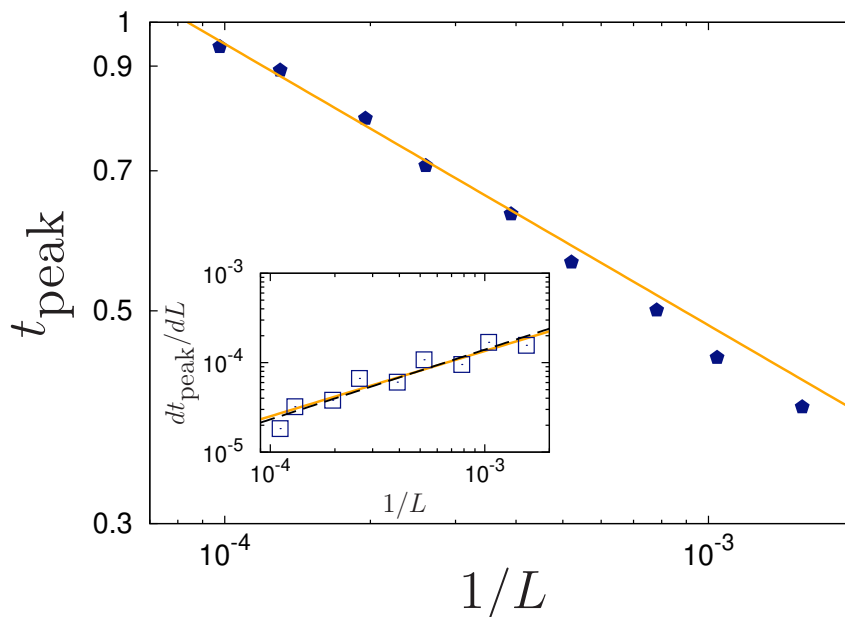
Figure 5.10: Position of the peak t_{peak} as a function of the system size L. The slope of the orange line is $\alpha \simeq 0.2935 \pm 0.03$. The inset shows $dt_{\text{peak}}/dL \sim L^{\alpha-1}$, whose slope provides another estimate for α, $\alpha \simeq 0.2696 \pm 0.03$. The dashed line corresponds to an exponent $\alpha = 0.22$. Since the peak is very broad for smaller system sizes, the smaller ones $L = 160, 320, 640$ were not used to fit the peak t_{peak}, thus omitted here.

For completeness, we also show the final evolution of the dynamical cluster size heterogeneity $H(t)$ for the ground and frozen states. Even though $H(t)$ only considers the unique cluster sizes, it can also distinguish the final evolution to the ground state or frozen stripes (Figure 5.11). Although the fate of the asymptotic state is determined at a time t_p, the evolution of the cluster size heterogeneity $H(t)$ for the different asymptotic states is similar up to a time much greater than $t_p \sim L^{0.4}$.

Typically, configurations evolving directly to the ground state will equilibrate in a time $t_{\text{eq}} \sim L^2$. Figure 5.11 highlights that all wrapping configurations (1d stripes, diagonal stripes or cross configuration, illustrated in Figure 2.10) reach a configuration with two unique domain sizes at $t/L^2 \sim 0.1$. Interestingly, the evolution to the diagonal stripes

is faster to reach a state with two domains than the other configurations. Subsequently, after reaching this configuration with two different domain sizes, the samples evolving directly to the ground state converge quickly to a fully aligned configuration, in a time $t_{eq} \sim L^2$. Meanwhile, the horizontal or vertical stripes will be "frozen" at $H(t) = 2$, the corresponding final number of stripes, which will not be altered since the number of domains does not change while the system is straightening the interfaces. The freezing time is the time when no spin updates are possible, i.e., flipping any spins increases the system's energy, as straight boundaries are stable configurations at $T = 0$ and the system is in a local minimum of energy. An example of this process for four stripes is shown in Figure 2.10f. Thus, due to the samples converging to frozen striped states, $H(t)$ does not converge to 1 when averaging over all samples. Differently from the horizontal or vertical stripes, diagonal stripes are not a stable configuration. Therefore, the domain walls will eventually diffuse and annihilate in a time $t_{eq} \sim L^3$ [51]. The slower relaxation of the diagonal stripes is evidenced by the plateau before collapsing to the ground state.
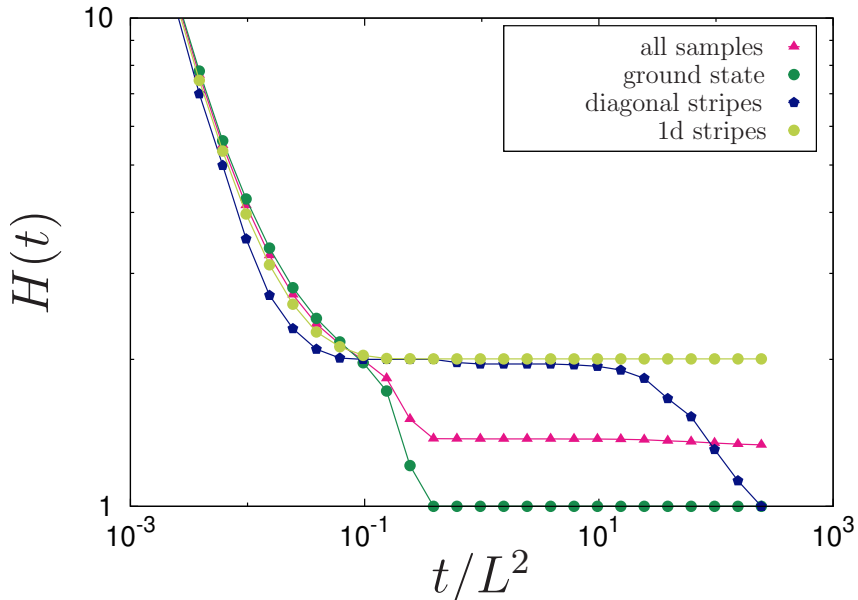
Figure 5.11: Final evolution of the dynamical cluster size heterogeneity $H(t)$ as a function of the rescaled time t/L^2 for the $2d$ Ising model after a quench from $T_0 \to \infty$ to $T_f = 0$ with linear size $L = 640$. From the wrapping probabilities in critical percolation, the system reaches the ground state in $t_{eq} \sim L^2$ with probability ~ 0.6290. Horizontal or vertical stripes (two or more) are stable configurations reached with probability ~ 0.334. Diagonal stripes are long lived configurations that reach the ground state in $t_{eq} \sim L^3$ with the probability ~ 0.039 [51, 54]. Due to the samples converging to striped states, averaging over all samples $H(t)$ does not converge to 1.

To check how universal the behavior of $H(t)$ is, we compare the behavior of $H(t)$ in the $2d$ Ising model after a quench from $T_0 \to \infty$ to $T_f = 0$ and the $2d$ voter model evolving from a fully uncorrelated state (Figure 5.12). The voter model is a simple spin model without an associated energy function named after its interpretation in terms of opinion dynamics [40–42]. In the voter model, a site chosen at random aligns with a

randomly chosen nearest neighbor. Thus, the probability of a spin flip does not depend on the energy variation, as in the Ising model, but is given by the fraction of nearest neighbors with opposite orientation. Hence, there is no bulk noise and the motion of the interfaces does not depend on the curvature, but is driven by interfacial fluctuations [43]. Actually, the voter and the Ising models are two particular cases of a family of stochastic systems with bimodal variables, up-down symmetry on a square lattice, and isotropic and short-ranged interactions [68]. The transition rates define this class of models, with the spin-independent variables in the transition rates acting as control parameters for bulk and interfacial noise [68]. For some particular choices of these parameters, the Ising, voter and majority voter dynamics may be recovered. Except for the Ising case, the dynamics for arbitrary control parameters do not satisfy detailed balance. Hence, the voter model is essentially out-of-equilibrium [69].

Despite the differences of the coarsening mechanism and the larger timescales in the voter model [31], the overall behavior of $H(t)$ is similar. Using the same definition for t_{p_1} and t_p as before, we can see in Figure 5.12 that these times are related to the end of the precursor peak and the end of the plateau, even if the critical properties of the percolating cluster in the voter model do not correspond to the critical percolation [31]. Remarkably, the precursor peak has roughly the same height for both models, suggesting a more general mechanism in the approach to a percolating state.

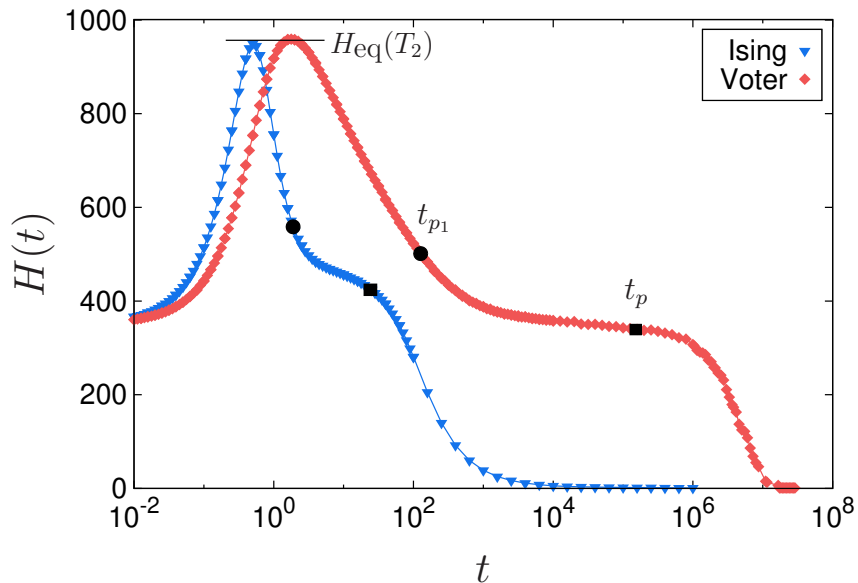Figure 5.12: Comparison between the time evolution of $H(t)$ for the 2d Ising model at $T_f = 0$ and the 2d voter model, both starting from an initially uncorrelated state ($T \to \infty$). The system linear size is $L = 1280$ and the time is in MCS. The precursor peak has roughly the same height for both models. The black horizontal line indicates $H_{\mathrm{eq}}(T_2, L)$, suggesting a common mechanism behind the peak.

Chapter 6

Conclusions

In this work, we studied the dynamical properties of the cluster size heterogeneity and its applications to the out-of-equilibrium Ising model. The equilibrium cluster size heterogeneity $H_{eq}(T)$ in the $2d$ Ising model presents two peaks at very different temperatures, which were associated with the thermal and percolative transitions [23]. In the thermodynamical limit, both the thermal and percolation transitions occur at T_c [70,71]. In finite systems, these transitions are marked by a peak in the measured quantities (e.g., mean cluster size, magnetic susceptibility) and occur at a different temperature than T_c, depending on the system size. Despite occurring at T_c in the thermodynamical limit, they have not yet merged for finite systems. Hence, the equilibrium cluster size heterogeneity $H_{eq}(T_c)$ was able to disentangle the percolative and thermal effects in equilibrium finite samples by separating them into two peaks. Motivated by those results and to further explore the role of the percolative transition in the dynamics, we investigated whether this quantity is useful to study out of equilibrium configurations. In particular, $H(t)$ was shown to distinguish between different regimes, demonstrating that it is an interesting measure to study the rich interplay between percolation and coarsening either at equilibrium or short-time scales during the dynamics. Besides, we have also investigated how different exponents of a power-law distribution affect the diversity of sizes in a system. Through a general model of independent and identically distributed integer random variables, we have shown that there is a value τ that maximizes the heterogeneity of the system.

In equilibrium, at high temperatures, thermal fluctuations break down large domains into small clusters, decreasing the average domain size with temperature and the size diversity. Decreasing the temperature, correlations between the spins grow, larger domains are formed, and the diversity of sizes increases; however, as $T < T_c$, a giant cluster fills most of the system, without much space for other clusters. So, both at $T \ll T_c$ or $T \gg T_c$, the size diversity is smaller than that close to T_c, where the distribution of domain sizes is a power-law. Therefore, one expects a peak in H_{eq} between these two extreme limits. Indeed there are two peaks present [23], one very close to T_c and a second one near the temperature where the percolating cluster first appears [72]. Since the equilibrium

cluster size heterogeneity gives information on two different length scales associated with percolation and coarsening, we aimed to investigate whether the dynamical cluster size heterogeneity $H(t)$ can give information on these regimes as well.

We extended the equilibrium measure of how heterogeneous the domains are to nonequilibrium situations deriving an analytical expression for $H(t)$, based on the analytical equations for the domain size distribution. Specifically, we explored $H(t)$ usefulness in the nonconserved order-parameter dynamics of the $2d$ Ising model after a sudden quench in temperature. We considered two relevant initial temperatures, starting at a state with $(T_0 \to \infty)$ or infinite range correlations $(T_0 = T_c)$. The fixed final temperature is $T_f = 0$. The measurement of $H(t)$ along the time evolution of the system made it possible to identify distinct temporal regimes during these quench protocols.

For quenches starting at T_c, $H(t)$ displays a plateau that increases very slowly, presenting a small peak before crossing over to the power-law coarsening regime. Initially, a stable percolating cluster is already present, and the domain size distribution follows a power law. The coarsening dynamics removes the smaller clusters from the system, and hence the $H(t)$ plateau, as most of the removed clusters do not have a unique size. In the latter regime, the domain size distribution is sparse, with many absent domain sizes and a small probability of two domains having the same size. Thus, the heterogeneity corresponds to the total number of clusters and decays as a power law. The analytical expression provided the proper scaling form for $H(t)$ and the correct dependence on the system size, which collapsed well $H(t)$ onto a universal curve for $T_0 = T_c$.

In contrast, when the quench is performed from $T_0 \to \infty$, in a few time steps, the system approaches the percolation critical state [12, 13]. The approach to the critical percolation state is characterized by a very pronounced peak in $H(t)$, which acts as a precursor of the percolating cluster being built. As expected, this peak is not captured by the analytical expressions, as the expression for the domain size distribution is not valid for $t < t_{p_1}$. The large percolating cluster formed at t_{p_1} is not stable against the dynamics. The two largest clusters grow by absorbing smaller domains and coexist until a later time t_p. At t_p, the largest cluster prevails over the others, and its percolating configuration will determine the final state of the system. The dynamics after the system has passed through the critical percolation point, $t > t_{p_1}$, is similar to the temporal regimes present in the quench starting at T_c. Nevertheless, $H(t)$ captured these regimes, in agreement with the numerical data and displayed an excellent collapse in these regions.

Besides being a precursor feature of the percolating cluster that appears soon afterward, the early peak $H(t_{\text{peak}})$ has a strong relation to the equilibrium measures $H_{\text{eq}}(T)$ of Ref. [23]. The height of both peaks is roughly the same, $H(t_{\text{peak}}) \simeq H_{\text{eq}}(T_2)$. Indeed, the equilibrium peak at T_2 [23] also anticipates the first appearance of a percolating cluster. As the temperature decreases, the correlation length grows, larger domains are formed, and a percolating cluster is formed at temperatures roughly below T_2. Similar to the equi-

librium case, where the peak at T_2 had a different scaling from the one at T_c, the data collapse from the analytic expression of $H(t)$ fails in the early regime. This supports that there is another growing length, different from $R(t) \sim t^{1/2}$, playing a role in the short time dynamics [29]. The peak region $t_{peak} < t < t_{p_1}$ is well collapsed with an exponent $\alpha \simeq 0.22$. Although the collapse in the right side of the peak is good, the characteristic times t_{p_1}, and t_p do not present a good convergence with this exponent. Thus, different values of the exponent α can collapse the other characteristic times, t_{p_1} and t_p. Recent works [29,31] discuss the approach to critical percolation and how the exponent α associated with this length scale depends on the microscopic dynamics and the lattice geometry. Nonetheless, the origin of the exponent α has to be better understood.

We have also analyzed $H(t)$ in the $2d$ voter model evolving from an initial disordered configuration. The voter model is an out of equilibrium model without an associated energy function. Remarkably, despite the voter dynamics not being curvature driven as in the Ising model, $H(t)$ displayed a similar behavior from the infinite temperature quench and distinguished different temporal regimes in the voter dynamics. The early peak height is roughly the same in the $2d$ voter and Ising models, suggesting a more general mechanism behind the formation of the first percolating cluster. Differently from the Ising model, the critical properties of the cluster formed at t_{p_1} do not correspond to critical percolation [31]. Even so, defining t_{p_1} and t_p as in the Ising model, indicate that these time scales are related, as in the Ising model, to the end of the precursor peak and the end of the plateau, which further indicates a more general mechanism in the approach to a percolating state. We hypothesize this relation could be due to a similarity of these models, as both are particular cases of a family of stochastic systems [68,73].

Motivated by the correspondence between the height of the dynamical peak $H(t_{peak})$ and equilibrium heterogeneity second peak $H_{eq}(T_2)$, we investigated also how different values of the exponent τ of the domain size distribution change the behavior of the heterogeneity. We considered a general statistical model that generated independent domains from a given probability distribution, whose only constraint is to fill the system area S, and explored the behavior of the heterogeneity. We started from a generic probability function and focused on the algebraic case due to the relevance of the cluster size heterogeneity in exploring critical properties of spatial models. Through this sort of mean-field approach, in the sense that the only constraint imposed is on the set of chosen domains, we obtained analytical expressions for the average domain size, average number of domains, and the average heterogeneity. For large values of τ, the distribution is steep, i.e., there is a higher probability of repeatedly extracting small domains, which results in a small heterogeneity. In the other limit, small τ, large clusters get more probable as the distribution decays slowly. Although it is more likely that all clusters have different sizes, the total number of clusters necessary to fill the area S is smaller; hence the diversity of sizes will also be small. We thus expected a maximum value of the heterogeneity at intermediate values of τ. Indeed, we have found a maximum heterogeneity at $\tau = 2$. In-

terestingly, this value is close to the exponent for geometrical domains in the Ising model, $\tau_I = 379/187 \simeq 2.027$ [47, 63], for physical clusters, $\tau = 31/15 \simeq 2.067$ [59], and at critical percolation is $\tau_p = 187/91 \simeq 2.055$ [19]. Instead of considering the geometrical domains, another possibility is to use the distribution of hull enclosed areas. Although the number of hulls is exactly the same as the number of geometrical domains, as each hull is associated with a single domain [13], they do not need to obey the area constraint and, indeed, their total area is larger than S. Remarkably, their exponent τ is exactly 2, which corresponds to the exponent that maximized the heterogeneity in our model with independent domains, whose only constraint was on the total area S. We thus speculate that the fewer constraints upon the domains, the closer their exponent will be to $\tau = 2$.

Another way to investigate the mechanism behind the height of the cluster size heterogeneity peak and the relation between the dynamical $H(t_{\mathrm{peak}})$ and equilibrium second peak $H_{\mathrm{eq}}(T_2)$ is to ask what geometrical properties play a role in the early time dynamics. What microscopic processes play a role in the formation of the first percolating cluster? In the zero-temperature Ising model, two types of flips are allowed: energy-lowering (energetic) ones or zero-energy (entropic) flips. Thus, what is the role of each type of flip in the dynamics? Does changing the acceptance probability of each type of flip alter the dynamics and equilibrium of the system? To answer the questions mentioned above, we have begun to explore how the details of the microscopic dynamics influence the macroscopic behavior of the system. Energetic flips are always accepted, then by altering the acceptance probability of the entropic spin flips, we observe the effects of each type of flip. Our preliminary results indicate that the energy-lowering flips are behind the formation of the first percolating cluster. Still, the zero-energy flips are essential to the stabilization of percolation and the final coarsening regime.

Finally, the cluster size heterogeneity was recently proposed to study equilibrium configurations. Its measurement in the equilibrium $2d$ Ising model was able to resolve the thermal and percolative effects. Here we have extended its measurement to out of equilibrium configurations, and $H(t)$ has proven to be a useful observable that unveils the rich interplay between percolation and coarsening dynamics either in equilibrium or at short-time scales. Still, the rich behavior of $H(t)$ suggests that its study in several extensions would be interesting. Although we focused here on geometric domains, the dynamical heterogeneity associated with the physical clusters [59], would also be of interest [23], along with the heterogeneity of hulls and perimeters. While we considered a temperature protocol of only a single sudden quench, $H(t)$ may be useful when exploring other quench procedures, such as the Kovacs protocol [74–77], that considers two sudden changes in temperature in order to measure memory effects, or a finite cooling rate, such as the Kibble-Zurek mechanism [72, 78–80]. Other interesting cases would be the Ising model with conserved order parameter [18, 31] or disorder [8, 30, 81]. Additionally, the analysis of the heterogeneity in other models and lattices is required to understand the universality of its behavior. The ($q > 2$) Potts model is a particularly interesting case, as

the time-dependence of the domain growth depends on the number of sides of each domain [14, 82, 83]. Preliminary results of $H(t)$ in the $2d$ $q > 2$ Potts model [64] indicate a peak in the heterogeneity, but further studies are needed to characterize the origin of this peak.

Appendix A

Dynamical cluster size heterogeneity

The paper included in this appendix is the complete text of Ref. [25], which is related to the results presented in chapter 5. Reproduced from Physical Review E 101, 012108 (2020); https://doi.org/10.1103/PhysRevE.101.012108

Dynamical cluster size heterogeneity

Amanda de Azevedo-Lopes [1], André R. de la Rocha,[1] Paulo Murilo C. de Oliveira,[2,3] and Jeferson J. Arenzon [1,3,*]

[1]*Instituto de Física, Universidade Federal do Rio Grande do Sul, CP 15051, 91501-970 Porto Alegre RS, Brazil*
[2]*Instituto de Física, Universidade Federal Fluminense, Av. Litorânea s/n, 24210-340 Boa Viagem, Niterói, RJ, Brazil*
[3]*Instituto Nacional de Ciência e Tecnologia–Sistemas Complexos, 22290-180 Rio de Janeiro RJ, Brazil*

Only recently has the essential role of the percolation critical point been considered on the dynamical properties of connected regions of aligned spins (domains) after a sudden temperature quench. In equilibrium, it is possible to resolve the contribution to criticality by the thermal and percolative effects (on finite lattices, while in the thermodynamic limit they merge at a single critical temperature) by studying the cluster size heterogeneity, $H_{eq}(T)$, a measure of how different the domains are in size. We extend this equilibrium measure here and study its temporal evolution, $H(t)$, after driving the system out of equilibrium by a sudden quench in temperature. We show that this single parameter is able to detect and well-separate the different time regimes, related to the two timescales in the problem, namely the short percolative and the long coarsening one.

I. INTRODUCTION

The ferromagnetic Ising model displays relatively homogeneous configurations when equilibrated either at temperatures $T \ll T_c$ or $T \gg T_c$, where T_c is its critical temperature. In the former case, thermal fluctuations in the giant, equilibrium background cluster of aligned spins are energetically inhibited but increase in probability with temperature. In the opposite limit, well above T_c, large domains of parallel spins are unstable against the thermal noise, which breaks them into small clusters whose average size decreases with temperature. At these extreme limits, the size diversity is smaller than that found close to T_c, where the distribution of allowed sizes is very broad, with a fully developed power law (in the thermodynamic limit, $L \to \infty$). Because neighboring parallel spins are not necessarily correlated, besides the geometric clusters described above, Coniglio-Klein (CK) clusters [1] may be built by removing a temperature-dependent fraction of the parallel pairs from the geometric clusters. These so called physical clusters have been useful in developing powerful simulation algorithms [2,3] and to unveil geometric properties for both models and experimental systems [4–9] that characterize both the equilibrium critical behavior [1,10] and the out-of-equilibrium dynamics [4]. The domain size distribution only becomes dense in the infinite-size limit or after ensemble averages are taken, while for a single, finite sample, space constraints forbid the presence of every possible cluster size, and the distribution gets truncated and sparse, subject to sample-to-sample fluctuations. A simple, global measure of the heterogeneity of a finite equilibrium configuration was introduced [11–15], only taking into account whether a given size is present in a configuration. The cluster size heterogeneity (H) is defined as the number of distinct cluster sizes,

irrespective of the number of equally sized domains, that are present in a finite-size sample.

The results for the equilibrium cluster size heterogeneity $H_{eq}(T)$ of the geometrical domains in the two-dimensional (2D) Ising model show a double peak structure at two very distinct temperatures. The small peak at $T_1 \simeq T_c$, associated with the thermal transition [14], is only observed for sufficiently large systems [15]. The peak grows as $H_{eq}(T_1) \sim L^{d/\tau}$, where $\tau = 379/187 \simeq 2.027$ is the Fisher exponent associated with the power-law cluster size distribution at the critical temperature of the Ising model [16,17]. In spite of the thermal and percolative transitions occurring at the same T_c, for finite systems these effects have not yet merged. Indeed, the percolative contribution appears as a second, much larger peak [15], at a temperature significantly higher than T_c [e.g., $T_2(L) \simeq 2T_c$ for $L = 640$]. The height of this second peak behaves as $H_{eq}(T_2) \sim L^{d/\tau'(L)}$. The exponent τ', associated with the height of the second peak, is closer to the percolation value, $\tau_p = 187/91 \simeq 2.055$, but it should cross over to τ as the two peaks merge in the thermodynamic limit. The double-peaked heterogeneity is a property of the geometric domains, while the physical (CK) domains, on the other hand, have a single peak similar to the susceptibility. Thus, for equilibrium finite samples, when describing the thermal and percolation transitions with the cluster heterogeneity of geometric domains, they seem to be disentangled, each one affecting the geometric properties more effectively at different temperatures (where the peaks are located), suggesting that the corresponding mechanisms may be different. The smaller the system is, the larger is the interval between these peaks. Whether this equilibrium separation translates to a temporal resolution is an interesting question. Thus, the main objective of this paper is to explore whether this measure may be useful to study not only equilibrium properties of simple models but their dynamics as well.

After a quench from infinite to a below-critical temperature, the out-of-equilibrium, single-flip dynamics of the

---

*arenzon@if.ufrgs.br

nonconserved order parameter 2D Ising model is first attracted by the percolative critical point and only then crosses over to the coarsening regime [18,19]. In the process, a percolation cluster first appears in the early stages (t_{p_1}) of the dynamics [18,19], but it only becomes stable on a longer, size-dependent timescale $t_p \sim L^{z_p}$ [20,21] where the exponent has been conjectured to be $z_p = 2/5$ [21] for the square lattice. This initially percolating cluster strongly correlates with the asymptotic state [20,22–28]. The domain growth eventually leads to the fully magnetized ground state for roughly 2/3 of the random initial configurations. The second most frequent outcome is a configuration of parallel stripes, while diagonal stripes have a much smaller probability (and a longer timescale). During the evolution, as the domains keep decreasing the excess energy at the curved interfaces, there appears a growing characteristic length associated with the coarsening regime, $\ell_d(t) \sim t^{1/z_d}$, with $z_d = 2$ [4].

The existence of a characteristic length obviously does not imply that the system is homogeneous, with domains similarly sized. A possible measure of the diversity of the actual sizes is the cluster size heterogeneity previously discussed, extended here to out-of-equilibrium configurations. While both the initial and the asymptotic equilibrium values of H_{eq} have been measured [15], there are many questions related to the intermediate time evolution of $H(t)$. In particular, since H_{eq} seems very responsive to the percolative equilibrium properties, does the dynamical size heterogeneity give information on the two regimes, approaching and departing from the critical percolation point, before the dynamics is dominated by coarsening? How distinct are these regimes? Is $H(t)$ monotonic in time or is there one or two peaks related to the equilibrium behavior? Is it possible for a single parameter to give information on the two length scales associated with coarsening? How do different initial and final temperatures change the behavior? We address some of these questions, showing that the dynamical cluster size heterogeneity, $H(t)$, is indeed a suitable observable that not only distinguishes among different dynamical regimes, but also provides quantitative access to the scaling laws related to the growth of correlations and of percolative clusters during the dynamics. Furthermore, we show that the time evolution of $H(t)$ correlates with the nature of the correlations present in the initial state, whether long-range if the quench is performed from $T_0 = T_c$, or absent from $T_0 \rightarrow \infty$. It is also noteworthy that the short-time regime of $H(t)$ resulting from the dynamics triggered from $T_0 \rightarrow \infty$ to $T = 0$ allows a quantitative connection with the percolation-related peak observed in the equilibrium heterogeneity, $H_{\mathrm{eq}}(T_2)$.

II. DYNAMICAL CLUSTER HETEROGENEITY

Following different temperature quench protocols that drive the system out of equilibrium, we study the 2D Ising model whose Hamiltonian is

$$\mathcal{H} = -J \sum_{\langle ij \rangle} \sigma_i \sigma_j, \qquad (1)$$

where $J > 0$, $\sigma_i = \pm 1$ is the spin at site i, and the sum is over all nearest-neighbor sites on an $L \times L$ square lattice with periodic boundary conditions (L is measured in units of the
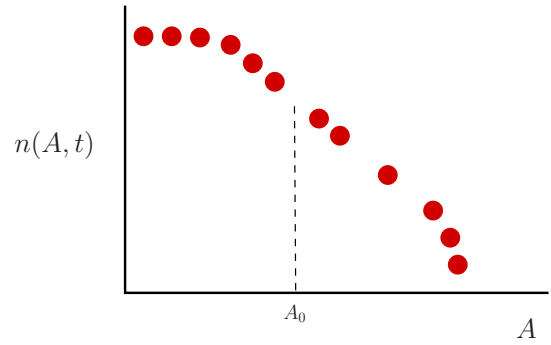

FIG. 1. Schematic cluster size distribution for a single, finite sample. Differently from an infinite system or averaged distribution, some sizes have no realizations. The smallest missing size, A_0, is indicated by a vertical dashed line, separating the dense region of the distribution, $A < A_0$, from the sparse one, $A > A_0$. Those sizes that are indeed present in the specific configuration define a measure of the cluster size heterogeneity (in this example, $H = 12$).

lattice spacing ℓ_0). We choose the initial temperature T_0 to be either infinite or the critical one, these equilibrium states thus differing by having zero or infinite range correlations, respectively. The fixed temperature adopted after the quench is $T = 0$. The simulations were performed on square lattices with linear sizes up to $L = 5120$. Averages up to 1000 samples were taken for the smaller systems, while larger sizes require fewer samples (100). When $T_0 = T_c$ it is necessary to equilibrate the system, and 1000 Swendsen-Wang steps were performed, while during the subsequent temporal dynamics, in all cases, a fast version of the single-spin Glauber algorithm at $T = 0$ was used [29]. Time is measured in Monte Carlo steps (MCSs), where one unit corresponds to N attempts to flip.

Along the time evolution of the system, we measure the dynamical cluster size heterogeneity $H(t)$, taking into account only the nonspanning clusters [the presence of one or more spanning clusters does not have a large influence on $H(t)$, except close to the asymptotic state, where it is small]. It is defined, as in the equilibrium case, as the number of different cluster sizes present at time t on a finite-size configuration (see the schematic depiction in Fig. 1). Although different domain definitions are possible, we consider here only geometrical domains, i.e., sets of connected parallel spins.

A. Quench from T_c to $T_f = 0$

After a quench from the equilibrium initial state at the Ising critical temperature ($T_0 = T_c$), the cluster size distribution of geometric domains evolves as [18,19]

$$n(A, t) \simeq \frac{c[\lambda(t + t')]^{\tau - 2}}{[A + \lambda(t + t')]^\tau}, \qquad (2)$$

where $n(A, t)dA$ is the average number of (nonspanning) clusters, per unit area, whose size is between A and $A + dA$. The constant $c \simeq 0.029$ [18,19] is very close to the Cardy-Ziff number [10], $c_h = 1/(8\pi\sqrt{3}) \simeq 0.023$, $\lambda \simeq 2$ (time and area units are unitary) is a temperature-dependent material constant (the chosen value is for $T = 0$), and t' is a microscopic
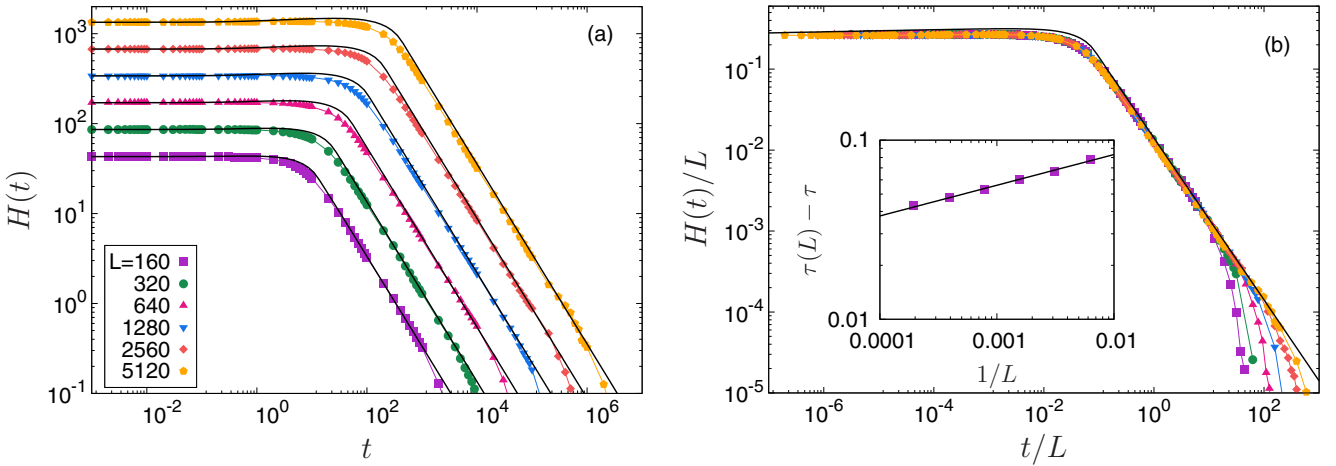
FIG. 2. Dynamical cluster size heterogeneity, $H(t)$, as a function of time (in MCS) after a temperature quench from $T_0 = T_c$ down to $T_f = 0$. For simplicity, only those samples that converged to a fully magnetized state were considered. (a) In the first regime, $t \lesssim t_0$, $H(t)$ presents a slow variation starting from $H_{\text{eq}}(T_c)$, Eq. (7), while in the power-law regime, the behavior is t^{-1}. The whole behavior is well approximated by Eq. (6) and shown as solid lines. We consider $c \simeq 0.029$, $\lambda \simeq 2$, and τ to take finite-size effects into account, as a fitting parameter. (b) The simulation data collapse well onto a universal curve, $H(t) = Lf(t/L)$, using the asymptotic value of the Fisher exponent, $\tau = 379/187$. The agreement with Eq. (6) is also very good. The inset shows that the values of $\tau(L)$ that better fit the data in panel (a) do converge to the correct value as L increases.

time such that $\lambda t' \simeq 1$. The above distribution is an average while the heterogeneity H is measured from single configurations as schematically shown in Fig. 1. At the moment of the quench, there is an already stable spanning cluster, $t_p \simeq t_{p_1} \simeq 0$ [20]. Differently from the averaged distribution of Eq. (2), for a single sample there are holes in the distribution, as not all possible sizes may be present. Denoting by $A_0(t)$ the smallest missing size at time t, the sample cluster size distribution is dense for $A < A_0(t)$ and sparse above it. If ℓ_0 is a microscopic length and $(\ell_0 L)^2$ is the area of the system, A_0 is the size such that $(L\ell_0)^2 n(A_0, t)\ell_0^2 \sim 1$. Thus, setting $\ell_0 = 1$, we obtain that

$$A_0(t) \simeq (\lambda t + 1)\left[\left(\frac{L\sqrt{c}}{\lambda t + 1}\right)^{2/\tau} - 1\right]\Theta(t - t_0) \quad (3)$$

and the dense region of the cluster size distribution, on average, disappears after a time

$$t_0 \simeq \frac{L\sqrt{c}}{\lambda}. \quad (4)$$

The cluster size heterogeneity after the quench, $H(t)$, is shown in Fig. 2(a) for different lattice sizes. The coarsening process moves the whole distribution to the left, removing the smallest clusters, initially changing very slowly the value of $H(t)$ up to $t \simeq t_0$. It then crosses over to a different regime, decreasing as a power law, when the dense region is about to disappear. Once the remaining distribution is sparse, almost all present cluster sizes appear only once, and $H(t)$ becomes equivalent to the number of clusters. These two contributions to $H(t)$ may be approximated by

$$H(t) \simeq A_0 + L^2 \int_{A_0}^{\infty} dA\, n(A, t), \quad (5)$$

where the first and second terms correspond, respectively, to the size of the dense region and the number of clusters in the sparse one. Using Eqs. (2) and (3) with Eq. (5), we get an

expression for $H(t)$ at all times:

$$H(t) \simeq \begin{cases} (\lambda t + 1)\left[\frac{\tau}{\tau - 1}\left(\frac{L\sqrt{c}}{\lambda t + 1}\right)^{2/\tau} - 1\right], & t \lesssim t_0, \\ \frac{L^2 c}{\tau - 1}\frac{1}{\lambda t + 1}, & t \gtrsim t_0. \end{cases} \quad (6)$$

Notice that $H(t \to \infty) = 0$ in the above expression because, in our definition, the spanning clusters are not accounted for. At $t = t_0 \simeq L\sqrt{c}/\lambda$, both terms give $H(t_0) \simeq L\sqrt{c}/(\tau - 1)$ while the initial value, corresponding to the equilibrium state at T_c, is

$$H(0) \simeq H_{\text{eq}}(T_c) \simeq \frac{\tau}{\tau - 1}c^{1/\tau}L^{2/\tau}. \quad (7)$$

Figure 2(a) also compares the simulations with the above expression for $H(t)$ as solid lines. The agreement is pretty good, except where there is a change of regime, close to t_0, where $n(A, t)$ is still significant and there may be more than one cluster with the same size, originating the small deviation seen in Figs. 2(a) and 3. Despite its exact value being known, we have considered τ as a fitting parameter in order to take finite-size effects into account. The inset of Fig. 2(b) shows the values of $\tau(L)$ obtained from each fit (performed only for the initial times, $t < 10^{-2}$) and how they converge to $\tau = 379/187$ as $L \to \infty$. Figure 2(b) also shows that the same data, when properly rescaled, present an excellent collapse. From Eq. (6) we see that the rescaling is $H(t) = L^{-1}f(t/L)$, where $f(x) \sim x^{-1}$ (a power-law decay) for $x \gg 1$, and $x^{1-2/\tau}$ (a very slow increase) for $x \ll 1$. There is a further, subtle feature of the numerical data, again well captured by Eq. (6), that can be seen in Fig. 3: $H(t)$ is not a monotonous function. It presents a maximum $H(t_{\max})$ whose location agrees well with the numerical data,

$$\frac{\lambda t_{\max} + 1}{L} = \sqrt{c}\left(\frac{\tau - 2}{\tau - 1}\right)^{\tau/2} \simeq 0.004, \quad (8)$$
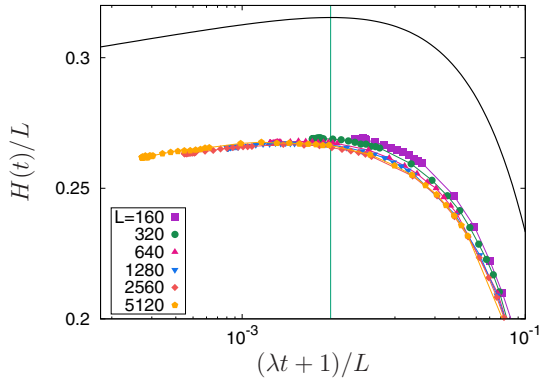
FIG. 3. Zoom into the region close to the end of the plateau, after a quench from $T_0 = T_c$, showing a very small peak at t_{max} (vertical line), Eq. (8). The height of the peak in Eq. (6) depends on the precise value of c, and the difference from the numerical data appears larger because of the chosen scale.

although the height has a small deviation (enlarged in Fig. 3 because of the chosen vertical scale).

B. Quench from $T_0 \to \infty$ to $T_f = 0$

When quenching the system from $T_0 \to \infty$ down to $T_f = 0$, the general cluster size heterogeneity behavior can be seen in Fig. 4(a). At the initial high temperature, despite spins being uncorrelated, small clusters of parallel spins are present. The initial heterogeneity is not very large and slowly grows with the system size, $H_{eq}(T \to \infty) \sim \ln L$ [12,14,15], as can be observed in Fig. 4(a). Soon after the quench, $H(t)$ presents a pronounced peak followed by a growing, intermediate plateau before the final power-law decrease toward the asymptotic

state. The dynamics is eventually attracted [22,24,25,27] to a state that is either fully magnetized or contains on- or off-axis stripes. Although the results are similar, for simplicity we kept only those samples that got, eventually, fully magnetized.

Differently from the previous case, the initial equilibrium state at $T_0 \to \infty$ is not critical. Nonetheless, before entering the scaling regime, the system first approaches the random site percolation critical state [18,19], with an average cluster size distribution given by a power law $A^{-\tau_p}$ whose Fisher exponent is $\tau_p = 187/91$. As discussed in the Introduction, the first occurrence of a percolating, albeit unstable, cluster is at the early time t_{p_1}, while at t_p it becomes stable. After the cluster size distribution becomes critical at t_{p_1}, its time evolution is well approximated by [18,19,21]

$$n(A, t) \simeq \frac{2c[\lambda(t + t_{p_1} + t')]^{\tau_p - 2}}{[A + \lambda(t + t_{p_1} + t')]^{\tau_p}}, \qquad (9)$$

where the factor 2 in the numerator comes from the existence of clusters with both positive and negative magnetizations, while in the related percolation problem only particle clusters, not voids, are accounted for. In analogy to the previous case, the behavior of $H(t)$ after a quench from $T_0 \to \infty$, calculated using Eq. (5), is given by

$$H(t) \simeq \begin{cases} (\lambda t + 1)\left[\frac{\tau_p}{\tau_p - 1}\left(\frac{L\sqrt{2c}}{\lambda t + 1}\right)^{2/\tau_p} - 1\right], & t_{p_1} < t \leqslant t_0, \\ \frac{2L^2 c}{\tau_p - 1}\frac{1}{\lambda t + 1}, & t \geqslant t_0, \end{cases}$$
$$(10)$$

where, in this case, $t_0 \simeq L\sqrt{2c}/\lambda$. As in the $T_0 = T_c$ case, $H(t)$ also has a broad and small maximum before t_0, more precisely at $(\lambda t_{max} + 1)/L = \sqrt{2c}[(\tau_p - 2)/(\tau_p - 1)]^{\tau_p/2} \simeq 0.011$. However, this maximum does not appear in the simulation, and $H(t)$ seems to always decrease. This is
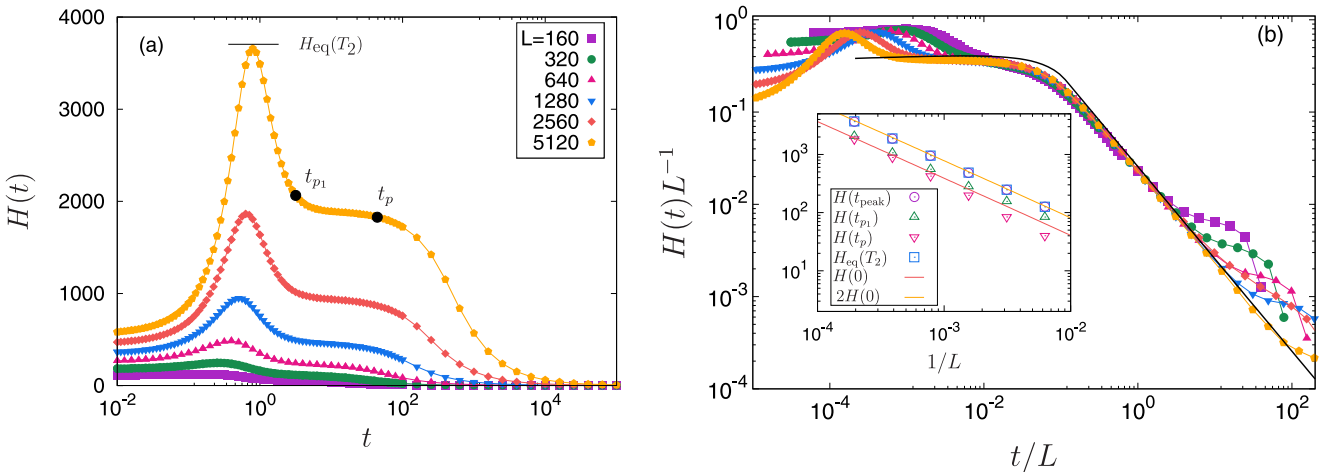
FIG. 4. (a) Dynamical cluster size heterogeneity $H(t)$ as a function of time (in MCS) after a temperature quench from $T_0 \to \infty$ down to $T_f = 0$. For simplicity, only those samples that converged to a fully magnetized state were considered. For the largest size, we indicate the times when a percolating cluster first appears and when it becomes stable, t_{p_1} and t_p, respectively. In Ref. [15] it was observed that the equilibrium heterogeneity, H_{eq}, has a second, larger peak at $T_2(L)$, well above $T_1 \simeq T_c$ where another, smaller peak is located. The value of $H_{eq}(T_2)$ agrees well with $H(t_{peak})$ and is shown, for the largest simulated size only, as a small horizontal line on top of the peak. (b) Data collapse. As the system size increases, a region between t_{p_1} and t_p, where $H(t)$ slowly changes, becomes apparent. The behavior for $t > t_{p_1}$ is well approximated by Eq. (10) with $\tau_p = 187/91$ (solid line). The inset shows, in the upper straight line, the height of the peaks $H(t_{peak})$ and $H_{eq}(T_2)$, indistinguishable at this scale, along with Eq. (12), as a function of the system size. The data below (triangles) correspond to the values of $H(t_p)$ and $H(t_{p_1})$ that, albeit different, get close as L increases.

because, for the sizes considered here, the region $t \lesssim t_0$ may not yet be fully developed, or it may be because of the presence of the initial, precursor maximum that reverses the behavior below t_{p_1}.

Since Eq. (9) considers an effective initial state at the percolation threshold, the above expression for $H(t)$ is not expected to capture any feature before t_{p_1}. Indeed, $t = 0$ corresponds to the beginning of the slowly changing region, which roughly extends between t_{p_1} and t_p (and whose width depends on L), observed in Figs. 4(a) and 4(b):

$$H(0) \simeq \frac{\tau_p}{\tau_p - 1}(L\sqrt{2c})^{2/\tau_p}. \quad (11)$$

In contrast with the $T_0 = T_c$ case, $H(t)$ has a very pronounced peak just before the appearance of the first percolating cluster, i.e., $t_{\text{peak}} < t_{p_1}$, which is a precursor feature of the percolating state. After the quench, as the correlations build larger clusters, the size distribution widens and $H(t)$ increases. However, as the largest cluster increases, less space remains for the other clusters. Thus, a state of maximum heterogeneity occurs slightly before t_{p_1} and the associated percolation transition. In particular, the height of the peak seems to correspond to the equilibrium heterogeneity at the second peak observed in Ref. [15], i.e., for each system size, $H(t_{\text{peak}}) \simeq H_{\text{eq}}(T_2)$, as indicated by a small horizontal line in Fig. 4(a) (only for the largest L). Moreover, we numerically observe that it is twice the height at t_{p_1}:

$$H(t_{\text{peak}}) \simeq H_{\text{eq}}(T_2) \simeq 2H(0) \simeq \frac{2\tau_p}{\tau_p - 1}(L\sqrt{2c})^{2/\tau_p}. \quad (12)$$

For $t \geqslant t_0$, the power-law behavior of $H(t)$ is similar to the $T_0 = T_c$ case and accounts for the number of clusters, differing only by the value of τ_p and the factor 2 in the numerator. The data for $t > t_{p_1}$ are well described by Eq. (10), as can be seen in Fig. 4(b).

Nonetheless, by rescaling both $H(t)$ and time by L [Fig. 4(b)], although the finite-size effects are somewhat stronger than in the $T_0 = T_c$ case, both the agreement with Eq. (10) and the collapse in the same region are very good.

Despite the strong, early peak being a precursor effect of the percolating cluster that appears soon afterward, $t_{\text{peak}} < t_{p_1}$, it has a strong connection with the equilibrium measures of Ref. [15]. Indeed, as the temperature is slowly decreased, the equilibrium peak at T_2 [15] also anticipates the first appearance of a percolating cluster. Interestingly, the data collapse in Fig. 4(b) fails in the very early regime, indicating that the dynamical scaling length $\xi(t) \sim t^{1/2}$ is not the sole relevant length scale after the quench. The precursor peak shifts to the left, indicating that a scaling factor L^α, with $\alpha < 1$, should be considered instead of L. Indeed, as seen in Fig. 5, a good collapse around the peak is obtained with $\alpha \simeq 0.22$. However, notice that although the peaks are well collapsed, neither the black circles indicating t_{p_1} nor the black squares for t_p present a good convergence. Different values of the exponent α can, on the other hand, collapse those characteristic times. For t_p, it was shown in Ref. [21] that the exponent is 0.4.

To check how universal the $H(t)$ behavior is, we compare in Fig. 6, for $L = 1280$, the behavior of $H(t)$ for the Ising model after a quench from $T_0 \to \infty$ and the Voter model (VM) evolving from a fully uncorrelated state. The VM is
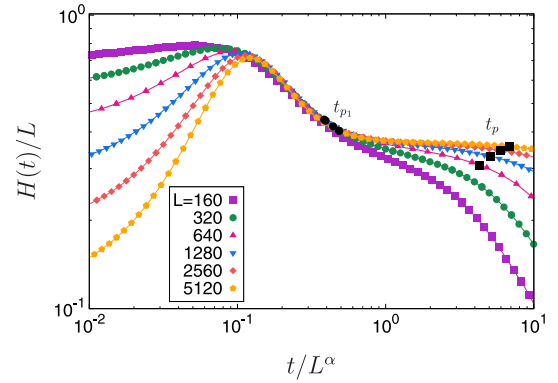

FIG. 5. Rescaling of the early time region near the peak of $H(t)$ after a temperature quench from $T_0 \to \infty$. The region that includes both the peak and t_{p_1} is well collapsed using $\alpha \simeq 0.22$.

interesting as there is no bulk noise, and detailed balance is not obeyed. Instead of considering the energy variation for a putative flip, as in the Ising model, in the VM the spin chooses and aligns with a single neighbor. As shown in Ref. [30], the timescales are all larger in the VM, nonetheless the overall behavior of $H(t)$ is similar, Fig. 6. Moreover, defining t_{p_1} and t_p as above (even if the critical properties of the percolating cluster do not correspond to critical percolation [30]), we can see in Fig. 6 that they are related, respectively, to the end of the precursor peak and the end of the plateau. A remarkable feature in this figure is the height of the early peak, which is roughly the same in both models, suggesting a more general mechanism.

III. CONCLUSIONS

In equilibrium at high temperatures, domains of parallel neighboring spins are not large and within a limited range of sizes, thus the number of different domain sizes in a given configuration, $H_{\text{eq}}(T)$, is small. Decreasing the temperature, spins become more correlated and the clusters increase and
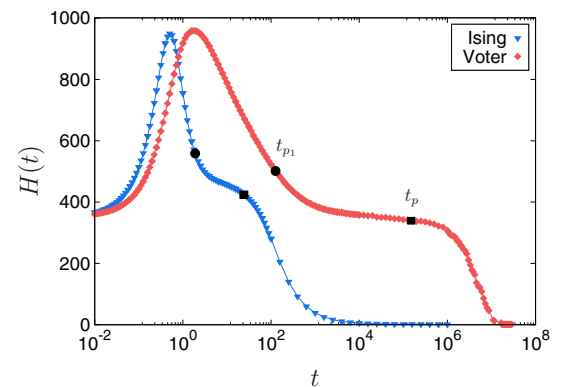

FIG. 6. Comparison between the time evolution of $H(t)$ for the Ising at $T = 0$ and the Voter model, both starting from an initially uncorrelated state ($T_0 \to \infty$). The system linear size is $L = 1280$ and time is in MCS. Notice that the precursor peak has roughly the same height for the two models, suggesting a common mechanism.

diversify, increasing H_{eq}. However, as some clusters get comparable to the size of the system, the lack of space tends to decrease the diversity. In the presence of these competing mechanisms, one expects a peak in H_{eq}. Remarkably, for geometric domains, two peaks are present [15], one near the temperature where the percolating cluster first appears [31] and a second one very close to T_c. We extended here this equilibrium measure of how heterogeneous the domains are in size to nonequilibrium situations, $H(t)$. Specifically, we explore its usefulness in the nonconserved order-parameter dynamics of the 2D Ising model after a sudden quench in temperature, confirming that this observable unveils the rich interplay between percolation and ferromagnetism either close to the phase transition (equilibrium) or at short-time scales during the dynamics.

For quenches starting at T_c, $H(t)$ presents an initial plateau that increases very slowly, attaining a shallow maximum before crossing over to a power-law behavior. In this latter regime, the sample size distribution is very sparse and the probability of two domains having the same size is small. The heterogeneity does correspond, in this time regime, to the total number of clusters and decays as a power law. When the system, instead, is first equilibrated at $T_0 \to \infty$ (random spin configuration), in addition to these regimes *after* it passes through the percolation critical point, there is also a very pronounced peak that is a precursor indication that a giant, percolating cluster is being built.

The rich behavior of $H(t)$ suggests that it would be interesting to consider several extensions, both in equilibrium and after a quench in temperature. While for the Ising model each domain has a single neighbor and its size decreases at the same, constant rate, for the ($q > 2$) Potts model domains may either decrease or increase as their time evolution, given by the von Neumann law, depends on their number of sides. The coarsening behavior is thus richer [32–34]. As a consequence, domains with the same area but a different number of sides have a larger probability of evolving into different sizes, increasing the heterogeneity. Such a mechanism, which breaks the degeneracy of areas depending on the number of sides, is absent in the Ising model. Another interesting case is the Ising model with conserved order parameter [30,35,36] or disorder [37–39]. Although we focused here on geometric domains, the heterogeneity associated with the Coniglio-Klein clusters [1] would also be of interest [15], along with the heterogeneity of perimeters. The dynamics of the 3D Ising model is more challenging [24,40,41], as multiple frozen percolating clusters coexist and, for sufficiently large systems, the ground state is never reached. In addition, the thermal and percolation transitions do not coincide. Finally, it would be important to verify our results in experimental setups [5,9].

[1] A. Coniglio and W. Klein, J. Phys. A **13**, 2775 (1980).

[2] R. H. Swendsen and J.-S. Wang, Phys. Rev. Lett. **58**, 86 (1987).

[3] U. Wolff, Phys. Rev. Lett. **62**, 361 (1989).

[4] A. J. Bray, Adv. Phys. **43**, 357 (1994).

[5] A. Sicilia, J. J. Arenzon, I. Dierking, A. J. Bray, L. F. Cugliandolo, J. Martinez-Perdiguero, I. Alonso, and I. C. Pintre, Phys. Rev. Lett. **101**, 197801 (2008).

[6] M. Castro, R. Cuerno, M. M. Garcia-Hernandez, and L. Vazquez, Phys. Rev. Lett. **112**, 094103 (2014).

[7] G. B. Deepa and R. Pratibha, Phys. Rev. E **89**, 042504 (2014).

[8] P. N. Timonin, Physica A **527**, 121402 (2019).

[9] R. Almeida and K. A. Takeuchi (private communication).

[10] J. Cardy and R. M. Ziff, J. Stat. Phys. **110**, 1 (2003).

[11] H. K. Lee, B. J. Kim, and H. Park, Phys. Rev. E **84**, 020101(R) (2011).

[12] J. D. Noh, H. K. Lee, and H. Park, Phys. Rev. E **84**, 010101(R) (2011).

[13] J.-P. Lv, X. Yang, and Y. Deng, Phys. Rev. E **86**, 022105 (2012).

[14] W. S. Jo, S. D. Yi, S. K. Baek, and B. J. Kim, Phys. Rev. E **86**, 032103 (2012).

[15] A. R. de la Rocha, P. M. C. de Oliveira, and J. J. Arenzon, Phys. Rev. E **91**, 042113 (2015).

[16] A. L. Stella and C. Vanderzande, Phys. Rev. Lett. **62**, 1067 (1989).

[17] W. Janke and A. M. J. Schakel, Phys. Rev. E **71**, 036703 (2005).

[18] J. J. Arenzon, A. J. Bray, L. F. Cugliandolo, and A. Sicilia, Phys. Rev. Lett. **98**, 145701 (2007).

[19] A. Sicilia, J. J. Arenzon, A. J. Bray, and L. F. Cugliandolo, Phys. Rev. E **76**, 061116 (2007).

[20] T. Blanchard, F. Corberi, L. F. Cugliandolo, and M. Picco, Europhys. Lett. **106**, 66001 (2014).

[21] T. Blanchard, L. F. Cugliandolo, M. Picco, and A. Tartaglia, J. Stat. Mech. (2017) 113201.

[22] B. Derrida, P. M. C. de Oliveira, and D. Stauffer, Physica A **224**, 604 (1996).

[23] A. Lipowski, Physica A **268**, 6 (1999).

[24] V. Spirin, P. L. Krapivsky, and S. Redner, Phys. Rev. E **63**, 036118 (2001).

[25] V. Spirin, P. L. Krapivsky, and S. Redner, Phys. Rev. E **65**, 016119 (2001).

[26] K. Barros, P. L. Krapivsky, and S. Redner, Phys. Rev. E **80**, 040101(R) (2009).

[27] J. Olejarz, P. L. Krapivsky, and S. Redner, Phys. Rev. Lett. **109**, 195702 (2012).

[28] T. Blanchard and M. Picco, Phys. Rev. E **88**, 032131 (2013).

[29] M. Newman and G. Barkema, *Monte Carlo Methods in Statistical Physics* (Oxford University Press, New York, 1999).

[30] A. Tartaglia, L. F. Cugliandolo, and M. Picco, J. Stat. Mech. (2018) 083202.

[31] H. Ricateau, L. F. Cugliandolo, and M. Picco, J. Stat. Mech. (2018) 013201.

[32] M. P. O. Loureiro, J. J. Arenzon, L. F. Cugliandolo, and A. Sicilia, Phys. Rev. E **81**, 021129 (2010).

[33] M. P. O. Loureiro, J. J. Arenzon, and L. F. Cugliandolo, Phys. Rev. E **85**, 021135 (2012).

[34] J. Denholm and S. Redner, Phys. Rev. E **99**, 062142 (2019).

[35] A. Sicilia, Y. Sarrazin, J. J. Arenzon, A. J. Bray, and L. F. Cugliandolo, Phys. Rev. E **80**, 031121 (2009).

[36] H. Takeuchi, Y. Mizuno, and K. Dehara, Phys. Rev. A **92**, 043608 (2015).

[37] A. Sicilia, J. J. Arenzon, A. J. Bray, and L. F. Cugliandolo, Europhys. Lett. **82**, 10001 (2008).

[38] F. Corberi, L. F. Cugliandolo, F. Insalata, and M. Picco, Phys. Rev. E **95**, 022101 (2017).

[39] F. Corberi, L. F. Cugliandolo, F. Insalata, and M. Picco, J. Stat. Mech. (2019) 043203.

[40] J. J. Arenzon, L. F. Cugliandolo, and M. Picco, Phys. Rev. E **91**, 032142 (2015).

[41] N. Vadakkayil, S. Chakraborty, and S. K. Das, J. Chem. Phys. **150**, 054702 (2019).

Appendix B

Maximal Diversity and Zipf's Law

The paper included in this appendix is the complete text of Ref. [26], which is a preprint related to the results presented in chapter 4. Reproduced from arXiv:2103.09143 [cond-mat.stat-mech]; https://arxiv.org/abs/2103.09143

Maximal Diversity and Zipf's Law

Onofrio Mazzarisi[1,2,*], Amanda de Azevedo-Lopes[3], Jeferson J. Arenzon[3,4], Federico Corberi[2,5]

[1]*Max Planck Institute for Mathematics in the Sciences, Inselstraße 22, 04103 Leipzig, Germany*
[2]*Dipartimento di Fisica "E. R. Caianiello",Università di Salerno,*
via Giovanni Paolo II 132, 84084 Fisciano (SA), Italy
[3]*Instituto de Física, Universidade Federal do Rio Grande do Sul, CP 15051, 91501-970 Porto Alegre RS, Brazil*
[4]*Instituto Nacional de Ciência e Tecnologia - Sistemas Complexos, Rio de Janeiro RJ, Brazil*
[5]*INFN, Gruppo Collegato di Salerno, and CNISM, Unità di Salerno,*
*Università di Salerno, via Giovanni Paolo II 132, 84084 Fisciano (SA), Italy**

Zipf's law describes the empirical size distribution of the components of many systems in natural and social sciences and humanities. We show, by solving a statistical model, that Zipf's law co-occurs with the maximization of the diversity of the component sizes. The law ruling the increase of such diversity with the total dimension of the system is derived and its relation with Heaps' law is discussed. As an example, we show that our analytical results compare very well with linguistics datasets.

Diversity is a central concept in ecology, economics, information theory, and other natural and social sciences. It can be quantified by diversity indices [1, 2], such as (species) richness, the Gini-Simpson index or Shannon entropy, which characterize the system under study from different angles. Loosely understanding the term, high diversity may represent an advantage in terms of resilience and performance. This is the case, for instance, in ecology, where well differentiated ecosystems are often (see, e.g., Ref. [3] for the debate on this topic) considered to be more stable [4–6], and in economy as well: strong countries have a well diversified production [7].

In most cases diversity is hindered by limiting factors. For an ecosystem the amount of energy and chemical factors available does not allow an unbounded increase of the population. Similarly, the number of different items produced by an economy is limited by its strength. The diversity drift is therefore a complex optimization process.

Elaborating on that, in this Letter we consider a quantity, the diversity index D, that takes the aforementioned restrictions into account. Its definition can be given in terms of richness [1], a quantity that counts the number of different types which are present in a collection of items. For instance, the set of integers $\{3, 7, 1, 9, 0, 1\}$ is richer than $\{3, 2, 3, 7, 7, 2\}$, because there are 5 different figures in the former and only 3 in the latter. We consider situations where types can be identified by quantitative labels s, as in the example above. D is the richness of the collection of entities $\{s_1, \ldots, s_N\}$, with arbitrary N, but subjected to the additive constraint $S = \sum_{n=1}^{N} s_n$. Here s_n represents the portion of the total resource S assigned to the n-th entity of the ensemble, i.e. its size. Entities can be cities [8] of a country with total population S, distinct words [9] occurring with absolute frequencies $\{s_n\}$ in a book of size S or genes [10] expressed with abundances $\{s_n\}$ where S is the total number of proteins synthesized in a cell.

These systems are instances where the Zipf's law [11,

12] is observed to hold. Other well known examples include [13] GDP of nations [14], firm sizes [15], species in taxa [16] and fragmentation processes [17]. To explain Zipfian behaviour many generative mechanisms have been proposed [18–24]; some of them, though, suffer drawbacks such as a lack of generality or limited predictive power in singling out the correct power law exponent. Zipf's law has been also framed in a broader statistical perspective [25–27]. For instance, it has been shown to be associated to maximally informative samples in modeling complex systems [26, 28].

In this Letter we show that the maximization of the diversity index D and the occurrence of Zipf's law in the distribution of the component sizes $\{s_n\}$ are naturally related. This is achieved by deriving, in a statistical model, a *diversity law* that can be used to estimate the index D of distributions of empirical data. We put our results to the test in the context of quantitative linguistics showing remarkable agreement with data taken from the Gutenberg English texts database [29]. Finally, within our approach we also recover in a simple way the expression of Heaps' law [30, 31] and discuss its relation with the diversity law.

The model.—Consider sets of independent and identically distributed integer random variables $\{s_n\}$, sampled from a generic probability distribution $p(s)$. We call s_n the size of the n-th component (or entity). $p(s)$ will be denoted as the *bare* distribution, since the effective (*dressed*) distribution of the s_n is shaped by the presence of a global constraint $\sum_{n=1}^{N} s_n = S$, where S is the total dimension of the system. N is the fluctuating number of entities that, according to the particular extraction of the $\{s_n\}$, is needed to fulfill the constraint. The probability of a particular configuration $\mathcal{C} \equiv [\{s_1, \ldots, s_N\}; N]$ is given by

$$p_S(\{s_1, \ldots, s_N\}; N) = \frac{1}{Z_S} \prod_{n=1}^{N} p(s_n) \delta_{\sum_{n=1}^{N} s_n, S}, \quad (1)$$

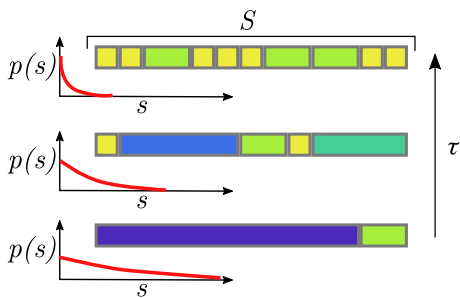where the constraint is enforced by the Kronecker delta.

FIG. 1. Pictorial representation of the problem. Power laws, $p(s) \sim s^{-\tau}$, are sketched with an increasing exponent τ (from bottom to top) alongside with relative typical realizations $\{s_n\}$. Entities of the same size are depicted as blocks of the same color and in all the cases they add up to S, the total length of the bar. For large values of τ, most of the entities have small and similar sizes, resulting in a poor diversity D. In the other limit, small τ, large sizes do get more probable but the total number of entities required to fill S is smaller. Consequently, diversity is again small. The diversity is expected to be maximal for an intermediate value of τ.

The quantities $Z_S = \sum_{N=1}^{\infty} Z_S(N)$ and

$$Z_S(N) \equiv \sum_{s_1=1}^{S} \sum_{s_2=1}^{S} \dots \sum_{s_N=1}^{S} \prod_{n=1}^{N} p(s_n) \delta_{\sum_{n=1}^{N} s_n, S} \quad (2)$$

play the role of partition functions in an ensemble where N is fluctuating or fixed, respectively. One obtains the probability of having a number N of entities as $p_S(N) = Z_S(N)/Z_S$. The dressed probability of observing a size s can be written using Eq. (2) as

$$p_S(s) = \frac{p(s)}{\sum_{N=1}^{\infty} N Z_S(N)} \sum_{N=1}^{\infty} N Z_{S-s}(N-1), \quad (3)$$

where the factor N appears because we do not distinguish among components.

If t_s is the number of times the value $s \in [1, S]$ is found in a given configuration $\mathcal{C}$, the diversity index D (hereafter also referred to as simply *diversity*) is defined as

$$D = \sum_{s=1}^{S} (1 - \delta_{t_s,0}), \quad (4)$$

namely the number of different values assumed by the entities. The probability $p_S(D)$ of observing a certain value of D is formally given in the Supplemental Material (SM) [32].

We are interested in highly diverse configurations, therefore we consider power law bare probability distributions, which grant access to a wide range of sizes,

$$p(s) = \frac{s^{-\tau}}{\Lambda(\tau, S)} \quad ; \text{for} \quad 1 \le s \le S, \quad (5)$$

and $p(s) = 0$ otherwise. The normalisation $\Lambda(\tau, S) = \zeta(\tau) - \zeta(\tau, S+1)$ is a generalized harmonic number and can be written in terms of the Riemann and Hurwitz zeta functions, $\zeta(x)$ and $\zeta(x, y)$ respectively.

Our goal is to compute the average diversity $\langle D \rangle_S$ and the value of τ which maximizes it (see Fig. 1). Given the complicated expression of $p_S(D)$, we directly determine $\langle D \rangle_S$ as follows. We split the range of sizes into $s \le s^*$ and $s > s^*$ [33], where s^* is defined by $\langle N \rangle_S p_S(s^*) = 1$; these two sectors contribute to $\langle D \rangle_S$ as

$$\langle D \rangle_S \simeq s^* + \langle N \rangle_S \sum_{s=s^*}^{S} p_S(s). \quad (6)$$

Indeed, given an average number of entities $\langle N \rangle_S$, there is at least one of them for each size $s \le s^*$, contributing to the first term on the r.h.s. of Eq. (6). The second term is the average number of entities with $s > s^*$. Since these are represented at most once this also corresponds to their contribution to $\langle D \rangle_S$.

With Eq. (6), the evaluation of $\langle D \rangle_S$ only depends on the knowledge of $\langle N \rangle_S$ and $p_S(s)$. These quantities can be computed numerically with an exact recursive method, as discussed in the SM [32]. For an analytical treatment of the problem it is possible to approximate the dressed probability distribution with the bare one, i.e. $p_S(s) \simeq p(s)$ (see the SM [32]). This simplification leads to an asymptotic expression for $\langle D \rangle_S$ which is accurate for large S. The average component size reads $\langle s \rangle_S = \sum_{s=1}^{S} s p_S(s) \simeq \sum_{s=1}^{S} s p(s) = \Lambda(\tau-1, S)/\Lambda(\tau, S)$, from which $\langle N \rangle_S$ can be obtained as $\langle N \rangle_S \simeq S/\langle s \rangle_S$. Using $\Lambda(x, S) \simeq \zeta(x) + S^{1-x}/(1-x)$ for $x \neq 0, 1$, $\Lambda(1, S) \simeq \ln S$ and $\Lambda(0, S) \simeq S$, valid for large S, we obtain

$$\langle N \rangle_S \simeq \begin{cases} (2-\tau)/(1-\tau) & ; \text{for} \quad \tau < 1 \\ \ln S & ; \text{for} \quad \tau = 1 \\ \zeta(\tau)(2-\tau)S^{\tau-1} & ; \text{for} \quad 1 < \tau < 2 \\ \zeta(2)S/\ln S & ; \text{for} \quad \tau = 2 \\ \zeta(\tau)S/\zeta(\tau-1) & ; \text{for} \quad \tau > 2, \end{cases} \quad (7)$$

which is in excellent agreement with the exact determination, see the SM [32]. From the definition $\langle N \rangle_S p_S(s^*) = 1$, we obtain $s^*(\tau, S) \simeq [S/\Lambda(\tau-1, S)]^{1/\tau}$ and, substituting in Eq. (6), one arrives at the sought after result for the average diversity: $\langle D \rangle_S \simeq s^* + (s^*)^{\tau} [\zeta(\tau, s^*) - \zeta(\tau, S+1)]$. Approximating the Riemann zeta function by $\zeta(x) \simeq (x-1)^{-1} + \gamma$, where $\gamma \simeq 0.577$ is the Euler constant, we can write

$$s^*(\tau, S) \simeq S^{1/\tau} \left[\gamma + (S^{2-\tau} - 1)/(2-\tau) \right]^{-1/\tau} \quad (8)$$

$$\langle D \rangle_S \simeq \frac{\tau s^* - (s^*)^{\tau} S^{1-\tau}}{\tau - 1}, \quad (9)$$

where the appropriate limits for $\tau = 1$ and 2 are taken.

This determination of $\langle D \rangle_S$ is portrayed in Fig. 2 and compared with the outcome of numerical simulations
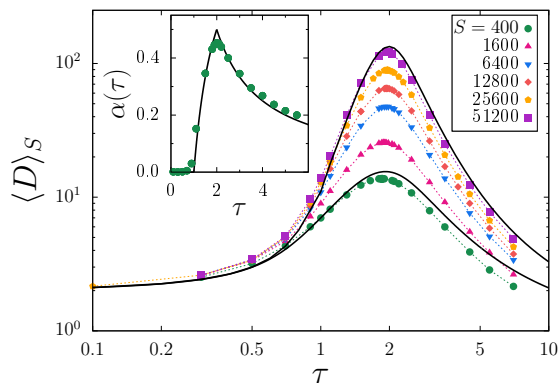
FIG. 2. Average diversity, $\langle D \rangle_S$, obtained through numerical simulations for various sizes S (see key), dashed lines are guides to the eye. Entities are extracted from the bare distribution Eq. (5) and the statistics is restricted over configurations respecting the global constraint. Results are averaged over 10^4-10^6 configurations. Solid lines (shown only for the extreme sizes), are the analytical solutions given by Eq. (9). Inset: The exponent $\alpha(\tau)$, defined below Eq. (10), as a function of τ. Solid line is the analytical result, dots are fits from the simulation data.

finding a very good agreement. For large S, the leading contribution to Eq. (9) is

$$\langle D \rangle_S \simeq \begin{cases} (2-\tau)/(1-\tau) & ; \text{ for } \tau < 1 \\ \ln S & ; \text{ for } \tau = 1 \\ \dfrac{\tau(2-\tau)^{1/\tau}}{\tau-1} S^{1-1/\tau} & ; \text{ for } 1 < \tau < 2 \\ 2\,(S/\ln S)^{1/2} & ; \text{ for } \tau = 2 \\ \dfrac{\tau}{\tau-1}\left[\dfrac{S}{\gamma+(\tau-2)^{-1}}\right]^{1/\tau} & ; \text{ for } \tau > 2 . \end{cases}$$

(10)

One has $\langle D \rangle_S \sim S^{\alpha(\tau)}$ with $\alpha(\tau) = 0$ for $\tau < 1$, $\alpha(\tau) = 1 - 1/\tau$ for $1 < \tau < 2$ and $\alpha(\tau) = 1/\tau$ for $\tau > 2$, see inset of Fig 2. In conclusion, for large S, $\langle D \rangle_S$ presents a pronounced peak at $\tau = 2$. This behavior is due to the competition between the abundance of entities $\langle N \rangle_S$, favored by large τ, and the diversity of their sizes which instead is enhanced by small τ, as shown in Fig. 1. We remark that the upper bound obtained by considering the deterministic partition $S \simeq 1+2+\ldots+D$ with $D \sim S^{1/2}$ overpowers the $\tau = 2$ case only by a logarithmic factor.

Let us mention that, although we explicitly solved the model for power law distributions, which yield maximum diversity, our calculations can be straightforwardly generalised to different $p(s)$. For instance, in the case of algebraic distributions with a lower cut-off, a case often representative of real situations [34], one recovers similar results provided that the cut-off is independent of S (see the SM [32]).

Diversity, Zipf's and Heaps' laws.— Since the diversity is determined once an empirical distribution of sizes
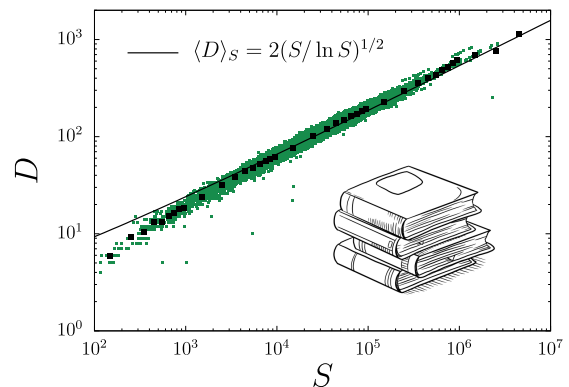

FIG. 3. Diversity index D evaluated from the data of Ref. [38]. Each green point is one of the more than 30000 English books in the Project Gutenberg database (accessed July 2014), while the black dots correspond to a logarithmic binning of the same data. The solid line is the result $\langle D \rangle_S = 2(S/\ln S)^{1/2}$, from Eq. (10) for $\tau = 2$, which corresponds to maximal diversity.

is given, we can use $\langle D \rangle_S$ given in Eq. (10) to estimate the diversity index D of power law distributed empirical data, regardless of the mechanism whereby they are produced. If this assumption holds, on the basis of our analytical arguments, one can conclude that if a system displays Zipf's law ($\tau \simeq 2$ [12, 35]) it is at the edge of maximal diversity and *vice versa*.

As an example we consider quantitative linguistics, the field in which Zipf's law has been originally observed in almost every human language [9, 36–38]. The regime of validity of the law in this context [39], its deviations [40] and the underlying mechanism(s) are still a matter of dispute. Nonetheless, large scale studies have been performed in order to validate that. For example, Moreno-Sánchez *et al.* [38] considered a very large set of English books (more than 30000) from the Gutenberg Project database. They checked how well some simple, one-parameter forms of the Zipf's law describe these data on the whole interval of frequencies, finding very good agreement with a distribution of exponents centered on $\tau \simeq 2$.

We use the filtered data of Ref. [38] and, for each book, measure the diversity index D. The total number of words a book contains is its total size S, the number of distinct words is the number of entities, N, and the size s of each entity is its absolute frequency, i.e. how many times that word appears. The diversity D is therefore the number of *different frequencies* a given text displays. The result of this analysis is shown in Fig. 3 along with Eq. (10) for $\tau = 2$. Notice that there are no free parameters in the plot. The agreement between our theoretical prediction and the experimental points is consistent with the results reported in Ref. [38] showing that a great deal of the books have τ close to 2.

The content of Eq. (7) is Heaps' law, which gives an es-

timate of the number of components of a system of total size S given that the empirical size distribution follows a power law with exponent τ. Our expression of the law for $\tau > 1$ is in accordance with Ref. [31] and complements the result with the cases with $\tau \leq 1$ and with the appropriate prefactors. Heap's law is expected to hold for systems which are robust in the statistics of their component ($p_S(s)$ in our notation) at varying S [31, 34]. This is captured in our approach, where Eq. (7) is only arrived at using distributions which have the same form for any S (the same applies to Eq. (10)).

In our approach, Heap's law (7) and the diversity law (10) imply each other, encoding dependencies on the system size on equal footings. However, notably, the latter naturally selects the exponent $\tau = 2$ as a special one. Moreover, our analysis of the Gutenberg dataset shows that the diversity law is obeyed up to the largest sizes considered ($S \simeq 10^7$), whereas it is known [41] that strong deviations from Heaps' law are caused by the finiteness of the vocabulary. Therefore, at least in the context of language, the diversity law appears more robust and this suggests that its use could be more suited to interpret the size dependence of empirical data.

Discussion.— The partition of a finite resource S among constituents informs numerous systems in diverse fields of science and humanities. In this Letter, by solving a paradigmatic statistical model, we have shown that a maximally diverse partition is accompanied by Zipf's law. When framed in terms of extremization of appropriate cost functions, problems are endowed with a complementary description and can be approached with new strategies. Our study suggests that, in some instances where Zipf's law is empirically observed, promoting diversity to the role of a driving force could provide further theoretical insights towards a deeper and more general comprehension.

* mazzaris@mis.mpg.de

[1] L. Jost, Entropy and diversity, Oikos **113**, 363 (2006).
[2] H. Tuomisto, A consistent terminology for quantifying species diversity? Yes, it does exist, Oecologia **164**, 853 (2010).
[3] A. R. Ives and S. R. Carpenter, Stability and diversity of ecosystems, Science **317**, 58 (2007).
[4] C. S. Elton, *The ecology of invasions by animals and plants* (Methuen & Co. Ltd., London, UK, 1958).
[5] D. Tilman, P. B. Reich, and J. M. Knops, Biodiversity and ecosystem stability in a decade-long grassland experiment, Nature **441**, 629 (2006).
[6] F. Arese Lucini, F. Morone, M. S. Tomassone, and H. A. Makse, Diversity increases the stability of ecosystems, PLOS ONE **15**, 1 (2020).
[7] A. Tacchella, M. Cristelli, G. Caldarelli, A. Gabrielli, and L. Pietronero, A new metrics for countries' fitness and products' complexity, Sci. Rep. **2**, 1 (2012).
[8] X. Gabaix, Zipf's law for cities: an explanation, The Quarterly journal of economics **114**, 739 (1999).
[9] S. T. Piantadosi, Zipf's word frequency law in natural language: A critical review and future directions, Psychon Bull Rev. **21**, 1112 (2014).
[10] C. Furusawa and K. Kaneko, Zipf's law in gene expression, Phys. Rev. Lett. **90**, 088102 (2003).
[11] G. K. Zipf, *Human Behaviour and the Principle of Least Effort: An Introduction to Human Ecology* (Addison-Wesley, Cambridge, MA, 1949).
[12] M. E. J. Newman, Power laws, Pareto distributions and Zipf's law, Contemp. Phys. **46**, 323 (2005).
[13] A. Clauset, C. R. Shalizi, and M. E. Newman, Power-law distributions in empirical data, SIAM review **51**, 661 (2009).
[14] M. Cristelli, M. Batty, and L. Pietronero, There is more than a power law in Zipf, Sci. Rep. **2**, 1 (2012).
[15] R. L. Axtell, Zipf distribution of US firm sizes, Science **293**, 1818 (2001).
[16] J. C. Willis and G. U. Yule, Some statistics of evolution and geographical distribution in plants and animals, and their significance, Nature **109**, 177 (1922).
[17] L. Oddershede, P. Dimon, and J. Bohr, Self-organized criticality in fragmenting, Phys. Rev. Lett. **71**, 3107 (1993).
[18] H. A. Simon, On a class of skew distribution functions, Biometrika **42**, 425 (1955).
[19] M. Levy and S. Solomon, Power laws are logarithmic Boltzmann laws, International Journal of Modern Physics C **7**, 595 (1996).
[20] M. Marsili and Y.-C. Zhang, Interacting individuals leading to Zipf's law, Phys. Rev. Lett. **80**, 2741 (1998).
[21] R. F. i Cancho and R. V. Solé, Least effort and the origins of scaling in human language, Proceedings of the National Academy of Sciences **100**, 788 (2003).
[22] F. Tria, V. Loreto, V. D. P. Servedio, and S. H. Strogatz, The dynamics of correlated novelties, Scientific Reports **4**, 1 (2014).
[23] B. Corominas-Murtra, R. Hanel, and S. Thurner, Understanding scaling through history-dependent processes with collapsing sample space, Proceedings of the National Academy of Sciences **112**, 5348 (2015).
[24] A. Mazzolini, M. Gherardi, M. Caselle, M. C. Lagomarsino, and M. Osella, Statistics of shared components in complex component systems, Phys. Rev. X **8**, 021023 (2018).
[25] T. Mora and W. Bialek, Are biological systems poised at criticality?, J. Stat. Phys. **144**, 268 (2011).
[26] M. Marsili, I. Mastromatteo, and Y. Roudi, On sampling

and modeling complex systems, J. Stat. Mech.: Theory and Experiment **2013**, P09003 (2013).

[27] D. J. Schwab, I. Nemenman, and P. Mehta, Zipf's law and criticality in multivariate data without fine-tuning, Phys. Rev. Lett. **113**, 068102 (2014).

[28] R. J. Cubero, J. Jo, M. Marsili, Y. Roudi, and J. Song, Statistical criticality arises in most informative representations, J. Stat. Mech.: Theory and Experiment **2019**, 063402 (2019).

[29] Project Gutenberg, `www.gutenberg.org`.

[30] H. S. Heaps, *Information Retrieval: Computational and Theoretical Aspects* (Academic Press, Inc., Orlando, FL, 1978).

[31] L. Lü, Z.-K. Zhang, and T. Zhou, Zipf's law leads to Heaps' law: Analyzing their relation in finite-size systems, PLOS ONE **5**, e14139 (2010).

[32] See Supplemental Material for an explicit expression for the probability distribution of the diversity $p_S(D)$, an exact computation of the dressed probability distribution $p_S(s)$ and $p_S(N)$, motivations for the approximation $p_S(s) \simeq p(s)$ and the case of power law bare distributions with a constant lower cut-off s_L. Ref. [42] is included.

[33] A. de Azevedo-Lopes, A. R. de la Rocha, P. M. C. de Oliveira, and J. J. Arenzon, Dynamical cluster size heterogeneity, Phys. Rev. E **101**, 012108 (2020).

[34] G. De Marzo, A. Gabrielli, A. Zaccaria, and L. Pietronero, Dynamical approach to Zipf's law, Phys. Rev. Research **3**, 013084 (2021).

[35] A. Corral, I. Serra, and R. Ferrer-i Cancho, Distinct flavors of Zipf's law and its maximum likelihood fitting: Rank-size and size-distribution representations, Phys. Rev. E **102**, 052113 (2020).

[36] E. U. Condon, Statistics of vocabulary, Science **67**, 300 (1928).

[37] M. Gerlach and E. G. Altmann, Scaling laws and fluctuations in the statistics of word frequencies, New J. Phys. **16**, 113010 (2014).

[38] I. Moreno-Sánchez, F. Font-Clos, and A. Corral, Large-scale analysis of Zipf's law in english texts, PLOS ONE **11**, 1 (2016).

[39] F. Font-Clos, G. Boleda, and A. Corral, A scaling law beyond Zipf's law and its relation to Heaps' law, New J. Phys. **15**, 093033 (2013).

[40] R. Ferrer i Cancho, The variation of Zipf's law in human language, Eur. Phys. J. B **44**, 249 (2005).

[41] L. Lü, Z.-K. Zhang, and T. Zhou, Deviation of Zipf's and Heaps' laws in human languages with limited dictionary sizes, Sci. Rep. **3**, 1 (2013).

[42] F. Corberi, Development and regression of a large fluctuation, Phys. Rev. E **95**, 032136 (2017).

SUPPLEMENTAL MATERIAL

Probability distribution of the diversity index D.— The formal expression of the constrained richness probability distribution $p_S(D)$ reads

$$p_S(D) = \frac{1}{D!} \sum_{N=D}^{S} N! \sum_{s_1}^{1,S} \sum_{s_2 \neq s_1}^{1,S} \sum_{s_3 \neq s_1,s_2}^{1,S} \cdots \sum_{s_D \neq s_1,\ldots,s_{D-1}}^{1,S} \sum_{\substack{k_1,k_2,\ldots,k_D \\ \sum_{i=1}^{D} k_i = N}}^{k_i=1,N-D+1} \frac{1}{\prod_{j=1}^{D} k_j!} \prod_{m=1}^{D} p(s_m)^{k_m} \delta_{\sum_{n=1}^{D} k_n s_n, S}, \tag{11}$$

Eq. (11) can be read out as follows. i) The product $\prod_{m=1}^{D} p(s_m)^{k_m}$ is the probability of a configuration where there are $\{k_m\}$ entities of sizes $\{s_m\}$. ii) One can go through all those configurations by summing over all the k_m, provided that $\sum_{i=1}^{D} k_i = N$, the total number of entities. Furthermore, each index k_i starts at 1, because each of the D different sizes must be represented by at least one component, up to $N - D - 1$, which is the situation in which all the other sizes, except s_i, are represented by single components. iii) The factor $N!/\prod_{j=1}^{D} k_j!$ ($N!$ has been moved to the beginning of the expression) is the number of ways to have a realisation of $\{k_m\}$. The extra factor $D!$ appears in order to avoid overcounting of configurations that have the same realisation of the entities due to the symmetry upon relabeling the sizes. iv) The δ function sets the system total size S. v) The sums over $s_1, \cdots, s_D$ are constrained not to overlap because, given D, there must be D entities of different sizes, no matter what these sizes are. vi) The sum over N starts from the given value of D, $N \geq D$, because it is not possible to have D different sizes in the configuration with less than D entities.

Exact solutions using recursive method.— Let us consider the computation of the quantities $p_S(s)$, Eq. (3), and $p_S(N) = Z_S(N)/Z_S$. The sums defining $Z_S(N)$ in Eq. (2) contain, *a priori*, a number S^S of terms, which cannot be enumerated by a fast computer even for relatively small values of S. However, due to the constraint imposed by the δ function, only a small fraction of such terms does not vanish. It was shown in Ref. [42] that using the recurrence relation

$$Z_S(N) = \sum_{s=1}^{\infty} p(s) Z_{S-s}(N-1), \tag{12}$$

that can be easily proved upon writing $\delta_{\sum_{n=1}^{N} s_n, S} = \delta_{\sum_{n=2}^{N} s_n, S-s_1}$, the algorithmic complexity is lowered to polynomial. With this tool we obtain an exact solution of the model up to relatively large values of S.

Let us start to discuss the dressed size probability $p_S(s)$. This quantity is plotted in Fig. 4 using an algebraic bare probability $p(s) \sim s^{-\tau}$ for different values of τ. The exact determination, obtained from Eq. (3), is compared with the outcome of numerical simulations
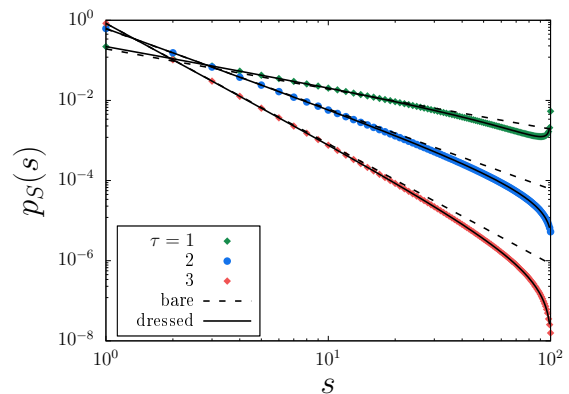

FIG. 4. The exact dressed probability distribution $p_S(s)$ obtained from Eq. (3) is compared with numerical simulations for a system of size $S = 100$, using a bare size distribution $p(s) \sim s^{-\tau}$ and different values of τ. Deviations only become large when s is close to S where $p_S(s)$ is small.

where, after extracting the random variables s_n, only the configurations respecting the constraint are kept. One sees a perfect agreement. As expected, the dressed and the bare distribution coincide, $p_S(s) \simeq p(s)$, up to values $s \lesssim S$ beyond which $p_S(s)$ gets strongly depressed. This suggests that the bare distribution $p(s)$ can be used, in place of $p_S(s)$, in the calculation of different quantities, thus simplifying the task.

The exact value of the average number of entities

$$\langle N \rangle_S = \sum_{N=1}^{S} N p_S(N), \tag{13}$$

can be computed by means of

$$p_S(N) = \frac{Z_S(N)}{Z_S}. \tag{14}$$

again evaluated with the recursive method. The result is shown in Fig. 5.

Algebraic distributions with lower cut-off.— We consider the case of power law bare distributions with a con-
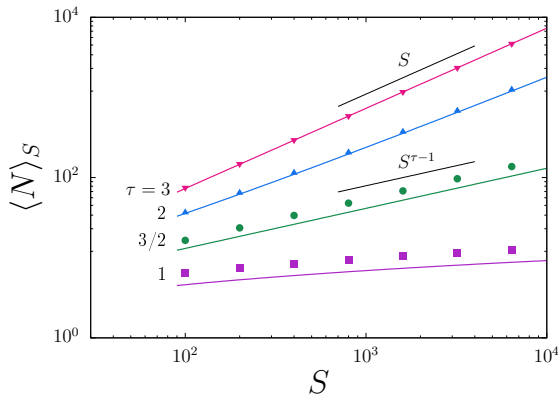
FIG. 5. Average number of domains as a function of the size of the system for different values of τ evaluated through Eq. (13). The solid lines represent the analytical evaluation of $\langle N \rangle_S$ using the bare probability distribution, as discussed in the main paper. It can be noticed that in the region $\tau < 2$ there is a shift by a constant prefactor, although the form is correctly predicted. The predicted asymptotic behaviour for $\tau = 3/2$ and 3, given by Eq. (7), is also indicated.

stant lower cut-off s_L

$$
p(s) = \begin{cases} 0 & ; \text{ for } \quad s < s_L \\ s^{-\tau}/\Lambda(\tau, s_L, S) & ; \text{ for } \quad s_L \leq s \leq S \\ 0 & ; \text{ for } \quad s > S , \end{cases} \quad (15)
$$

where $\Lambda(\tau, s_L, S) = \zeta(\tau, s_L) - \zeta(\tau, S)$, where $\zeta(x, y)$ is the Hurwitz zeta function. We denote the average number of entities $\langle N \rangle_{S, s_L}$ and the average diversity $\langle D \rangle_{S, s_L}$ in this

case. Equation (6) can be cast as

$$
\langle D \rangle_S \simeq s^* - s_L + \langle N \rangle_S \sum_{s=s^*}^{S} p_{S, s_L}(s), \quad (16)
$$

where $p_{S, s_L}(s)$ is the appropriate dressed probability distribution. Also in this case we can approximate, for large S, $p_{S, s_L}(s) \simeq p(s)$. Therefore we can write the average size of the entities as $\langle s \rangle_{S, s_L} \simeq \Lambda(\tau - 1, s_L, S)/\Lambda(\tau, s_L, S)$ and $\langle N \rangle_{S, s_L} \simeq S/\langle s \rangle_{S, s_L}$. For large S we can approximate $\Lambda(x, s_L, S) \simeq \zeta(x, s_L) + S^{1-x}/(1-x)$ for $x \neq 0, 1$ and, noticing that $\zeta(x, s_L) = \zeta(\tau) + \text{const.}$, on has $\Lambda(1, s_L, S) \simeq \ln S$ and $\Lambda(0, s_L, S) \simeq S$. We obtain

$$
\langle N \rangle_{S, s_L} \simeq \begin{cases} (2 - \tau)/(1 - \tau) & ; \text{ for } \quad \tau < 1 \\ \ln S & ; \text{ for } \quad \tau = 1 \\ \zeta(\tau, s_L)(2 - \tau)S^{\tau - 1} & ; \text{ for } \quad 1 < \tau < 2 \\ \zeta(2, s_L)S/\ln S & ; \text{ for } \quad \tau = 2 \\ \zeta(\tau, s_L)S/\zeta(\tau - 1, s_L) & ; \text{ for } \quad \tau > 2 , \end{cases} \quad (17)
$$

which is the same as Eq. (7) with all the Riemann zeta functions replaced by Hurwitz ones. Therefore, with $s^* \simeq (S/\Lambda(\tau - 1, s_L, S))^{1/\tau}$, we can write

$$
\langle D \rangle_S \simeq s^* - s_L + (s^*)^\tau [\zeta(\tau, s^*) - \zeta(\tau, S + 1)], \quad (18)
$$

which, to leading order in S, reads

$$
\langle D \rangle_{S, s_L} \simeq \begin{cases} (2 - \tau)/(1 - \tau) - s_L & ; \text{ for } \quad \tau < 1 \\ \ln S & ; \text{ for } \quad \tau = 1 \\ \dfrac{\tau(2 - \tau)^{1/\tau}}{\tau - 1} S^{1 - 1/\tau} & ; \text{ for } \quad 1 < \tau < 2 \\ 2 (S/\ln S)^{1/2} & ; \text{ for } \quad \tau = 2 \\ \dfrac{\tau}{\tau - 1} \left[\dfrac{S}{\zeta(\tau - 1, s_L)} \right]^{1/\tau} & ; \text{ for } \quad \tau > 2 . \end{cases} \quad (19)
$$

Bibliography

[1] A. Bray, "Theory of phase-ordering kinetics," *Advances in Physics*, vol. 43, no. 3, pp. 357–459, 1994.

[2] R. Prozorov, A. F. Fidler, J. R. Hoberg, and P. C. Canfield, "Suprafroth in type-I superconductors," *Nature Physics*, vol. 4, pp. 327–332, 2008.

[3] D. J. Keavney, Y. Choi, M. V. Holt, V. Uhlíř, D. Arena, E. E. Fullerton, P. J. Ryan, and J.-W. Kim, "Phase coexistence and kinetic arrest in the magnetostructural transition of the ordered alloy FeRh," *Scientific reports*, vol. 8, no. 1, pp. 1–7, 2018.

[4] A. Chirkova, F. Bittner, K. Nenkov, N. Baranov, L. Schultz, K. Nielsch, and T. Woodcock, "The effect of the microstructure on the antiferromagnetic to ferromagnetic transition in ferh alloys," *Acta Materialia*, vol. 131, pp. 31 – 38, 2017.

[5] L. McNally, E. Bernardy, J. Thomas, A. Kalziqi, J. Pentz, S. P. Brown, B. K. Hammer, P. J. Yunker, and W. C. Ratcliff, "Killing by type VI secretion drives genetic phase separation and correlates with increased cooperation," *Nature communications*, vol. 8, no. 1, pp. 1–11, 2017.

[6] J. C. M. Mombach, R. M. C. de Almeida, and J. R. Iglesias, "Mitosis and growth in biological tissues," *Phys. Rev. E*, vol. 48, pp. 598–602, Jul 1993.

[7] R. Schlicht and Y. Iwasa, "Forest gap dynamics and the Ising model," *Journal of Theoretical Biology*, vol. 230, no. 1, pp. 65 – 75, 2004.

[8] A. Sicilia, J. J. Arenzon, I. Dierking, A. J. Bray, L. F. Cugliandolo, J. Martínez-Perdiguero, I. Alonso, and I. C. Pintre, "Experimental test of curvature-driven dynamics in the phase ordering of a two dimensional liquid crystal," *Phys. Rev. Lett.*, vol. 101, p. 197801, Nov 2008.

[9] G. Heppke and D. Moro, "Chiral order from achiral molecules," *Science*, vol. 279, no. 5358, pp. 1872–1873, 1998.

[10] D. J. Earl, M. A. Osipov, H. Takezoe, Y. Takanishi, and M. R. Wilson, "Induced and spontaneous deracemization in bent-core liquid crystal phases and in other phases doped with bent-core molecules," *Phys. Rev. E*, vol. 71, p. 021706, Feb 2005.

[11] L. F. Cugliandolo, "Geometric aspects of ordering phenomena," *Comptes Rendus Physique*, vol. 18, no. 1, pp. 5 – 18, 2017.

[12] J. J. Arenzon, A. J. Bray, L. F. Cugliandolo, and A. Sicilia, "Exact results for curvature-driven coarsening in two dimensions," *Phys. Rev. Lett.*, vol. 98, p. 145701, Apr 2007.

[13] A. Sicilia, J. J. Arenzon, A. J. Bray, and L. F. Cugliandolo, "Domain growth morphology in curvature-driven two-dimensional coarsening," *Phys. Rev. E*, vol. 76, p. 061116, Dec 2007.

[14] M. P. O. Loureiro, J. J. Arenzon, L. F. Cugliandolo, and A. Sicilia, "Coarsening in the Potts model: out-of-equilibrium geometric properties," *Journal of Physics: Conference Series*, vol. 246, no. 1, p. 012022, 2010.

[15] K. Barros, P. L. Krapivsky, and S. Redner, "Freezing into stripe states in two-dimensional ferromagnets and crossing probabilities in critical percolation," *Phys. Rev. E*, vol. 80, p. 040101, Oct 2009.

[16] J. Olejarz, P. L. Krapivsky, and S. Redner, "Fate of 2d kinetic ferromagnets and critical percolation crossing probabilities," *Phys. Rev. Lett.*, vol. 109, p. 195702, Nov 2012.

[17] T. Blanchard and M. Picco, "Frozen into stripes: Fate of the critical Ising model after a quench," *Phys. Rev. E*, vol. 88, p. 032131, Sep 2013.

[18] A. Sicilia, Y. Sarrazin, J. J. Arenzon, A. J. Bray, and L. F. Cugliandolo, "Geometry of phase separation," *Phys. Rev. E*, vol. 80, p. 031121, Sep 2009.

[19] D. Stauffer and A. Aharony, *Introduction To Percolation Theory*. Taylor & Francis, 1994.

[20] H. K. Lee, B. J. Kim, and H. Park, "Continuity of the explosive percolation transition," *Phys. Rev. E*, vol. 84, p. 020101, Aug 2011.

[21] J. D. Noh, H. K. Lee, and H. Park, "Scaling of cluster heterogeneity in percolation transitions," *Phys. Rev. E*, vol. 84, p. 010101, Jul 2011.

[22] W. S. Jo, S. D. Yi, S. K. Baek, and B. J. Kim, "Cluster-size heterogeneity in the two-dimensional Ising model," *Phys. Rev. E*, vol. 86, p. 032103, Sep 2012.

[23] A. R. de la Rocha, P. M. C. de Oliveira, and J. J. Arenzon, "Domain-size heterogeneity in the Ising model: Geometrical and thermal transitions," *Phys. Rev. E*, vol. 91, p. 042113, Apr 2015.

[24] J.-P. Lv, X. Yang, and Y. Deng, "Scaling of cluster heterogeneity in the two-dimensional Potts model," *Phys. Rev. E*, vol. 86, p. 022105, Aug 2012.

[25] A. de Azevedo-Lopes, A. R. de la Rocha, P. M. C. de Oliveira, and J. J. Arenzon, "Dynamical cluster size heterogeneity," *Phys. Rev. E*, vol. 101, p. 012108, Jan 2020.

[26] O. Mazzarisi, A. de Azevedo-Lopes, J. J. Arenzon, and F. Corberi, "Maximal Diversity and Zipf's Law," *arXiv e-prints*, p. arXiv:2103.09143, Mar. 2021.

[27] A. de Azevedo-Lopes, R. Almeida, and J. J. Arenzon, "The formation of a critical cluster in the Ising model after a quench." in preparation.

[28] T. Blanchard, F. Corberi, L. F. Cugliandolo, and M. Picco, "How soon after a zero-temperature quench is the fate of the Ising model sealed?," *EPL (Europhysics Letters)*, vol. 106, no. 6, p. 66001, 2014.

[29] T. Blanchard, L. F. Cugliandolo, M. Picco, and A. Tartaglia, "Critical percolation in the dynamics of the 2d ferromagnetic Ising model," *Journal of Statistical Mechanics: Theory and Experiment*, vol. 2017, no. 11, p. 113201, 2017.

[30] F. Corberi, L. F. Cugliandolo, F. Insalata, and M. Picco, "Coarsening and percolation in a disordered ferromagnet," *Phys. Rev. E*, vol. 95, p. 022101, Feb 2017.

[31] A. Tartaglia, L. F. Cugliandolo, and M. Picco, "Coarsening and percolation in the kinetic 2d Ising model with spin exchange updates and the voter model," *Journal of Statistical Mechanics: Theory and Experiment*, vol. 2018, no. 8, p. 083202, 2018.

[32] A. Sicilia, J. J. Arenzon, A. J. Bray, and L. F. Cugliandolo, "Geometric properties of two-dimensional coarsening with weak disorder," *EPL (Europhysics Letters)*, vol. 82, p. 10001, mar 2008.

[33] E. Ising, "Beitrag zur Theorie des Ferromagnetismus," *Zeitschrift für Physik*, vol. 31, no. 1, pp. 253–258, 1925.

[34] L. Onsager, "Crystal statistics. I. a two-dimensional model with an order-disorder transition," *Phys. Rev.*, vol. 65, pp. 117–149, Feb 1944.

[35] J. G. Amar and F. Family, "Diffusion annihilation in one dimension and kinetics of the Ising model at zero temperature," *Phys. Rev. A*, vol. 41, pp. 3258–3262, Mar 1990.

[36] A. J. Bray, "Universal scaling function for domain growth in the Glauber-Ising chain," *Journal of Physics A: Mathematical and General*, vol. 23, pp. L67–L72, jan 1990.

[37] A. Coniglio and M. Zannetti, "Multiscaling in growth kinetics," *Europhysics Letters (EPL)*, vol. 10, pp. 575–580, nov 1989.

[38] T. J. Newman, A. J. Bray, and M. A. Moore, "Growth of order in vector spin systems and self-organized criticality," *Phys. Rev. B*, vol. 42, pp. 4514–4523, Sep 1990.

[39] S. M. Allen and J. W. Cahn, "A microscopic theory for antiphase boundary motion and its application to antiphase domain coarsening," *Acta Metallurgica*, vol. 27, no. 6, pp. 1085 – 1095, 1979.

[40] P. Clifford and A. Sudbury, "A model for spatial conflict," *Biometrika*, vol. 60, no. 3, pp. 581–588, 1973.

[41] R. A. Holley and T. M. Liggett, "Ergodic theorems for weakly interacting infinite systems and the voter model," *The Annals of Probability*, vol. 3, no. 4, pp. 643–663, 1975.

[42] T. Liggett, T. Liggett, and S. Chern, *Stochastic Interacting Systems: Contact, Voter and Exclusion Processes*. Springer, 1999.

[43] I. Dornic, H. Chaté, J. Chave, and H. Hinrichsen, "Critical coarsening without surface tension: The universality class of the voter model," *Phys. Rev. Lett.*, vol. 87, p. 045701, Jul 2001.

[44] T. Liggett, *Interacting particle systems*. Springer-Verlag, 1985.

[45] R. J. Glauber, "Time-dependent statistics of the Ising model," *Journal of Mathematical Physics*, vol. 4, no. 2, pp. 294–307, 1963.

[46] J. Cardy and R. M. Ziff, "Exact results for the universal area distribution of clusters in percolation, Ising, and Potts models," *Journal of Statistical Physics*, vol. 110, pp. 1–33, Jan 2003.

[47] A. L. Stella and C. Vanderzande, "Scaling and fractal dimension of Ising clusters at the d=2 critical point," *Phys. Rev. Lett.*, vol. 62, pp. 1067–1070, Mar 1989.

[48] S. R. Broadbent and J. M. Hammersley, "Percolation processes: I. Crystals and mazes," *Mathematical Proceedings of the Cambridge Philosophical Society*, vol. 53, no. 3, p. 629–641, 1957.

[49] D. Stauffer, "Scaling theory of percolation clusters," *Physics Reports*, vol. 54, no. 1, pp. 1–74, 1979.

[50] A. Lipowski, "Anomalous phase-ordering kinetics in the Ising model," *Physica A: Statistical Mechanics and its Applications*, vol. 268, no. 1, pp. 6 – 13, 1999.

[51] V. Spirin, P. L. Krapivsky, and S. Redner, "Fate of zero-temperature Ising ferromagnets," *Phys. Rev. E*, vol. 63, p. 036118, Feb 2001.

[52] V. Spirin, P. Krapivsky, and S. Redner, "Freezing in Ising ferromagnets," *Phys. Rev. E*, vol. 65, p. 016119, Dec 2001.

[53] J. Kalda, "Description of random gaussian surfaces by a four-vertex model," *Phys. Rev. E*, vol. 64, p. 020101, Jul 2001.

[54] H. T. Pinson, "Critical percolation on the torus," *Journal of Statistical Physics*, vol. 75, no. 5–6, pp. 1167–1177, 1994.

[55] J. L. Cardy, "Critical percolation in finite geometries," *Journal of Physics A: Mathematical and General*, vol. 25, no. 4, p. L201, 1992.

[56] G. Watts, "A crossing probability for critical percolation in two dimensions," *Journal of Physics A: Mathematical and General*, vol. 29, no. 14, p. L363, 1996.

[57] N. Jan, D. Stauffer, and A. Aharony, "An infinite number of effectively infinite clusters in critical percolation," *Journal of Statistical Physics*, vol. 92, pp. 325–330, Jul 1998.

[58] C. Fortuin and P. Kasteleyn, "On the random-cluster model: I. introduction and relation to other models," *Physica*, vol. 57, no. 4, pp. 536 – 564, 1972.

[59] A. Coniglio and W. Klein, "Clusters and Ising critical droplets: a renormalisation group approach," *Journal of Physics A: Mathematical and General*, vol. 13, pp. 2775–2780, aug 1980.

[60] F. Corberi, "Development and regression of a large fluctuation," *Phys. Rev. E*, vol. 95, p. 032136, Mar 2017.

[61] T. M. Apostol, "An elementary view of Euler's summation formula," *The American Mathematical Monthly*, vol. 106, no. 5, pp. 409–418, 1999.

[62] D. E. Knuth, *The art of computer programming, volume 1: Fundamental algorithms*. Addison-Wesley Professional, 1997.

[63] W. Janke and A. M. J. Schakel, "Fractal structure of spin clusters and domain walls in the two-dimensional Ising model," *Phys. Rev. E*, vol. 71, p. 036703, Mar 2005.

[64] A. R. de la Rocha, "Geometria e heterogeneidade na dinâmica no modelo de Potts," Master's Thesis, UFRGS, 2013.

[65] E. Newman and G. Barkema, *Monte Carlo Methods in Statistical Physics*. Clarendon Press, 1999.

[66] J. Olejarz, P. L. Krapivsky, and S. Redner, "Zero-temperature relaxation of three-dimensional Ising ferromagnets," *Phys. Rev. E*, vol. 83, p. 051104, May 2011.

[67] J. Hoshen and R. Kopelman, "Percolation and cluster distribution. I. cluster multiple labeling technique and critical concentration algorithm," *Phys. Rev. B*, vol. 14, pp. 3438–3445, Oct 1976.

[68] M. J. de Oliveira, J. F. F. Mendes, and M. A. Santos, "Non-equilibrium spin models with Ising universal behaviour," *Journal of Physics A: Mathematical and General*, vol. 26, no. 10, p. 2317, 1993.

[69] A. Tartaglia, L. F. Cugliandolo, and M. Picco, "Percolation and coarsening in the bidimensional voter model," *Phys. Rev. E*, vol. 92, p. 042109, Oct 2015.

[70] K. Binder, ""Clusters" in the Ising model, metastable states and essential singularity," *Annals of physics*, vol. 98, no. 2, pp. 390–417, 1976.

[71] A. Coniglio, C. R. Nappi, F. Peruggi, and L. Russo, "Percolation points and critical point in the Ising model," *Journal of Physics A: Mathematical and General*, vol. 10, no. 2, p. 205, 1977.

[72] H. Ricateau, L. F. Cugliandolo, and M. Picco, "Critical percolation in the slow cooling of the bi-dimensional ferromagnetic Ising model," *Journal of Statistical Mechanics: Theory and Experiment*, vol. 2018, no. 1, p. 013201, 2018.

[73] M. J. de Oliveira, "Linear Glauber model," *Phys. Rev. E*, vol. 67, p. 066101, Jun 2003.

[74] A. Kovacs, "Glass transition in amorphous polymers: a phenomenological study," *Adv. Polym. Sci*, vol. 3, pp. 394–508, 1963.

[75] L. Berthier and J.-P. Bouchaud, "Geometrical aspects of aging and rejuvenation in the Ising spin glass: A numerical study," *Phys. Rev. B*, vol. 66, p. 054404, Aug 2002.

[76] J. J. Arenzon and M. Sellitto, "Kovacs effect in facilitated spin models of strong and fragile glasses," *The European Physical Journal B - Condensed Matter and Complex Systems*, vol. 42, no. 4, pp. 543–548, 2004.

[77] Y. Lahini, O. Gottesman, A. Amir, and S. M. Rubinstein, "Nonmonotonic aging and memory retention in disordered mechanical systems," *Phys. Rev. Lett.*, vol. 118, p. 085501, Feb 2017.

[78] T. W. B. Kibble, "Topology of cosmic domains and strings," *Journal of Physics A: Mathematical and General*, vol. 9, pp. 1387–1398, aug 1976.

[79] W. H. Zurek, "Cosmological experiments in superfluid helium?," *Nature*, vol. 317, no. 6037, pp. 505–508, 1985.

[80] G. Biroli, L. F. Cugliandolo, and A. Sicilia, "Kibble-Zurek mechanism and infinitely slow annealing through critical points," *Phys. Rev. E*, vol. 81, p. 050101, May 2010.

[81] F. Corberi, E. Lippiello, and P. Politi, "One dimensional phase-ordering in the Ising model with space decaying interactions," *Journal of Statistical Physics*, vol. 176, pp. 510–540, 2019.

[82] M. P. Loureiro, J. J. Arenzon, and L. F. Cugliandolo, "Geometrical properties of the Potts model during the coarsening regime," *Phys. Rev. E*, vol. 85, p. 021135, Feb 2012.

[83] J. Denholm and S. Redner, "Topology-controlled Potts coarsening," *Phys. Rev. E*, vol. 99, p. 062142, Jun 2019.